A Study of Fluxons Propagating in Annular Josephson Junctions

By

Luke Hyland

Doctoral Thesis

Submitted in partial fulfilment of the requirements

For the award of

DPhil of Loughborough University

October 8th 2012

Abstract

In this research we looked at how fluxons propagate in an annular Josephson junction containing a microshort. We studied this from a theoretical stance and looked at how a single fluxon based on the sine-Grodon soliton equation propagates in this type of junction. It has been seen from a variety of studies that fluxons have many applications through the use of Josephson junctions. The aim of this thesis was to see whether a fluxon will show new properties whilst coming into contact with a microshort located in the junction. We also explored the different geometries a Josephson junction can have and whether that would show the fluxon to present new phenomena.

We will also examine point particle systems. With this in mind we took a keen interest in how the interaction between two of these particles in a double well potential would present itself and whether a relationship would become apparent. Alongside the point particle system we modelled fluxons in a double well potential and comment on the similarities with the point particle system.

With the aid of the computer programmes Mathematica and COMSOL Multiphysics we were able to compute these different theoretical models and present the work in a logical order with a progression from a single point particle in a double well potential to a fluxon in a heart-shaped Josephson junction. We have looked at current theories and ideas present in this area of condensed matter physics and have explained these in the subsequent thesis.

Acknowledgements

Contents

1 <u>Introduction</u>

This research project hopes to improve upon current knowledge in the area of condensed matter physics which concerns fluxons and Josephson junctions. It builds upon previous works relating to different junction geometries which contain a device known as a microshort. The paper "Vortex Qubit Based on an Annular Josephson Junction Containing a Microshort" by the authors A.N. Price, A. Kemp, D.R. Gulevich, F.V. Kusmartsev and A.V. Ustinov[1] has been the springboard platform of this research.

The project commences with double well potentials and point particles propagating in them. This can be classically thought of as a "w" shaped ramp with a marble placed in various initial starting points. By releasing the marble one can see which well the ball will come to rest. Through the use of the computer programme Mathematica a code can be written to determine which "well" a particle will rest in from the various initial positions and velocities applied to the system. After the completion of the one point particle a system of two non-interacting particles is undertaken. Following on from this a two point particle interacting system will be investigated.

The next stage of the research will look at moving from the "simple" point particle to a more complex fluxon model. This model will have to consider the new potential associated with the microshort as well as the equations associated with a fluxon.

Once all of these codes were constructed and analysed the project will go onto consider designing Josephson junctions with the aid of the computer programme COMSOL Multiphysics. The fluxon will be placed in the junction and left to propagate and one hopes, undergo some different transformations. First to be considered will be an annular junction, then a square junction and finally a heart shaped junction. By examining these three structures with a

---

[1] A.N. Price, A. Kemp, D.R. Gulevich, F.V. Kusmartsev and A.V. Ustinov. "Vortex Qubit Based on an Annular Josephson JunctionContaining a Microshort" (03/07/08).

microshort it is hoped that some new advances will be observed so that future technologies that will be able to make use of these techniques will prosper.

The literature review will go into detail on the history of the soliton and its three main forms. Also there will be a focus on the Josephson junction itself and how it came to be an important implement to be used in various capacities within the area. There is also an emphasis on the mathematical proofs and conditions that are applied to each of the research projects compiled. Due to the ease of talking from just a mathematical viewpoint the physics orientated research project will be emphasised with the many applications that these other projects indicate.

As with any standard experimental piece the analysis of each of the results will be explored and explained and then summarised in a conclusion. The conclusion will also touch upon further research models that with improvements could yield better results then ones obtained at this time. Finally the appendix will include all hard copies of the codes used in this project. These will be explained and hopefully give one the insight of the evolution of the research conducted. This will provide enough information to be able to take on the problem if one desires. An artefact is also located at the end of the thesis which is a draft of a paper we hope to get published.

2 <u>Literature Review</u>

This introductory chapter looks briefly at the historical significance of the soliton and how after a dormant period it evolved to become such a hot topic with research projects all over the world today. There are three main equations that give rise to soliton solutions and these are sine-Gordon (SG) equation, the Kortweg-de Vries (KdV) equation and the nonlinear Schrödinger (NLS) equation. These soliton solutions were found to have many different applications and have explained several phenomena in the physical world. There is also a focus on Josephson junctions where the historic information will be looked into as well as what it is used for in today's scientific society. Due to the nature of some of the results achieved a sub chapter will look into the mathematical phenomenon of fractals. To end the review one observes properties associated with fluxons in double-well potentials such as the depinning and bias currents. The review in particular takes some recent studies and their contribution to the research project.

2.1 Solitons

There are three solitons that are most well known, the sine-Gordon solitons also sometimes known as FK solitons (due to their discoverers Frenkel and Kontorova), the KdV (Korteweg-de Vries) or Russell solitons (named after John Scott Russell) and finally the envelope or group solitons. They all exhibit uncanny similarities but also have some intriguing differences.

The first discovery of a solitary wave was in 1834 by John Scott Russell. Russell, a Scottish scientist, first documented this observation whilst observing the movement of a canal barge. While observing the barge he noticed a water wave on the surface that he had not recognised before. His description of this "meeting" with the solitary wave is as follows:[2]

"I was observing the motion of a boat which was rapidly drawn along a narrow channel by a pair of horses, when the boat suddenly stopped – not so the mass of water in the channel which it had put in motion; it accumulated round the prow of the vessel in a state of violent agitation, then suddenly leaving it behind, rolled forward with great velocity, assuming the form of the large solitary elevation, a rounded, smooth and well defined heap of water, which continued its course along the channel apparently without change of form or diminution of speed. I followed it on horseback and overtook it still rolling on at a rate of some eight or nine miles an hour, preserving its original figure some 30 feet long and a foot to a foot and a half in height. Its height gradually diminished and after a chase of one or two miles I lost it in the windings of the channel. Such in the month of August 1834 was my first chance interview with that singular and beautiful phenomenon which I have called the Wave of Translation…"

Solitary wave solutions are just waves that propagate without change of form and have some localised shape. In 1844, John Scott Russell came up with four pieces of criteria to demonstrate

---

[2] R.K.Dodd, Solitons and Nonlinear Wave Equations (London: Academic Press, 1982)

solitary waves whilst using a water tank. The first of these facts were that solitary waves have the form of the shape, $h \operatorname{sech}^2[k(x - vt)]$ where h is the height of the wave, v is the velocity, t is time, and k is the wave vector. Secondly, a sufficiently large initial mass of water produces two or more independent solitary waves. Thirdly, solitary waves cross with each other but do not undergo "a change of any kind" and finally a wave of height h and propagating in a channel of depth d has a velocity given by the following equation,

$$v = \sqrt{g(d + h)} \tag{2.1.1}$$

Where the parameter g corresponds to gravity, d denotes the channel depth and the other parameters are the same as noted earlier. The previous equation also implies that large amplitude solitary waves travel faster than smaller ones. [3]

2.2 The KdV Soliton

In 1895, Korteweg and de Vries derived a nonlinear evolution equation governing wave propagation in a shallow channel of water,[4]

$$\frac{\partial \eta}{\partial \tau} = \frac{3}{2}\sqrt{\frac{g}{h}}\frac{\partial}{\partial \xi}\left(\frac{1}{2}\eta^2 + \frac{2}{3}\alpha\eta + \frac{1}{3}\sigma\frac{\partial^2\eta}{\partial\xi^2}\right) \tag{2.2.1}$$

Where,

$$\sigma = \frac{1}{3}h^3 - \frac{Th}{\rho g} \tag{2.2.2}$$

[3] R.Rajaraman, Solitons and Instantons (North-Holland Physics Publishing, 1987)
[4] P.G.Drazin, R.S.Johnson, Solitons: An Introduction (Cambridge University Press, 1989)

And η is equal to the surface elevation of the wave above the "normal" equilibrium h, α is a small arbitrary constant related to the uniform motion of the liquid, g is the gravitational constant, T is the surface tension and ρ corresponds to the density. Equation (2.2.1) has solitary wave solutions. Through the use of the following transformations the equation can be put into a nondimensional form,

$$t = \frac{1}{2}\sqrt{\frac{g}{(h\sigma)}}\tau \tag{2.2.3}$$

$$x = -\sigma^{-1/2}\xi \tag{2.2.4}$$

$$u = \frac{1}{2}\eta + \frac{1}{3}\alpha \tag{2.2.5}$$

Which in turn yields the standard KdV equation,

$$u_t + 6uu_x + u_{xxx} = 0 \tag{2.2.6}$$

The KdV equation had many other applications but this wasn't noted until 1960 by Gardner and Morikawa. They came across this equation when studying collision free hydromagnetic waves. Other application examples where the KdV equation aroses are stratified internal waves, ion-acoustic waves, plasma physics and lattice dynamics.

The solitary wave solution to this equation is,

$$u(x,t) = 2K^2 sech^2\left\{\kappa\left(x - 4K^2t - x_0\right)\right\} \tag{2.2.7}$$

Where K and x_0 are constants and the terms $2K^2$ and $4K^2$ are the amplitude and velocity terms respectively. Here, the velocity is proportional to the amplitude thus confirming one of Russell's earlier criteria for a solitary wave that the taller, larger amplitude waves will propagate faster

than the shorter, smaller ones. The KdV equation (2.2.6) in physical terms arises if the water waves are strictly one dimension, (x, t).

Physicists Norman Zabusky and Martin Kruskal took on an extensive mathematical analysis and considered the initial value problem for the KdV equation,

$$u_t + uu_x + \delta^2 u_{xxx} = 0 \qquad (2.2.8)$$

Also, they used the following initial condition,

$$u(x,0) = \cos(\pi x), \quad 0 \le x \le 2 \qquad (2.2.9)$$

Where $\delta = 0.022$ and that u, u_x, u_t are all periodic on [0, 2] for all of t. Zabusky and Kruskal found that after a short time the wave would steepen and almost produce a shock. At this point $\delta^2 u_{xxx}$ (the dispersive term) becomes significant and thus the nonlinear and dispersive terms balance each other out. It was these American physicists who came up with the term "soliton".[5]

The KdV soliton is prevalent in physical systems that consist of weak nonlinear and weak dispersive waves (The remnants of a wave impulse). All of the KdV soliton will propagate in the same direction. The solitons velocity is proportional to its height but the length on the other hand is inversely proportional to the square root of the height.

2.3   The Group Soliton (NLSE)

One of the Fourier modes that occurs when looking at linear waves and instabilities in homogeneous media has the form,[6]

$$\phi(x,t) = Ae^{i(kx-\omega t)} \qquad (2.3.1)$$

[5] A.T.Filippov, The Versatile Soliton (Springer Distributor, 2010)
[6] E.Infeld, G.Eowlands. Nonlinear Waves, Solitons and Chaos (Cambridge University Press, 1990)

Where A is the amplitude and also a constant. The solutions for this particular mode have to follow the dispersion relation, $D(\omega, k, \mu) = 0$. For example an acoustic wave for small k will have the following form,

$$\omega^2 = c^2 k^2 + \cdots, \tag{2.3.2}$$

Where the parameter c, corresponds to the velocity of sound. The dispersion relation introduced previously contains μ, which in this instance is a controlling the system externally and is known as a control parameter. For weakly nonlinear systems the dispersion relation has the form,

$$\omega = \omega(k, \mu, |\Phi|^2) \tag{2.3.3}$$

The disturbance can be written with the fundamental linear frequency ω_0 and the wave number k_0 terms which then gives the amplitude factor,

$$\Phi(x, t) = a(x, t) e^{i(k_0 x - \omega_0 t)} \tag{2.3.4}$$

Now by comparing (2.3.1) to (2.3.4) one obtains,

$$a = a_0 e^{i[(k-k_0)x - (\omega[k,\mu,|a|^2] - \omega_0)t]}$$

Then for values of k's near k_0 a Taylor expansion is implored to expand ω for weakly nonlinear cases,

$$\omega(k, \mu, |a|^2) = \omega\left(k_0, \mu_0, 0\right) + \omega_k(k - k_0) + \frac{1}{2}\omega_{kk}(k - k_0)^2 + \tag{2.3.5}$$
$$\omega_\mu(\mu - \mu_0) + \omega_{|a|^2}|a|^2 + \cdots,$$

and in this equation the suffix's stand for partial differentials with respect to the variable associated with it. By now being able to choose ω_0 one can achieve the result,

$$i\left(\frac{\partial a}{\partial t} + vg\frac{\partial a}{\partial x}\right) + \frac{1}{2}\omega_{kk}\frac{\partial^2 a}{\partial x^2} - [(\mu - \mu_0)\omega_\mu + \omega_{|a|^2}]a = 0 \qquad (2.3.6)$$

which is a form of the nonlinear Schrodinger equation (NLSE). The quantities v_g, ω and ω_{kk} can be obtained by linear theory whereas the quantity $\omega_{|a|^2}$ is obtained by nonlinear theory. The equation (2.3.6) is very universal in that one can do a mathematical process similar to the above method but instead of calculating in terms of frequency one could do so with the wave number with $k = k(\omega, \mu, |a|^2)$ as a solution to the dispersion relation that was used initially. A case where one would want to have this different form of the NLSE would be if one was exploring the instability that causes growth in space but such that time dependence is controlled.

A more eye pleasing version of the NLSE is as follows,

$$iu_t + u_{xx} + 2|u|^2 u = 0 \qquad (2.3.7)$$

In contrast to the KdV equation and also the sine-Gordon equation, the dependent variable is complex rather than real. The evolutions of the magnitude and phase of u are governed by this equation. This equation, the NLSE is a generalization nonlinearly of the linear equation:

$$iu_t + u_{xx} + u = 0 \qquad (2.3.8)$$

Solutions of this comprise both an envelope and a carrier wave. This can be seen in Fig (2.3.2).[7] A carrier wave is defined as an electromagnetic wave that can be modulated, as in frequency, amplitude or phase to transmit speech, music, images or other signals.[8]

---

[7] http://www.mathpages.com/home/kmath210/Image3229.gif
[8] "Carrier Wave", [Online] Farlex, Available from: http://www.thefreedictionary.com/carrier+wave [Accessed on 28/12/08]
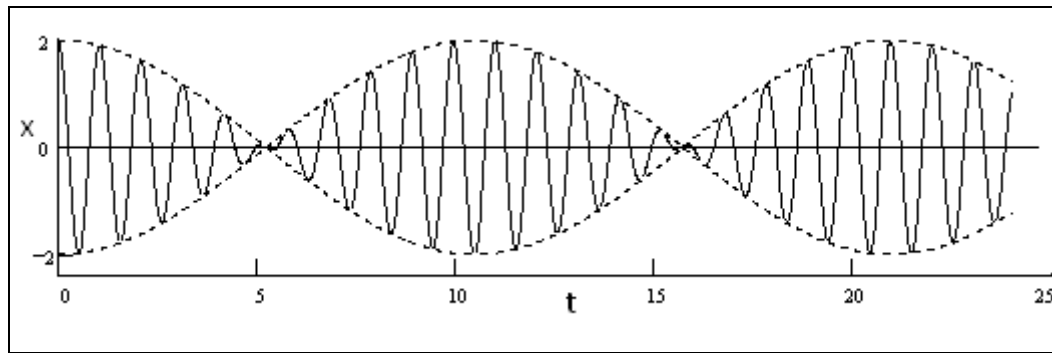
Figure 2.3.2 The Group Wave

The group soliton appears in weak nonlinear and strongly dispersive media. It is basically a wave that is smoothly modulated and monochromatic. Unlike the KdV soliton its velocity is independent of amplitude. The length of the KdV soliton is inversely proportional to the amplitude.

2.3.1   Freak Waves

In the year 2000, freak waves were observed from space. Before this it was thought that these waves were just an old sailor's tale with no scientific truth attached to them. During a three week experiment, 10 giant waves were detected of at least 25m (approximately 81 ft) in height.

During the 1980s and 1990s researchers have noted that just over 200 super carriers (which are ships that are longer than 200m) have been lost at sea. It is thought that some of these incidents are related to the freak wave phenomena.

To prove that it wasn't just bad weather that had caused these losses, 11 organizations from around the EU formed the project MaxWave. As part of the project, ESA tasked two of its Earth-scanning satellites, ERS-1 and ERS-2 to monitor the oceans via radar. These radars sent back rectangle images of the sea's surface measuring 6 x 2.5 miles (10 x 5km) which were taken at intervals of 200km.

During this three week period the Breman and the Caledonian Star (2 tourist liners) were struck by rogue waves measuring 30m in height in the South Atlantic Ocean. By capturing these waves on film and therefore proving their existence, a new phase of research was decided upon. This

was known as WaveAtlas. This project was to last 2 years, and the goal being to discover how these waves were created and which parts of the oceans are more susceptible than others.[9]

Waves produced by a storm can be diffracted and reflected when they approach waters that are shallower. This occurs occasionally on the Norwegian Coast and figure (2.3.1.1) shows this:[10]
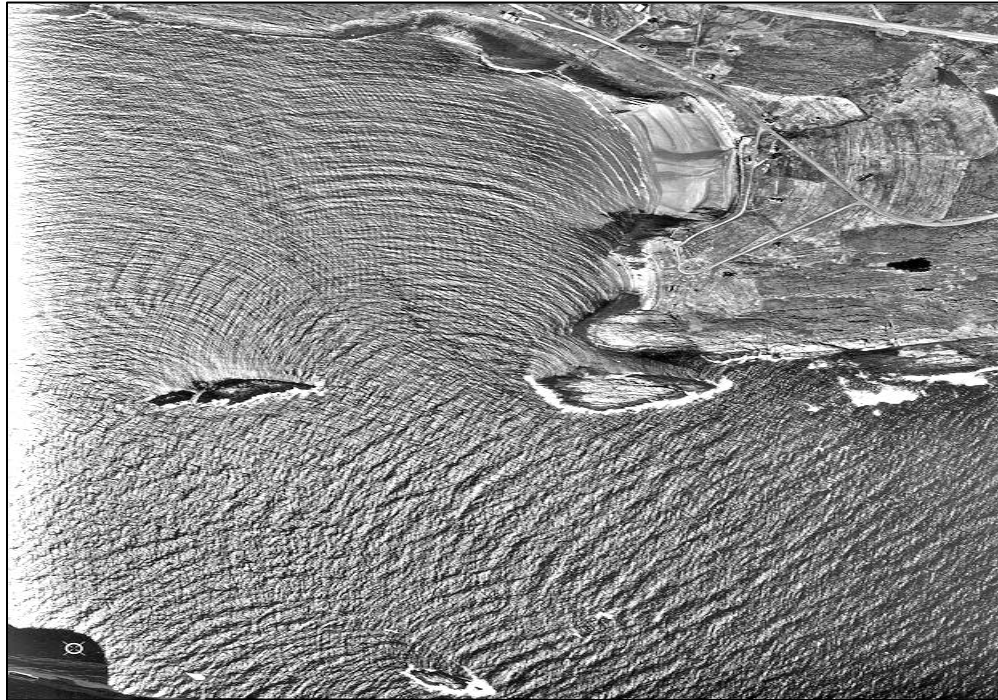
Figure 2.3.1.1 An image of the shallow waves along the Scandinavian coastline.

Figure (2.3.1.2) shows a time series of surface elevation (m) as a function of time (s) for the "New Year Wave" which was detected on the 1st January 1995 in the North Sea. As one can see from the figure (2.3.1.2) the wave surface elevation spikes to more than double in size at the time, t = 270 s.

---

9   ""Freak Waves Spotted From Space", [Online] MarineTalk2, Available from: http://www.marinetalk.com/articles-marine-companies/art/Freak-Waves-Spotted-from-Space-xxx000120257IN.html [Accessed on 12/11/08]

10 "Freak Waves, Rogue Waves, Extreme Waves and Ocean Wave Climate", [Online] University of Bergen, Available from: http://www.math.uio.no/~karstent/waves/index_en.html [Accessed on 12/11/08]
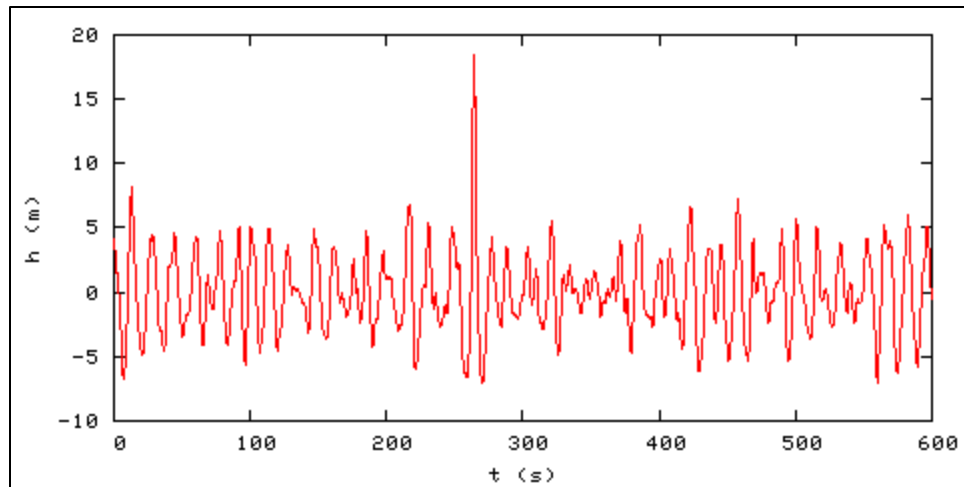
Figure 2.3.1.2 The New Year Wave

So what causes these anomalies in the open water? There were 3 possible candidates proposed,

1. Time-space focusing
2. Current focusing
3. Nonlinear focusing

The first 2 "candidates" are a result of linear theory and the last, nonlinear. The latter being the one of most interest to us and will be explored furthered in the next section.

2.3.2 Nonlinear focusing

In the 1960's it was shown that if in one end of a long tank a uniform set of periodic waves are produced then they will split into groups spontaneously. These "groups" become more prominent as they travel along the tank. Linear theory says that these waves should have stayed uniform and periodic in profile. The NLSE was then developed to explain this phenomenon qualitatively. The figures (2.3.2.1 to 2.3.2.4) show a set of three waves, the top (red) wave is equal to the evolution according to the higher order modified NLSE, the middle (green) wave is the evolution according to the cubic NLSE and the bottom (blue) wave corresponds to the linear evolution.

19

This is a mathematical simulation and shows a time series measured at four different "stations".
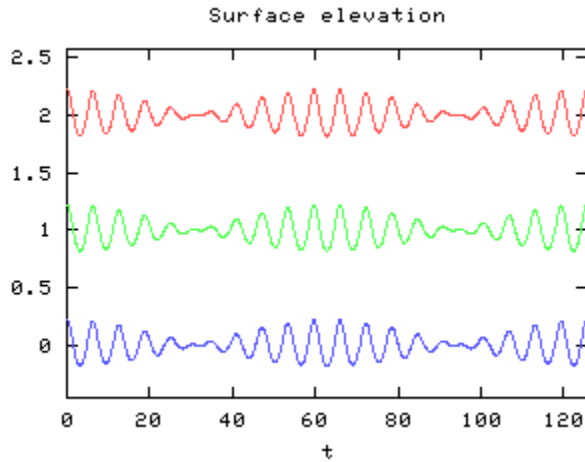
Fig 2.3.2.1 Time Station 1.
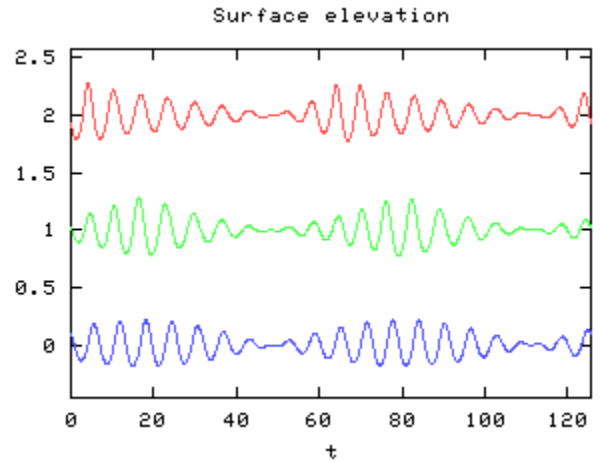
Fig 2.3.2.2 Time Station 2.
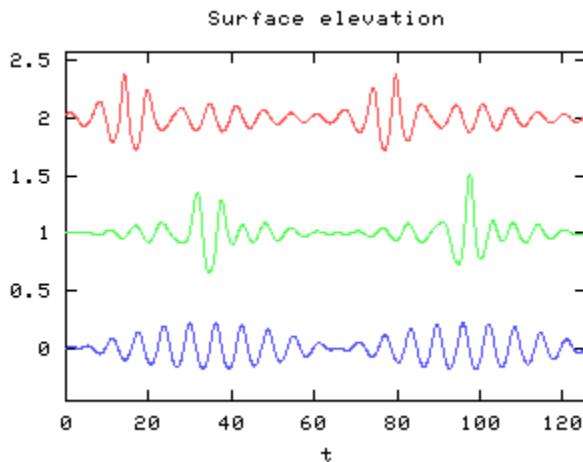
Fig 2.3.2.3 Time Station 3.
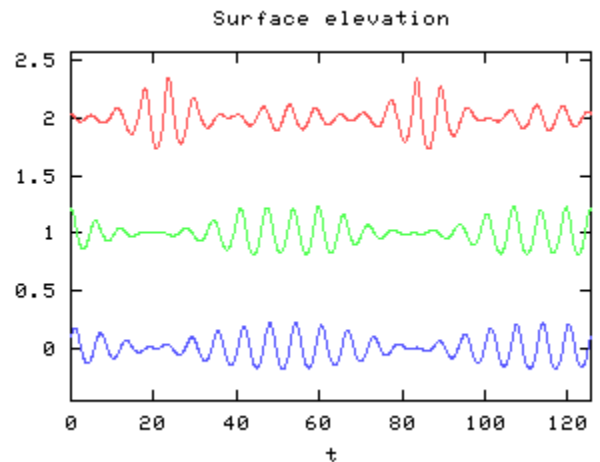
Fig 2.3.2.4 Time Station 4.

From the figures we see that the blue wave depending upon linear effects does not differ in its shape in any of the time stations. The red and green nonlinear waves however, have peaks occur in their time series and this led researchers to suggest that they may be related to the freak wave phenomena. The upper wave has been proven to be the most realistic with regards to the physical world.

Another popular candidate for freak waves is the simplest NLSE. This starts as a periodic wave train where the amplitude is modulated weakly. This is known simply as a breather wave. As this wave propagates, the waves develop a strong focusing of wave energy by having a small part of

the wave will "breathe" and use itself up at the cost of the neighbouring waves. The drawings in figure (2.3.2.5) help visualise what is occurring for this breather wave,
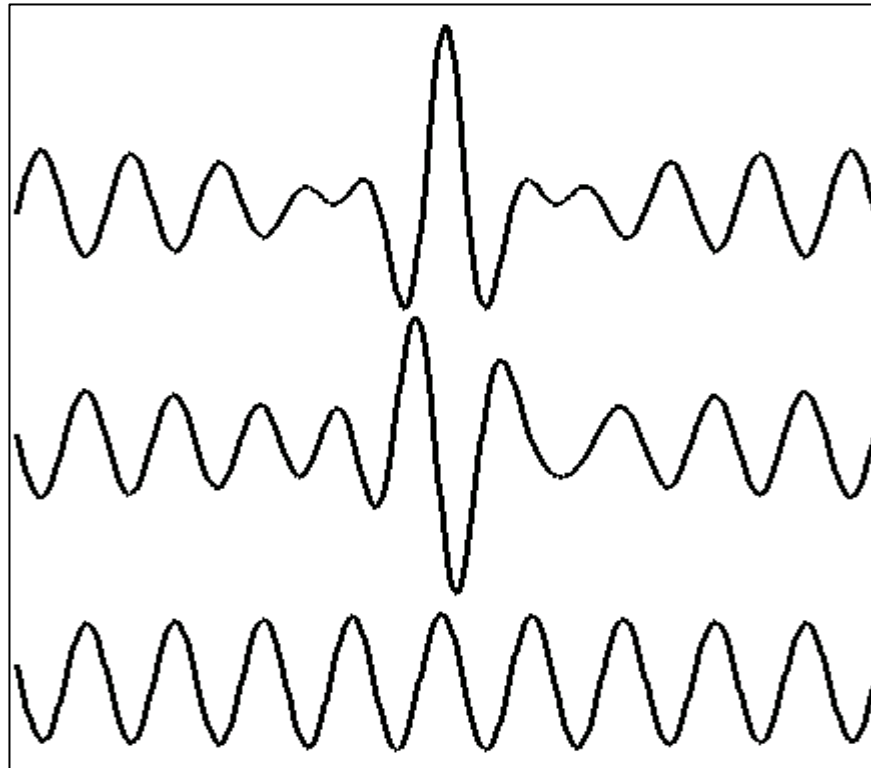
Fig 2.3.2.5 A three step drawing of how a "breather" wave acts.

A minor pitfall to this theory is that it only works though if the wave starts out as periodic in form. If the wave has varying periods or lengths then it becomes more complicated and unpredictable for one to predict a peak.

2.4 The sine-Gordon soliton

The previous two types of solitons can be denoted as particles when specific conditions are applied. Friction however causes trouble for these first two types of solitons. Under friction the

KdV soliton becomes smaller and longer.[11] As this occurs the soliton will look as if it is degrading. This change in form corresponds to an exponential law. The velocity and amplitude are proportional to,

$$e^{(-t/\tau)} \tag{2.4.1}$$

Where τ is the "lifetime" of the soliton whereas the length expands proportionally to,

$$e^{t/2\tau} \tag{2.4.2}$$

If the friction force (which τ is proportional to) is sufficiently large then the lifetime parameter τ will be negligible. A KdV soliton will also preserve its shape under a small amount of friction.

The group soliton is also quite temperamental under friction but its velocity remains unaffected and the length is proportional to,

$$e^{(t/\tau)} \tag{2.4.3}$$

The sine-Gordon soliton is very robust in comparison to the other two solitons. It will hold its shape under friction and will slow down and come to rest at a certain point rather than deform. The sin part of the equation is responsible for this stability and produces this topological nature.

The simplest form of this equation is[12],

$$v_{tt} - v_{xx} + \sin v = 0 \tag{2.4.4}$$

Where v_{tt} and v_{xx} are the partial differentials with respect to x and t. Due to the robust nature of this "soliton" many studies use it as a basis for their experiments. In most instances

[11] Ibid, A.T.Filippov, The Versatile Soliton (Springer Distributor, 2010)
[12] "Sine-Gordon Equation". Wolfram Mathworld [Online] Available from: http://mathworld.wolfram.com/Sine-GordonEquation.html [Accessed on 08/12/08]

Josephson junctions go hand in hand with the sine-Gordon soliton and this will be explored later on in this review.

2.5   Integrability

There are several tests that can be done to test for complete integrability. There is the numerical test, generalized symmetries, Hirota's direct method, and the Painlevé test. Each of these methods is examined in the following sub chapters. [13]

2.5.1   The Numerical Test

The KdV equation when let to evolve numerically produces solitons in one direction and radiation in the other. By solving a nonlinear ODE you can obtain a travelling wave solution. The amplitude will dictate the speed of the wave, so larger amplitude waves travel quicker then smaller amplitude waves. If two of these waves pass through each other/exchange identities then the existence of solitons is indicated. These numerical tests give hints that the equation is integrable.

2.5.2   Generalized Symmetries

Nonlinear evolution equations are well known to be related to infinite hierarchies of isospectral flows, associated with a single spectral problem. Isospectral is a term used in mathematics for two linear operators that are supposed to have the same spectrum (eigen values). These isospectral flows commute with the natural Lie bracket of vector fields.

13 Fordy, Allan P. Soliton Theory: a survey of results. (Manchester University Press, 1990)

2.5.3   Hirota's Direct Method

If the equation can be used to construct an N-soliton solution (arbitrary N) then Hirota's method can be used. This shows that the equation is capable of being integrable. A lot of Hirato's collaborators and others have used this method to good effect. The coupled KdV equation that Hirato and Satsuma discovered was a three soliton solution. This is the most powerful tool to use as a test.

2.5.4   The Painlevé test

The last of these mini tests is the Painlevé test. From the paper "Exact Linearisation of a Painlevé Transcendent" by M.J.Ablowitz and H.Segur, they suggest that the similarity solutions of some of the more well known soliton equations satisfy some particular second order differential equations which were discovered by Painlevé and Gambier between the years of 1893 and 1906. The scientists Ablowitz, Segur and Ramani came up with a method that would test these equations for this property.

The Painlevé test, Hirota's direct method and Generalised symmetries have all been used to calculate exact solubility with successful results.

2.6   Fractals

A fractal is a geometry that displays the property of self symmetry. These structures must be of the same type on all scales, though they need not have exactly the same structure at all scales.

In the 1960's, Benoit Mandelbrot[14], a French mathematician considered a simple idea, how long is the coast of Britain? Obviously this is a difficult thing to do practically, especially with a meter rule! But if one measured with a rule on hands and knees and then measured again by flight say, then the results obtained would be different.

In 1975 Mandelbrot came up with the word fractal, because he thought these figures would be fractured and broken up. With the use of a computer he finally saw what he was contemplating about. Fractals are very complex and a good property they have is that the resulting picture has surprising depth. So, if one is to zoom in on one of these pictures you would see the same amount of detail as before. A basic example of this is demonstrated by the Sierpinski triangles.

Other physical examples of fractals are the Internet, the coastline, clouds and even evolution.

2.6.1 The Magnetic Pendulum

The magnetic pendulum experiment consists of an iron sphere as the pendulum being placed in the centre of three magnets.[15] The magnets are coloured so that one can see the propagation of the pendulum. This is shown in figure (2.6.1.1).
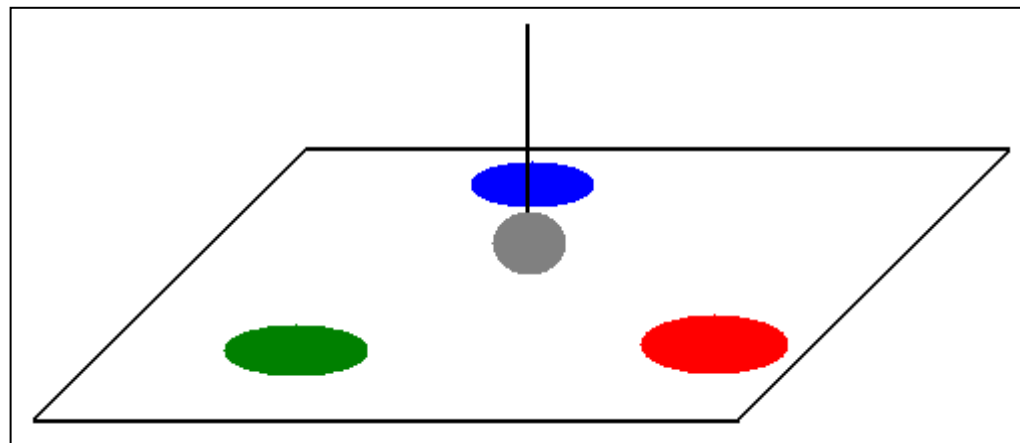
Figure (2.6.1.1) The Magnetic Pendulum Experimental Setup

[14]"Benoit Mandlebrot" [Online] NNDB, Available from: http://www.nndb.com/people/752/000022686/ [Accessed on 10/08/12]
[15] R. Müller, "The Magnetic Pendulum" Institute of Persuasive Computing, Switzerland. [Accessed on 15/10/10]

When the sphere is released from it's initial position (x_0, y_0) it will move towards the magnets. The pendulum will come to rest over one of the magnets because the system is dissipative due to the friction that arises. The system has proven to be quite sensitive, for example a small change to the initial starting point can result in the pendulum resting at a different magnet. The results of these are shown as maps, so if the pendulum starts at $(1, 0)$ and comes to rest at the green magnet then on the map $(1, 0)$ will be a denoted as a green point.

The model is described by a system of equations,

$$\ddot{x}(t) + R\dot{x}(t) + Cx(t) = \sum_{i=1}^{n} \frac{x_i - x(t)}{\left(\sqrt{(x_i - x(t))^2 + (y_i - y(t))^2 + d^2}\right)^3} \tag{2.6.1.1}$$

$$\ddot{y}(t) + R\dot{y}(t) + Cy(t) = \sum_{i=1}^{n} \frac{y_i - y(t)}{\left(\sqrt{(x_i - x(t))^2 + (y_i - y(t))^2 + d^2}\right)^3} \tag{2.6.1.2}$$

These represent a magnetic pendulum that is propagating over n magnets. All three of the magnets are on the same plane and the shortest distance between the magnet and sphere is d. The co-ordinates, x_i and y_i correspond to the magnets. R represents the friction force. A backward force is created when there is a movement to $(x(t), y(t))$, this pulls the pendulum back to the $(0, 0)$ condition. This force is modelled proportionally to the pendulum's amplitude. This is represented by the parameter C.

$$R = \frac{1}{5}, C = \frac{1}{2}, d = \frac{1}{4}. \tag{2.6.1.3}$$

The simulation uses a Verlet-Leapfrog integration that computes the system of differential equations. For each of the iterations the energy is calculated. The simulation is stopped when the energy is lower than the threshold E_T. The trajectories were then recorded for all virtual positions in a grid on the plane of the magnets. As said, each trajectory is coloured with respect to the magnet it rests at. The following fractal maps were produced by a Unix cluster using "Message Passing".
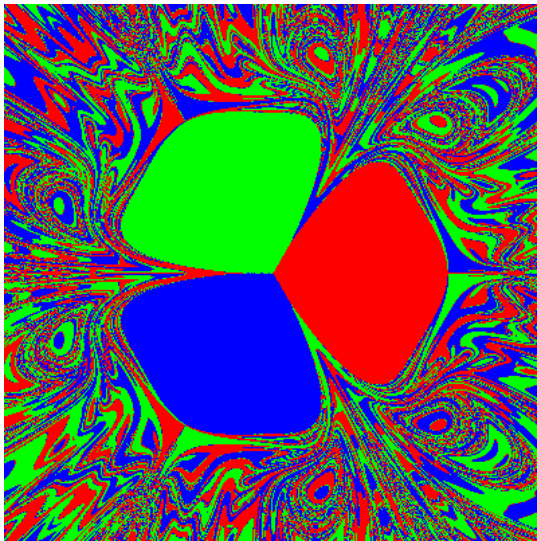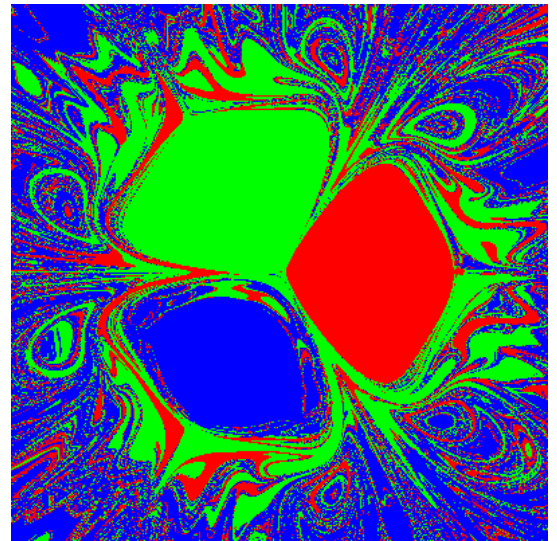

Figure (2.6.1.2) Sample 1.
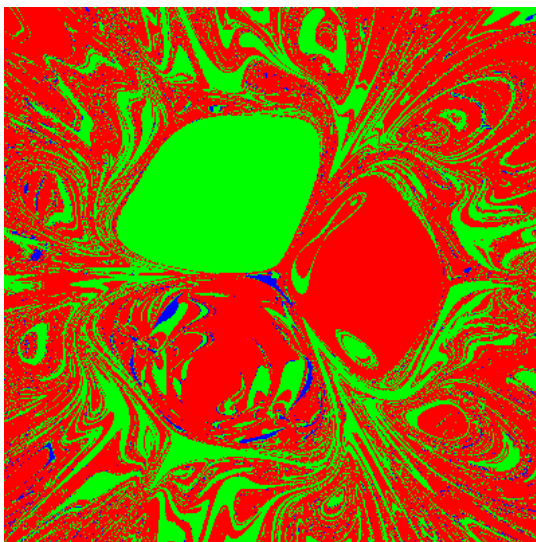

Figure (2.6.1.3) Sample 2.
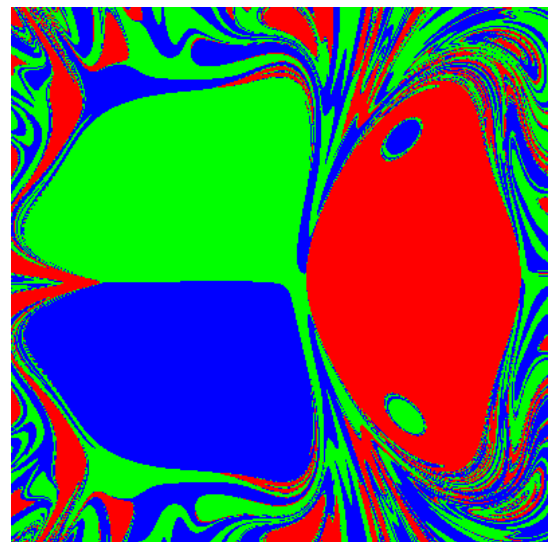

Figure (2.6.1.4) Sample 3.

Figure (2.6.1.5) Sample 4.

2.7   Josephson Junctions

2.7.1   Historical Background

A Josephson junction consists of two layers of a superconducting material surrounding a thin layer of a nonsuperconducting material. Josephson junctions were predicted by Brian Josephson in 1962 and were the subject for his Nobel Prize for Physics win in 1973. He had predicted that electrons that were paired could propagate from one of the superconducting layers to the other through the thin insulator. On either side of the insulator the wavefunctions interfere and this leads to a variety of quantum phenomena. His other prediction involved the form of the current and voltage relations for the junction.[16]

The first Josephson junction was made up from soft materials such as lead. These junctions degraded when thermally cycled between room temperature and an operating temperature, usually about 4 Kelvin.[17]

Josephson Junctions have some very important applications especially in instruments like SQUID's, which are quantum mechanical circuits. There is an effect known as the "Josephson Effect" where there is a current flow across two weakly coupled superconductors separated by a thin insulating barrier.

There are two equations which govern the Josephson junction. They are known as the superconducting phase evolution equation and the Josephson relation (weak-link current-phase).

16"What are Josephson Junctions? How Do They Work?" [Online] Scientific American, Available from: http://www.scientificamerican.com/article.cfm?id=what-are-josephson-juncti [Accessed on 26/ 8/ 09]

17   "Josephson Junctions" [Online] UCL, Available from: http://www.ee.ucl.ac.uk/~pwarburt/jj.htm [Accessed on 5/4/09]

These equations are respectively as follows:[18]

$$U(t) = u(t) = \frac{\hbar}{2e}\frac{\partial \phi}{\partial t}$$ (2.8.1.1)

$$I(t) = I_c \sin(\phi(t))$$ (2.8.1.2)

where U(t) is the voltage across the Josephson Junction and I(t) is the current. Φ(t) is the phase difference over the junction and I_c is the critical current of the junction (a constant). In a Josephson junction, the two superconductors which as stated before are separated by an insulating layer can experience the tunnelling of Cooper pairs of electrons as they travel through this. Cooper pair of electrons are a pair of weakly bounded electron in a superconductor. These were discovered by the American physicist Leon. N. Cooper and they also have the properties shared by bosons and therefore reside together in the groundstate.[19] A wavefunction can represent the Cooper pairs on each side of the junction and this wavefunction is similar to that of a free particle wavefunction. There are two effects in a Josephson junction, AC and DC.

The DC Josephson effect has a current which is proportional to the wavefunctions difference in phase that can flow in the junction with an absence of voltage. It occurs with the absence of an external electromagnetic field. The value of this current normally takes the value between $-I_c$ and I_c.

In the AC effect the junction oscillates with a frequency that is proportional to the voltage across the junction. The current will obviously be an AC current and will have an amplitude of I_c and its frequency is $(2e/h) \cdot U_{DC}$. The current drive I_{ext} becomes,

$$I_{ext} = C_j \frac{dv}{dt} + I_j \sin \phi + \frac{V}{R}$$ (2.8.1.3)

This shows that a Josephson junction is a good voltage-to-frequency converter. Frequencies these days can be measured very accurately and because of this the Josephson junction is the standard measure of voltage.

---

18 "Josephson Effect" [Online] Wikipedia http://en.wikipedia.org/wiki/Josephson_effect [Accessed on 10/8/09] Original Source - Barone A, Paterno G. *Physics and Applications of the Josephson Effect*. (New York: JohnWiley & Sons; 1982)

19 The Free Dictionary, "Cooper Pairs", [Online] Farlex, Available from: http://www.thefreedictionary.com/Cooper+pair [Accessed on 5/4/09]

The wavefunction that describes a Cooper pair of electrons in a superconductor is exponential as is the case of the free particle wavefunction. Actually, all Cooper pairs in a superconductor can be described by a single wavefunction in the absence of voltage. This is because all of the pairs have the same phase and are therefore coherent.

Quantum mechanical tunnelling can occur for the Cooper pairs without separating the pairs when they are in the two superconductors which are separated by the nano thick layer of insulator. To explain what happens in the DC effect, Clarke,[20] envisions the pairs on both sides of the superconductors penetrating the insulating region and "locking together" in phase. If these conditions are obeyed then a current will flow through the junction even if there is an absence of an applied voltage, this is the DC Josephson junction effect.

There are many devices based upon the characteristics of a Josephson junction as they are very valuable in high speed circuits. These junctions can be made to switch in times of a few picoseconds. A Josephson junction has a low power dissipation making it useful in high-density computer circuits where the resistive heating limits the applicability of normal, conventional switches.[21]

As mentioned before Josephson junctions are used in the device called a SQUID. The image in figure (2.8.1.1) shows what one looks like.

[20] J.Clarke. "SQUIDs", (01/08/94)
[21] "Josephson Devices", [Online] HyperPhysics, Available from: http://hyperphysics.phy-astr.gsu.edu/Hbase/solids/squid.html#c3 [Accessed on 10/5/09]
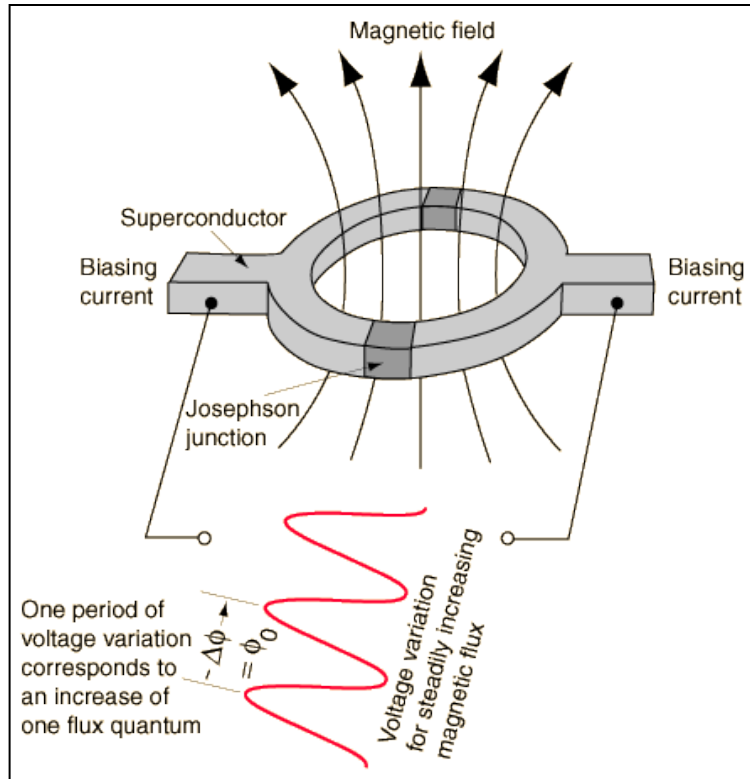
Figure (2.8.1.1) A Schematic for a SQUID machine.

This equipment is sensitive to the total magnetic field that passes through the loop. The voltage that is measured across the device is very strongly correlated to the total magnetic field around the loop. SQUID's are used for MRI's, (magnetic resonance imaging). SQUID magnetometers are used in geological research in particular detecting the remains of changes in the Earth's field in rocks.[22]

Superconducting Tunnel Junction Detectors (STJ's) are used in astronomy and astrophysics as they are devices that have a very good effectiveness across the spectrum from ultraviolet to infrared. They also go into x-rays. These have also been used in the William Herschel Telescope located in the Canary Islands.

---

22   "SQUID Magnetometer", [Online] HyperPhysics, Available from: http://hyperphysics.phy-astr.gsu.edu/Hbase/solids/squid.html [Accessed on 15/5/09]

2.8   Shape Waves in 2D Josephson Junctions[23]

The (1+1)D sine-Gordon (SG) model is fully integrable and as well as this has both soliton and breather solutions. The (1+1)D SG model represents a fluxon in a Josephson Junction. This is suitable for a 1D system but what about realistic situations? For a 2D Josephson Junction, one has to use the (2+1)D SG equation. Unfortunately this is not fully integrable like the (1+1)D sine-Gordon model.

In the (2+1)D sine-Gordon equation there are exact solutions that describe the movement of excitations of an arbitrary shape along a Josephson vortex. A useful analogy of this is to think of two tables joined together and that when they are moving in the positive x direction. The excitation will move in the y direction. This excitation can be represented as a marble propagating along the crease of the two tables. Figure (2.8.1) shows this idea.
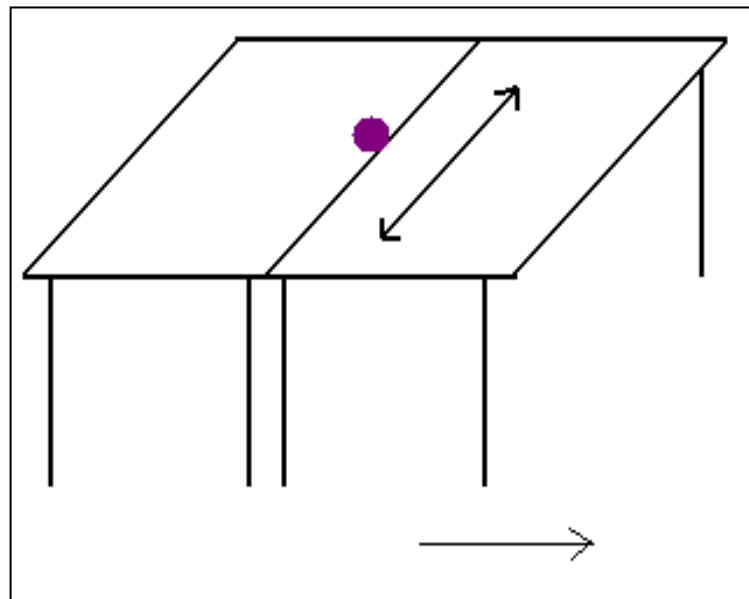

Figure (2,8.1) - The Shape Wave Analogy.

The marble is able to freely propagate in the y direction (between the two tables) whilst the table is moving in the x direction. These excitations have useful properties, for example the excitation could have a transmission of pulses of electromagnetic radiation which can be helpful to the transmission of information in certain Josephson devices (high frequency in particular).

23 D.R. Gulevich, F.V. Kusmartsev, S. Savel'ev, V.A. Yampol'skii and Franco Nori, "Shape and Wobbling Wave Excitations in 2D Josephson Junctions: exact solutions of 2+1 sine-Gordon model" (15/8/08)

Obviously these excitations occur as demonstrated in the previous diagrams (on an arbitrary shape fluxon or Josephson Vortex).

$$U_{tt} - U_{xx} - U_{yy} + \sin U = 0 \qquad (2.8.1)$$

This is the 2D sine-Gordon equation.[24] In this equation the quantity U is known as the superconducting phase difference across the Josephson Junction.

To obtain results/solutions to this equation one has to do a Lorentz transform to the stationary 2D sine-Gordon equation.

$$U(x, y, t) = 4\tanh^{-1} e^{[y - f(x \pm t)]} \qquad (2.8.2)$$

This equation gives a general set of solutions and describes various shapes for an excitation of a certain shape. This is because of the arbitrariness of f. One study chose to use the a value of f as

$$f = 8/\cosh[(x - x_0 \pm t)/2] \qquad (2.8.3)$$

as it is localized in a finite area. With this in mind for f, equation (2.8.3) gives arise to a shape wave (excitation) that sustains it's shape when moving, also known as a solitary wave.

For the shape wave to be in the form of a soliton then another aspect must be satisfied, this being that the "waves" must remain intact after a collision. So through the use of the function:

$$U(x, y, t) = 4\tanh^{-1} e^{[y - f(x + t) \pm f(x - t)]} \qquad (2.8.4)$$

24 D.R.Gulevich, F.V. Kusmartsev, Sergey Savel'ev, V.A. Yampol'skii and Franco Nori. "Shape Waves in 2D Josephson Junctions: Exact Solutions and Time Dilation" (18/9/08)

When $t \to -\infty$, it describes two solitary shape waves heading towards one another (when the ±
is a minus) or a solitary wave and it's "anti partner" (when the ± is a plus). Due to the fact that
when $|f'(x + t)f'(x - t)| \ll 1$ for all values of x and t then one can only approximately satisfy
1. This leads to the conclusion that some waves may lose their form after conclusion. This is true
for solitary waves of large amplitudes as their interactions are destructive even though they
retain form up to this point. At the point of interaction the waves experience annihilation and
hence dissipate the energy away from the vortex.

On the other hand smaller amplitude waves that satisfy $|f'(x + t)f'(x - t)| \ll 1$ only dissipate
smaller amounts of energy and so keep their form after they interact, thus being solitons.

The images below show a simulation of 2 large amplitude "solitary wave" shape waves and
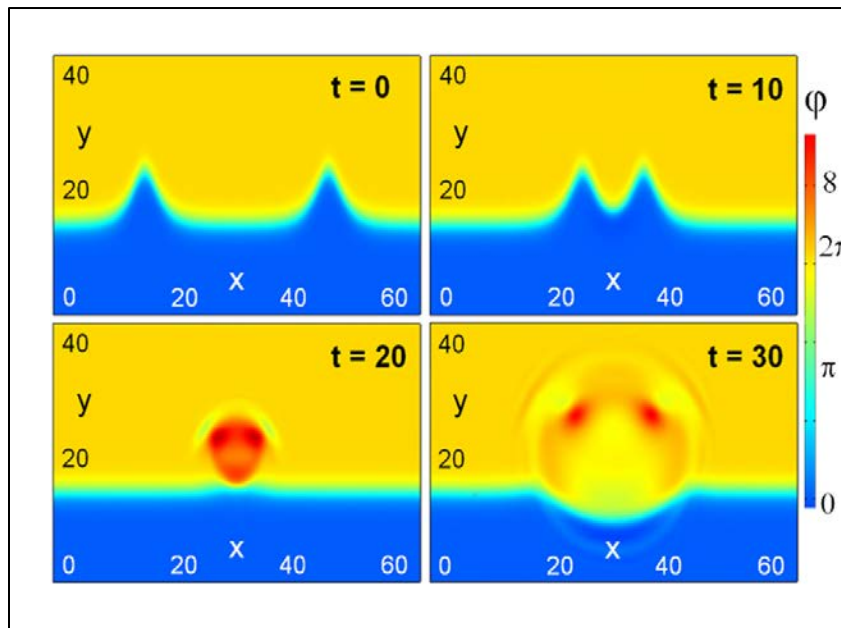what happens when they interact.

Figure (2.8.2) Two Large Amplitude Solitary Waves Interacting.

2.9 Linear Junctions

2.9.1 Zero field Steps

From many previous experiments it has been found that fluxon motion are so called zero-filed steps (ZFS's) at voltages, $V_n = n\phi_0 \bar{c}/L$. These appear in the I-V curves of a junction. This phenomenon was discovered in 1973 by Fulton and Dynes and it is they who suggested that the number of fluxons oscillating in the junction is equal to the step index n. If a fluxon arrives at a junction's boundary then it undergoes reflection into an anti-fluxon which will propagate in the opposite direction to which it was travelling as a fluxon. The reason it propagates this way is due to the bias current.[25]

Solitons in a long Josephson junction have a quantized magnetic flux known as $\Phi_0 = 2 \times 10^{-15} Vs$. A soliton is coined the term fluxon when in a Josephson junction due to this flux. One of the earliest ways of seeing fluxon motion was to examine the current-voltage characteristics of the junction. The fluxons are shown by current singularities that appear. In a study by Gelubov, Ustinov and Serpuchenko they use a normalised sine-Gordon equation,

$$\varphi_{xx} - \varphi_{tt} = f(x)sin\varphi + \alpha\varphi_t + \gamma \qquad (2.9.1.1)$$

The lattice which is inhomogenous can be approximated by the following function,

$$f(x) = 1 + f_0 \sum_{n=1}^{N} \delta(x - an - x_0) \qquad (2.9.1.2)$$

---

[25] Ustinov, A.V, "Solitons in Josephson Junctions – Basic model and fluxon properties", (University Erlangen-Nürnberg, 1998)

Where the parameter a is the lattice spacing normalised to λ_J. The following condition has to be satisfied for resonance to occur between the soliton and plasma mode,

$$m\frac{2\pi\beta}{l} = \omega_{PL}$$

(2.9.1.3)

Where β is the velocity of the soliton normalised to the swihart velocity $\bar{c}$, m is the resonance number and l is the length of the junction normalised to λ_J. These conditions are also valid in an annular junction. By examining when the plasma waves frequency ω_{PL}, are not equal to unity and also depend upon the parameters α and β. It was found that the resonance appeared at certain values of β,

$$\beta_m = \left[(1 - 2l/ma)^2 + (l/\pi m)^2\right]^{1/2},$$

(2.9.1.4)

Where,

$$m < (2l/a)\left(1 - \beta_m^2\right)^{-1},$$

(2.9.1.5)

And

$$\beta_m < 1.$$

(2.9.1.6)

The first resonance to occur at voltages, $V_m = \phi\beta_m\bar{c}$ is known as the first zero field step. These plasma waves occur at the inhomogenous parts of the junction. This could be at the imperfect junction boundaries or at the tunnel barrier.

 In a paper published in 1982 the ZFS's are described as,

"These branches named anomalous current singularities or zero field steps are explained as the d.c.-manifestation of the oscillatory motion of N solitions in the tunnelling barrier"[26]

The study by Ustinov et al[27], went on to confirm these theories by experimentation. The samples used were Nb-NbO$_x$-Pb and they were linear overlapping junctions. The size of these junctions was approximately 500x20 µm^2. The inhomogeneities were formed by silicon oxide (SiO) film islands on a nicrobium (Nb) film. This sample is then evaporated and patterned. Then the Pb layer was oxidised and evaporated also. The SiO layer was 800Å in thickness and the islands were 10x20µm^2 in dimensions. To keep the experiment reliable and true the same substrate was used for all four control junctions.

2.9.2 Flux Cloning

Fluxons in Josephson junctions will clone themselves when certain conditions are met.[28] This is normally due to the initial vortex coming into contact to an additional Josephson transmission line. Figure (2.9.2.1) illustrates an example of such a geometry which has been shown to produce cloning,
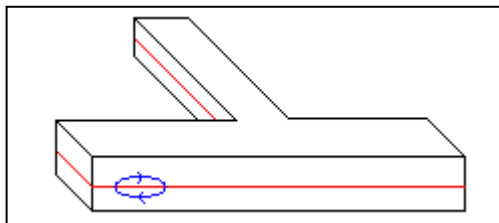

Figure (2.9.2.1) A Representation of a Fluxon in a T-junction.

[26] P.S.Lomdahl, 0.H.Soerensen and P.L.Christiansen "Soliton Dynamics and Zero Field Steps in Josephson Tunnel Junctions." (26/10/81).

[27] I.V. Vernik, N. Lazarides, M.P. Sorensen, A.V. Ustinov, N.F. Pederson and V.A. Oboznov (5/2/1996).

[28] D.R.Gulevich, F.V.Kusmartsev "Flux Cloning in Josephson Transmission Lines" (07/07/06).

In the case of a T-junction one can see that the AJTL is located in the middle of the main Josephson transmission line (MJTL) and extends outwards perpendicularly. The paper, Fluxon Cloning in Joesphson Transmission Lines by D. R.Gulevich and F. V. Kusmartsev shows success in cloning a sine-Gordon fluxon in a T-shaped junction. The author of this research project also attempted using a fluxon based on the NLSE which proved to be more unstable then the SG fluxon. In fact when this fluxon came into contact with the boundaries of the T-junction the NLSE completely dissipated.

2.9.3   Stacked junctions as Josephson Superlattices

A lot of work has been put into the experimental and theoretical idea fluxons in coupled JTL's. Due to the discovery of the intrinsic Josephson effect in some high temperature superconductors it was convincingly shown that they are natural superlattices of Josephson junctions that are formed on the atomic structure scale.

The junctions are densely packed due to the spatial period of the superlattice being only 15Å. A typical superconductor would be $Ba_2Sr_2Cu_2O_{8+y}$ (BSCCO). A copper oxide bilayer about as thin as 3Å form a superconducting electrode. This is separated by the non conducting BiO.

 Josephson junctions that have many layers naturally have complex dynamics. One now looks at stacked JTL's which are formed by a few layers. The simplest case of this is of the two stacked junctions and is illustrated in Figure (2.9.3.1).
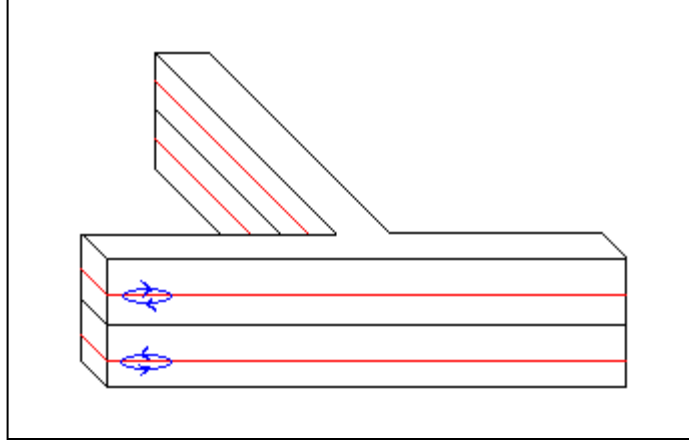
Figure (2.9.3.1) A Stacked T-Junction Superlattice.

According to the model derived by Sakai for the arbitrary strong coupling between junctions, they can be described by a system of coupled perturbed sine-Gordon equations,

$$\frac{1}{1-S^2}u_{xx}^A - u_{tt}^A = \sin u^A + \alpha u_{tt}^A + \gamma^A + \frac{S}{1-S^2}u_{xx}^B \qquad (2.9.3.1)$$

And

$$\frac{1}{1-S^2}u_{xx}^B - u_{tt}^B = \sin u^B + \alpha u_{tt}^B + \gamma^B + \frac{S}{1-S^2}u_{xx}^A \qquad (2.9.3.2)$$

Here $u^A(x,t)$ and $u^B(x,t)$ are the superconducting phase differences across the stacked junctions A and B respectively. The quantities of γ^A and γ^B are bias currents and from the tunnel barrier thickness d, the middle electrode thickness t and the thickness of the top and bottom electrodes t_e the coupling coefficient S can be calculated. The coefficient S has the form of,

$$-[(d/\lambda_L + \coth(t/\lambda_L) + \coth(t_e/\lambda_L)) \sinh(t/\lambda_L)]^{-1} \qquad (2.9.3.3)$$

If the coupling parameter S has $t \gg \lambda_L$ then it will vanish. The parameter S, is associated with the screening currents in superconducting electrodes. These are shared by the fluxons belonging to different layers. It has been shown experimentally that the value for S lies between -0.2 to -0.9.

The coupling equations give rise to in phase and out of phase oscillations within the two junctions. The velocities are respectively as follows:

$$\bar{c}_- = \frac{\bar{c}}{\sqrt{1-S}} \qquad (2.9.3.4)$$

And,
$$\bar{c}_+ = \frac{\bar{c}}{\sqrt{1+S}} \qquad (2.9.3.5)$$

The velocities were measured experimentally for the double junction stacks with a different thickness for d of the common superconducting layer. In the experiment, as d decreased the coupling increased and therefore increased the difference between $\bar{c}_-$ and $\bar{c}_+$. The experimental data seems to be in agreement with the theory. There are different configurations possible for fluxon chains in a two layered junction. One would be a configuration or repulsion of fluxons and the second would be the mutual attraction between fluxons in different layers. Fluxon configurations in a two layered junction can be written as [N|M], where N is the number of fluxons in one of the LJJ and M is the number of fluxons in the other LJJ. An anti-soliton can be written as (N, M< 0).[29]

---

[29] Ibid. Ustinov, A.V, "Solitons in Josephson Junctions" (1998)

2.10 Annular Junctions

2.10.1 Uses of Annular junctions

Superconductors are better used than semiconductors as radiation detectors due to the energy
gaps, typically for a superconductor it would be of 1meV whereas a semiconductor will be
roughly 1eV.

Annular junctions have been used as a promising start to become radiation detectors. The
reason annular Josephson junctions were suggested as a better geometry for such detectors
was due to being able to reduce the Josephson effect and also Fiske resonations. Once the
external magnetic field has been removed after a successful entrapment of a single fluxon there
is no need for a parallel magnetic field to be active as the detector works away. This is an
improvement upon the previously suggested quartic or diamond shaped junction. One
particular experiment looked at a set of junctions with differing internal diameters inside a chip.

In this case a trilayer of Nb/Al-AlO$_x$/Nb is used as the main part of the junction. The S1 substrate
is formed of Si wafer. The insulator was composed of SiO and is surrounded by anodized Nb
strips. The experiment commenced in an atmosphere of argon with a DC magnetron set at a
rate of 1.48nm/s. The trilayer was composed of 200nm Nb, 10nm Al and finally 100nm Nb. The
tunnel barrier was created by leaving the Al film in the presence of Oxygen at a pressure of
3.5x10^{4}Pa for t = 1800s. The authors used Reactive Ion Etching (RIE) in a CF$_4$ plasma for the Nb
layers whilst using a wet etching of Al. A photoresist layer was made with the geometry of the
junction. Then RIE was used upon this creating a top electrode with a hole. The photoresist layer
provided an anodised surrounding which would then go on to be replaced with two SiO
insulation layers. These insulation layers were of 400nm in thickness.

There were two proposed models for the junctions in this experiment however only one of the
model's experimental results were presented. Type 1 had the SiO insulating layers cover the
internal and exterior junction boundaries and had a hole appearing in the middle of the

junction. Type 2 was simililar in that it had a SiO film covering the junction boundaries but it had a wiring made through a small area (4 x 3 μm^2). This set up also had an integrated Au control line attached to the junction. The first results presented by the group were from the first type of junction. Type 1 has an external diameter of 16μm and an internal diameter of 7.5μm. By using a copper Helmholtz coil a parallel magnetic field was present. After a single magnetic fluxon was trapped in the junction the external magnetic field was switched off. From this, the first Fiske step (resonance) appeared at V_{f1}=550 $\pm$22μV. Two subsequent Fiske steps were detected also although their resonance peaks were negligible compared to that of the first peak. This complies with the theory that states with the external magnetic field absent only a Fiske step of V_{n1} (k=n) will have a prolific amplitude.

Following on from these discoveries further research was undertaken to explore this unique ability the AJJ exhibits once a fluxon is trapped. One significant change was to the geometry of the junction. Instead of only the top and bottom electrodes a third geometry was added. This adds a control current which is where the magnetic field is created. The AJJ was made on a Sapphire/Molybdenum/SiO substrate and had an external diameter of 100μm and an internal diameter of 60μm. The experiment consisted of each terminal set at an angle of α=90°. This new geometry was proposed to theoretically suppresses the Josesphson effect in two ways however, the results did not prove this as they were not able to achieve the balance between injecting a current into the system without heating the Aluminium wiring. There was also an unsuccessful attempt in trapping magnetic flux quanta by a cooling process.

There was success in trapping multiple fluxons when an external parallel magnetic field was applied to the system. This was set at a value above the critical value of the base aluminium electrode but below that of the top electrode. An I-V characteristic which had suppressed Fiske resonances and I_c was obtained once the external magnetic field had been turned off, in this case in particular, twelve fluxons were trapped. A pulse spectrum was calculated by a ^{55}Fe X ray

source and the energy resolution was approximately 100eV for the K_α line for the top electrode.[30]

The annular Josephson junction has several applications. One such instance is a Josephson fluxon pump. This implement is aimed to develop a series of fluxons without the use of an external magnetic field which is prevalent in the research outlined in this thesis.

In the paper "Josephson fluxon pump: Theoretical aspects and experimental implementation of elementary flux quanta generator with BSCCO" there are two models suggested and they are primarily formed of an annular junction with an additional Josephson transmission line attached to it in different positions. These are named aptly the σ pump junction and T-pump junction.

A singular fluxon will be trapped in the annular part of the pump and then left to oscillate toward the additional transmission line (ATL). At this point of contact the fluxon will clone a new fluxon that will oscillate in the T junction. The "old" fluxon will then continue around the AJJ and then come into contact with the (ATL) and form another new fluxon. Importantly this process happens when a driving current is switched on. The critical current of the system is given by,

$$\gamma_c^T = \frac{4W}{(2W_0 + W)} \tag{2.10.1.1}$$

Where W and W_0 correspond to the widths of the JTL and the AJJ respectively.

There is however some problems with the T junction model when trying to apply it on a larger scale. This is because the main vortex may experience energy losses when it comes into contact with the JTL. The extra branch in the σ-pump case is situated as a smooth addition to the model rather than the abrupt JTL in the T-pump. This is why the σ is preferred geometry out of the two

---

[30] M.P. Lisitskii, G..Ammendola, D.V. Balashov, A. Barone, R. Cristiano, E. Esposito, L. Frunzio, V.G. Gubankov, C. Nappi. S.Pagano, L.Parlato, G.Peluso, G.Pepe. "Annular Josephson Junctions for Radiation Detectiton: Fabrication and Investigation of the Magnetic Behaviour" (2000)

models as it has a better application to the larger scale. Using (EQN number) the potential energy of the system can be calculated to be,

$$V(x_0) = 8W(x_0) - \gamma(\Delta R + W/2)2\pi x_0 \qquad (2.10.1.2)$$

The fluxon used is of the sine-Gordon soliton form and is described by (EQN number) with the following Neumann boundary conditions applied,

T pump - $\nabla\varphi.n = 0$ for the internal boundary and,

$\gamma\nabla R$ on the external boundary.

σ pump - $\nabla\varphi.n = 0$ on the internal boundary and,

$\gamma(\Delta R + W/2)$ on the external boundary.

For the additional JTL's boundary the following condition was applied,

$$\vec{n}\nabla\varphi|_{\partial\Omega_{JTL}} = \gamma W/2$$

The simulations were computed with COMSOL multiphysics and showed that in both cases a new fluxon was produced when the main fluxon came into contact with the JTL. The current for the systems was set at $\gamma = 0.3$ and the damping parameter $\alpha = 0.1$.

The research then goes on to examine the Current-Voltage characteristics of the two pumps, theoretically and experimentally. The numerical results were calculated for both pumps, with the T-pump showing a hysteresis relationship while the σ-pump did not show this kind of relationship.

The T-pump is capable of producing both fluxons and antifluxons due to the fact that it can have a negative driving current applied to it. The pump is to be experimentally made a reality by the use of a BSCCO crystal.

It has also been proposed that these pumps can function as a set of multilayered junctions. The pumps if they were to be stacked could produce multiple fluxon trains propagating in parallel.[31]

2.11 Quantum Properties of Solitons and Potential Wells

2.11.1 Quantum Solitons

When the climate changes and we enter a new season, in particular the autumn/winter changeover, we see birds migrate. They tend to fly in the shape of a V. The reason they fly in this shape is so that the stronger birds at the front take the brunt of the force and therefore make it easier for the weaker birds to keep up with the pack.

Light, meaning photons, can replicate this trick and travel over intercontinental distances in optical fibers. In the fibers the photons travel in the form of solitons. These pulses rely on the refractive index being dependent on wavelength and intensity as each pulse composes of a different wavelength. The blue wavelength will travel at the front and the red wavelength will travel at the back. This dispersion is known as a chirp.

The photons use another effect of the fiber and that's it's nonlinearity. This comes from the refractive index which also depends on the intensity. The peak of a soliton will experience a higher refractive index and is so delayed with respect to it's "wings". This dispersion gives rise to a chirp which then opposes the chirp created by the dispersion caused by the wavelength. This arrangement occurs for solitons of a specific shape. Even though these pulses can travel for distances without loss of shape there is no guarantee that the information has been transmitted faithfully. The pulse has to make sure it has to combat any sort of spreading and also noise. This noise comes from the imperfections of the fiber (this may be from the random fluctuations of the laser generating the pulse or strains in the fiber). These factors can be improved upon

---

[31] D.R. Gulevich, M. Gaifullin, O.E. Kusmartseva, F.V. Kusmartsev and K. Hirata "Josephson Fluxon Pump:Theoretical aspects and Experimental Implementation of Elementary Flux Quanta Generator with BSCCO" (13/06/12).

technical improvements but one factor that cannot be cancelled out by this is the quantum mechanical properties of light. Quantum noise arises from the uncertainty principle because there is an incompatibility between the generation and detection processes for light pulses. Solitons are made up of the purest light possible – coherent light, from a laser. The E field of a coherent state has a non-zero expectation value that oscillates sinusoidally in time just like a classical oscillating field.

A photodiode will detect solitons and hence measures the energy and also counts the number of photons N in the soliton. The quantum eigenstates corresponding to these eigenvalues are known as number states. Unfortunately a coherent state is not an eigenstate of the photo-number operator and so must be expressed as a superposition of all photon-number states. This means that the most likely outcome detected would be N when a coherent soliton pulse arrives at the photodiode. In general though a different result will be found each time a measurement is made. This uncertainty which is found in experiments is known as quantum noise.
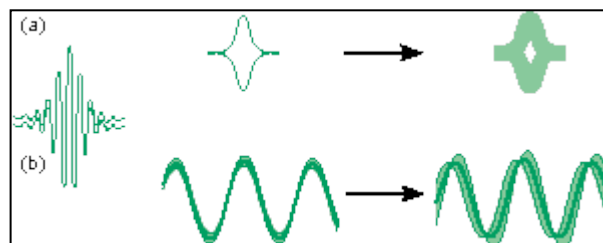
Figure (2.11.1.1) The noise associated with the waves.

This noise arises from the laser emission and light detection involving 2 different observables, the energy of a pulse and an amplitude of the E field. These 2 observables have no common eigenstates. Stopping this noise is a tricky business and in the 1990's a large amount of time went into trying to quash quantum noise for once and for all. The thought at the time was to investigate a property of light called squeezing. This "squeezing" is linked to the uncertainty principle.

Take this for example:

$$\Delta x \Delta p > h/2 \qquad\qquad (2.11.1.1)$$

where Δx is the uncertainty in position, Δp is the uncertainty of momentum and h is plank's constant. A similar equation exists for photon number n and phase Φ in an electromagnetic field. For this case the uncertainty relation is known as:

$$\Delta n \Delta \Phi = 1 \qquad\qquad (2.11.1.2)$$

In the uncertainty principle when $\Delta x \Delta p = h/2$ we have a state where there is no excessive noise. This is known as a minimum uncertainty state. A coherent state is a particular kind of this state in which the uncertainties in a pair of conjugates are equal, so $\Delta n \Delta \Phi = 1$.

Squeezing enables one to lower the uncertainty in one variable and raise the uncertainty in the other variable while keeping the equality satisfied (e.g. $\Delta n < 1$ and $\Delta \Phi > 1$ but $\Delta n \Delta \Phi = 1$). This was achieved in 1985 by Dick Slusher and co workers in the U.S. Soliton squeezing was first demonstrated experimentally in 1991 by Michael Rosenbluh and Bob Shelby at IBM in San Jose. In this experiment Rosenbluh and Shelby directed their efforts on squeezing the in-phase quadrature of the soliton and not the photon number. The quadrature of the soliton is the sine or cosine component and is measured by combining the soliton with a stronger reference beam called a local oscillator in an interference experiment.[32]

---

[32] Quantum Solitons, [Online] Available from: http://physicsworld.com/cws/article/print/1285 [Accessed on 11/1108]

2.11.2 Qubits

Josephson junctions give rise to qubits. Various JJ's have been tested as qubits successfully. Longer JJ's have also been hypothesized to implement qubits albeit that they have quantized vortices if supercurrent at present. Vortices have also been shown to have the phenomenon quantum tunnelling applied to them at milli-Kelvin temperatures as well as having macroscopic quantum properties.[33] Various Josephson junctions have been used to construct different types of qubits such as charge, phase and flux qubits.

The bit is a basic unit for information processing in a computer. This unit can be in either state 0 or 1. As one would expect the basic unit in quantum computing is the quantum bit, known as qubit for short. The qubit is similar to the bit in that it can be in one of two states. However it is written in the following form $|0\rangle$ and $|1\rangle$.

The qubit differs from the classical bit as it can also be in a superposition state. The superposition state, $|\varphi\rangle$ can be written as,

$$|\varphi\rangle = \alpha|0\rangle + \beta|1\rangle \qquad\qquad (2.11.2.1)$$

Here, α and β are complex numbers.

Even though a qubit can exist in these superposition states, when a measurement is taken it will not be found here. It will be located in either the $|0\rangle$ or $|1\rangle$ state. To calculate the probability of locating the qubit in either state one must find the modulus squared of parameters α and β. So,

$|\alpha|^2$: Tells us the probability of finding $|\varphi\rangle$ in state $|0\rangle$ and,

$|\beta|^2$: Tells us the probability of finding $|\varphi\rangle$ in state $|1\rangle$.

These probabilities must be equal to one when summed,

---

[33]Ibid. A.N. Price, A. Kemp, D.R. Gulevich, F.V. Kusmartsev and A.V. Ustinov. "Vortex Qubit Based on an Annular Josephson JunctionContaining a Microshort" (03/07/08).

$$|\alpha|^2 + |\beta|^2 = 1 \qquad (2.11.2.3)$$

In an event that has N results and one can denote the probability of finding i, as p_i, then the summation of these can be written as,

$$\sum_{i=1}^{N} p_i = p_1 + p_2 + \cdots + p_N = 1 \qquad (2.11.2.4)$$

Thus normalizing the probability.[34]

2.11.3 Qubit Chips

In 2007, two research teams in America reported that they were able to form for the first time a chip-based example of a quantum bus. A quantum bus is a term used for a device that can either combine two qubits into a superposition state or move the information between qubits in a quantum computer. These results were said to be a main stepping stone to the formation of a full scale quantum computer.

These two teams composed similar "buses", in the shape of an undulating curve of wire between two loops of aluminium. The team located at the National Institute of Standards and Technology in Boulder, Colorado have managed to store a photon for about a microsecond before it is then absorbed by a second qubit. The leader Raymond Simmonds said of the experiment that it is,

---

[34] D.McMahon "Quantum Computing Explained" (John Wiley and Sons Inc, 2008).

"sort of like having a guitar string and plucking it,"

And that the result yielded is,

" is a basic memory circuit that can transfer a quantum state from one qubit to another".

The other research group located in the Department of Applied Physics at Yale University came up with a system that had a longer wire and caused the single quantum state to switch between two qubits. By creating this flip flop effect with many qubits one can create a large entanglement, which is what causes a quantum computer to run.

By constructing a bus, researchers hope that they will be able to connect more qubits together as they would then be allowed to communicate directly with each other rather then just with their nearest neighbour.[35]

2.11.4 Particles in a Double Potential Well

A double well potential is created when a fluxon, for example interacts with a microshort and an external magnetic field is applied. Perturbation theory can be used to gain an expression for the field induced double well potential and also the depinning current as a function of magnetic field strength.

The double potential well has been used in the past to provide understanding in a variety of areas. One example occurs in Mass Spectrometry where it was noted that the double well

---

[35] "Quantum Chip Sends Information by Bus" [Online] Scientific American, Available from http://www.scientificamerican.com/article.cfm?id=quantum-chip-bus-information [Acessed on 15/5/10]

potential model would help explore ion-molecule reactions.[36] These reactions are key in chemistry and for supporting analytical mass spectrometric characterization.

There are numerous forms of a double well potential and one example can be described by the following equation.

$$u(x) = -Ax^2 + Bx^4 \qquad\qquad (2.11.4.1)$$

This particular form has many applications and is used in the fields of quantum mechanics, field theory and statistical physics. This type of double potential well has no exact analytical results, though it was found that with a certain choice of parameters for the following potential,

$$V(x) = V_0(A\cosh\alpha x - 1)^2 \qquad (0 < A < 1) \qquad\qquad (2.11.4.2)$$

that exact eigenvalues are present.[37]

Double potential wells can be tuned according to which parameters the "experiment" requires. Figure (2.11.4.1) demonstrates an example of how a magnetic field can be tuned. The following graph was produced show how tuneable the magnetic field can be.[38]

[36] H.Konwent. P.Machnikowski and A. Radoszt. "A certain Double Well Potential Related to SU(2) Symmetry" (1995).

[37] J.I. Brauman, "Some Historical Background on the Double Well Potential Model" (1995).

[38] Ibid . A.N. Price, A. Kemp, D.R. Gulevich, F.V. Kusmartsev and A.V. Ustinov. "Vortex Qubit Based on an Annular Josephson JunctionContaining a Microshort" (03/07/08).
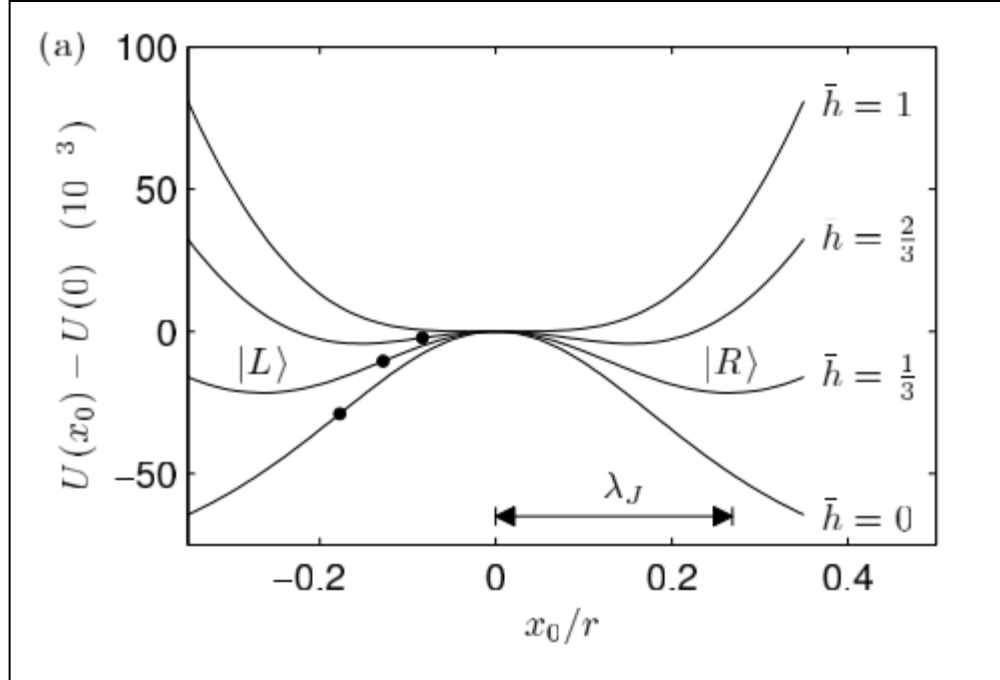
Figure (2.11.4.1) This graph shows how different values of $\bar{h}$ can be applied to a double well potential to manage the barrier height that occurs.

Figure (2.11.1) shows the 4 different plots for the four different magnetic fields between the values of $0 < \bar{h} < 1$, where $\bar{h}$ corresponds to the magnetic field and has the form,

$$\bar{h} \equiv \frac{h\pi\text{sech}(\pi/2r)}{\mu r^2} \qquad (2.11.4.3)$$

As the magnetic field is in increased the potential barrier falls for the microshort and the separation between $|L\rangle$ and $|R\rangle$ decreases. The black dots represent the point where the vortex "escapes" from the left well and passes through the microshort. The critical current is known as the amount of bias current needed to overcome the pinning potential (let the vortex propagate into the other well). When the curvature $U_{xx}(x_0)$ of the potential at the point $x_0 = 0$ is positive then the barrier disappears. The $|L\rangle$ and $|R\rangle$ are the classical states for the vortex.

2.11.5 Depinning and Bias Currents

There have been numerous studies of the double well potential in relation to vortex qubits over the past decade. The paper – "Double-Well Potential in an Annular Josephson Junction" by P.D Shaju and V.C. Kuriaskose[39] takes a direct look at the potential associated with the junction and how a particle would behave in such a system. With a microshort in the junction it's noted that its strength is dependent upon the dielectric barrier, so, as the barriers thickness increases the strength of the microshort decreases. To model the fluxons dynamics in an AJJ with a microshort the perturbed sine-Gordon equation partial differential equation was applied,

$$\varphi_{tt} - \varphi_{xx} + \sin\varphi = -\frac{\partial}{\partial x}(\Delta\bar{B}\cdot\bar{n}) - \delta(x)\mu\sin\varphi - \varphi_t\alpha - \gamma \qquad (2.11.5.1)$$

Where $\varphi(x,t)$ is the phase difference across the junction electrodes, the spatial coordinate is x and is normalized to λ_J and the time t is normalized to the inverse plasma frequency ω_0^{-1} where $\omega_0 = \tilde{c}/\lambda_J$. The parameter $\tilde{c}$ is the maximum velocity of the electromagnetic waves in the junction. $\bar{B}$ corresponds to the strength of the magnetic field. $\Delta = 2\lambda_L$ is the effective penetration depth of the magnetic field into the junction. λ_L is the London penetration depth of the superconducting electrodes, $\bar{n}$ represents the direction of the vortex's magnetic moment, μ is the current density associated with the mircroshort and is normalized to the maximum Josephson current j_0. The parameter $\alpha = 1/(\omega_0 RC)$, where R is the resistance per unit length and $C = \epsilon_T\epsilon_0 W/t_{ox}$ is the capacitance. t_{ox} is the thickness of the oxide layer and W is the width of the junction. And finally $\gamma = j/j_0$ which is the normalized amplitude of a dc bias current normalized to j_0.

---

[39] P.D.Shaju, V.C.Kuriakose. "Double Well Potential in Annular Josephson Junction" (27/09/04)

The term, $-\frac{\partial}{\partial x}(\Delta\bar{B}\cdot\bar{n})$ is the interaction of the external field with the junction. The second term $-\delta(x)\mu\sin\varphi$ corresponds to the Josephson current density associated with the microshort. The third term $-\varphi_t\alpha$ is where the internal damping due to the quasi particle current is taken into consideration. The last term γ is a parameter that shows the energy input from the bias current.

A double well potential was obtained through various steps. Firstly the perturbed sine-Gordon equation can be re-written as,

$$\varphi_{tt} - \varphi_{xx} + \sin\varphi = b\sin(kx) - \delta(x)\mu\sin\varphi - \varphi_t\alpha - \gamma \qquad (2.11.5.2)$$

The parameter $b = 2kB/B_{cl}$, with $B_{cl} = \Phi_0/(\pi\Delta\lambda_J)$ which corresponds to the first critical field for the fluxon penetration in a long Josephson junction. The parameter $k = 2\pi/l$ and is the normal spatial periodicity of the magnetic field in the junction, l represents the length of the Josephson junction (taking note that it is normalized to λ_J). The last parameter Φ_0 is the magnetic flux quantum and is equal to $h/2e = 2.064 \times 10^{-15} Wb$. The closed boundary conditions for this junction are,

$$\varphi(l) = \varphi(0) + 2\pi N, \qquad\qquad \varphi_x(l) = \varphi_x(0) \qquad (2.11.5.3)$$

Where N corresponds to the number of fluxons trapped in the system. By making the parameters, $\gamma = \mu = b = \alpha = 0$ the newly rewritten perturbed equation has the form,

$$\varphi(x,t) = 4\tan^{-1}\left[exp\frac{\sigma(x-\xi)}{\sqrt{1-u^2}}\right], \qquad (2.11.5.4)$$

ξ in this equation stands for the instantaneous location and is equal to $ut + \xi_0$, u is the velocity and is once again normalized, the polarity $\sigma = \pm 1$ and the initial position of the vortex is represented by ξ_0. The Hamiltonian associated with the vortex is,

$$H^{SG} = \int_{-\infty}^{\infty} \left[\frac{1}{2}(\varphi_t^2 + \varphi_x^2) + 1 - \cos\varphi \right] dx \qquad (2.11.5.5)$$

And the dissipative rate is calculated by,

$$\frac{d}{dt}(H^P) = - \int_{-\infty}^{\infty} [-b\sin(kx) + \delta(x)\mu\sin\varphi + \alpha\varphi_t + \gamma]\varphi_t dx \qquad (2.11.5.6)$$

Substituting the vortex solution to the perturbed sine-Gordon equation into the previous two equations and then applying McLaughlin and Scott's[40] perturbative analysis one obtains the expression,

$$\frac{du}{dt} = -\frac{\pi b}{4}(1-u^2)^{3/2}\operatorname{sech}\left[\frac{\pi^2}{l}\sqrt{1-u^2}\right]\sin(k\xi) + \frac{\mu}{2}(1-u^2)\operatorname{sech}^2\left[\frac{\xi}{\sqrt{1-u^2}}\right]\tanh\left[\frac{\xi}{\sqrt{\sqrt{1-u^2}}}\right] -$$

$$\alpha u(1-u^2) + \frac{\pi}{4}\gamma(1-u^2)^{3/2} \qquad (2.11.5.7)$$

as a solution. Considering the classical picture in which the particle has a rest mass of $m_0 = 8$, the potential has the following relation,

$$\frac{\partial U_{eff}}{\partial \xi} = -m_0 \frac{du}{dt} \qquad (2.11.5.8)$$

Now with the substitution of $\frac{du}{dt}$ of (2.11.5.7) into (2.11.5.8) one obtains the potential,

$$U_{eff}(\xi_0) = -bl\operatorname{sech}\left(\frac{\pi^2}{l}\right)\cos(k\xi_0) + 2\mu\operatorname{sech}^2\xi_0 - 2\pi\gamma\xi_0 \qquad (2.11.5.9)$$

---

[40] D.W. McLaughlin, A.C. Scott. "Perturbation Analysis of Fluxon Dynamics" (01/10/78)

With the following adjustments $\gamma = 0, b = 0.1, l = 10$ and $\mu = 0.5$ a double potential well is formed. This can be seen in fig (2.11.5.1) which is constructed via Mathematica.
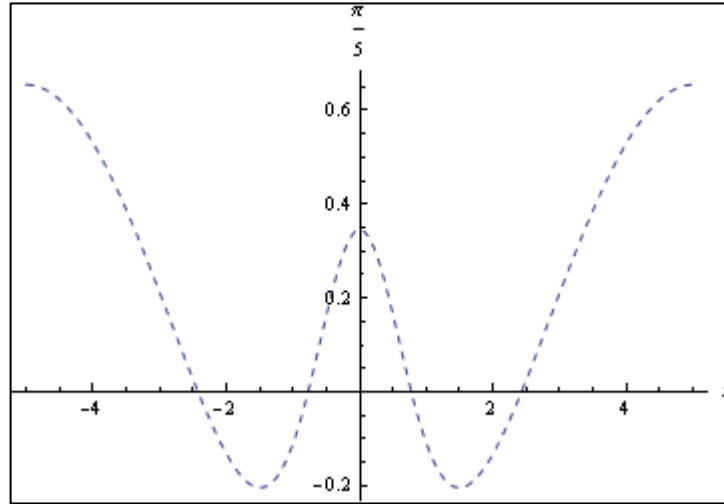
Figure (2.11.5.1) A plot of the suggested double well potential parameters.

The paper goes on to look at how the bias and depinning current effect the system. In the model proposed the vortex depinning current is dependent upon the microshort's strength μ or magnetic field strength b depending on the state concerned. In state A, the dependent is the microshort whereas in state B the depinning current depends upon the magnetic field. Both of these states have a point when the depinning current is exceeded and so the vortex will exit from the potential well and continue propagating around the junction. To exceed these depinning currents a bias current has to be applied to the system. These correspond to the strength of the microshort and magnetic field respectively.

The depinning current is the "force" which keeps the vortex in the potential well. It needs to be overcome for a vortex to carry on propagating through the junction. The bias current can aid this and when applied it can slant the double well potential so that a vortex can escape and continue moving along. This illustration of how the bias current can effect the potential can be seen in fig (2.11.5.2).
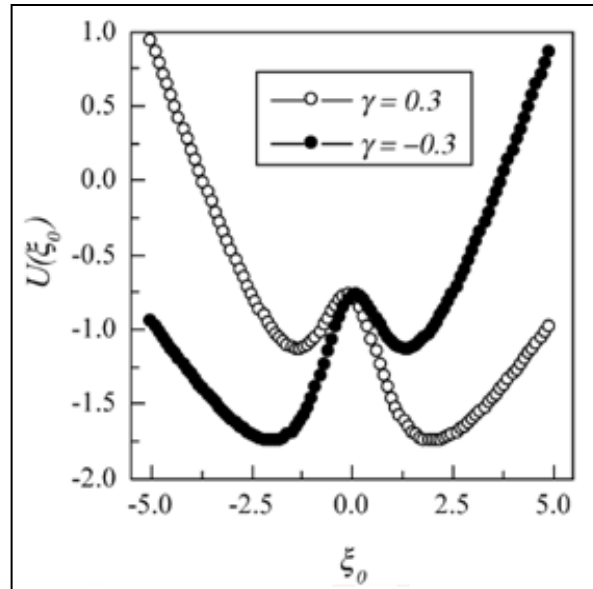
Fig (2.11.5.2) A double well potential tilting in form due to the bias current.[41]

In the case where the bias is too low and the vortex is pinned into one of the wells it is known as the zero-voltage state. On the contrary when the bias current is high enough the trapped vortex will start to propagate in the junction. This movement caused by the vortex contributes to the finite voltage states. The vortex depinning current is where the zero-voltage switches to a finite value. The paper also suggests that an experimental realisation of this particular model may help find an application for the processing in quantum computing and also quantum information processing.

---

[41] Ibid. P.D.Shaju, V.C.Kuriakose. "Double Well Potential in Annular Josephson Junction" (27/09/04)

3 __Methods and Results__

The project started with using Mathematica and a surplus tutorials and background reading associated with nonlinear equations was completed before work could begin with the point particle problem. This helped construct the basis for the future Mathematica tasks. With the single particle problem it was decided to commence with the potential,

$$u(x) = (x^2 - 1)^2$$

which gives arise to a double well. These wells are stable states and are where the particle will come to rest after it has oscillated for a certain period of time. The particle had varying initial conditions (initial position and initial velocity) which were changed to gain many results. The results were then constructed onto a graph of initial velocities against the initial position of the particle. Following on from this, three more cases were explored via Mathematica. These were two particles, a single fluxon and two interacting fluxons. The latter two cases are directly related to the physical problem and were used to help construct a theoretical animation of fluxons contending with a microshort in an annular Josephson junction. All of the codes in full are located in the appendix with a written commentary.

The results are also included in this section and are appropriately titled after the method of research undertaken. A couple of extra graphs are added to give a progression of how the final result was obtained. This can be seen in particular in our first case. Due to the later scenarios (Results 3.1.9 to 3.2.6) having animations as their results we have put together a snapshot of the animation at particular times. This gives the reader an idea of how the propagating fluxon/fluxons behave in the double well potential or Josephson junction.

3.1 Mathematica

3.1.1 Fluxons in Closed loops

A fluxon in a closed Josephson junction loop which has an external magnetic field H applied to it will align itself with the direction of the field. A driving force is needed in the system for the fluxon to propagate around the Josephson junction; this is achieved by applying a uniform dc bias through the superconducting electrodes. The geometry of this case is simple and the fluxon can easily align itself, this can be seen in Figure (3.1.1.1).
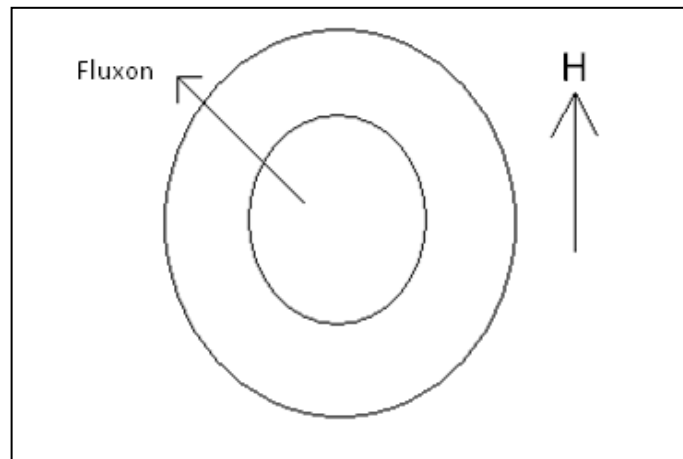
Figure (3.1.1.1) A Simple Annular Junction with a Propagating Fluxon.

The potential associated with the fluxon at this point of alignment has the form of $u(x) = x^2$ and this is shown in fig (3.1.1.2).
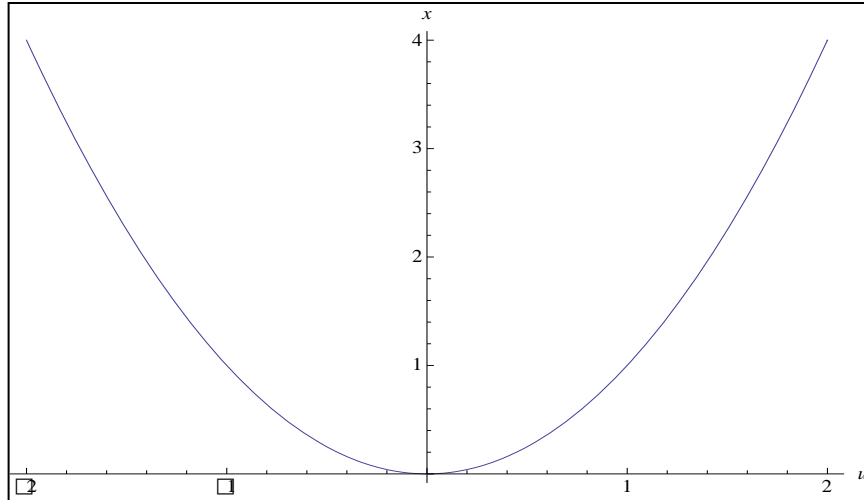
Figure (3.1.1.2) A graph of U(x) = x^2

Now one introduces a potential barrier to the system. This can be seen in figure (3.1.1.3) as a "junction" and is located at the top of the geometry.
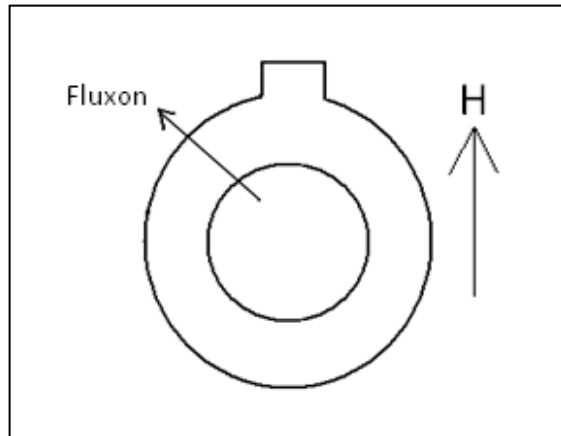
Figure (3.1.1.3) An annular geometry with a "junction".

This new addition produces a different potential and this has the form $U(x) = (x^2 - 1)^2$. This is shown in fig (3.1.1.4). The fluxon will not be stable at this point of alignment unlike the previous case and will instead rest in either adjacent well.
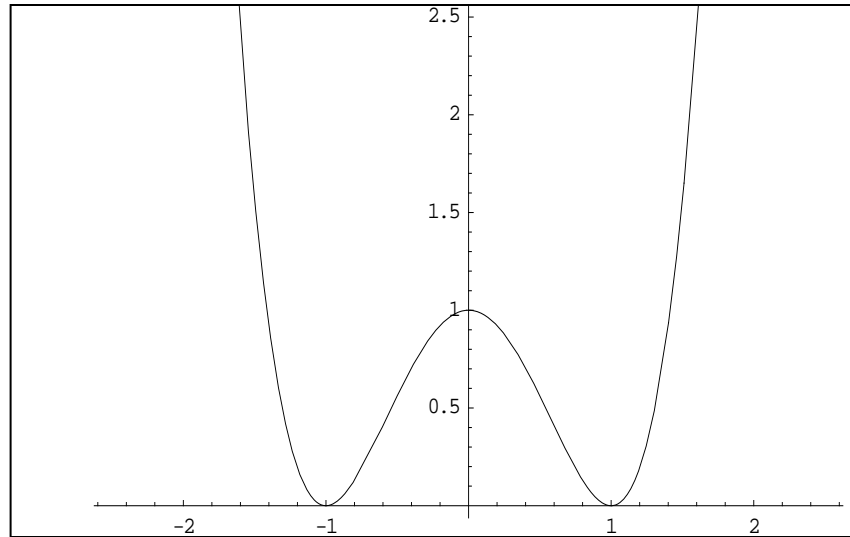
Figure 3.1.1.4 A graph of U(x) = $(x^2-1)^2$

Mathematica was used to carry out this investigation. With varying initial conditions and the system being described by nonlinear equations, a computer programme was written. The first part of the numerical analysis considered a single particle in a double well potential.

3.1.2 Single Particle in a Double Well Potential

The simplest case for investigating fluxons in an annular Josephson junction was to start with a single point particle oscillating in a double well potential. The potential used creates a potential barrier which the particle cannot rest at (an unstable point in the system). With the application of damping the particle will come to rest in one of the two wells.

The system was constructed firstly with Newton's second law,

$$\ddot{x} - F + \alpha\dot{x} = 0 \qquad\qquad (3.1.2.1)$$

Where $\ddot{x}$ corresponds to the acceleration to the particle, $\dot{x}$ is velocity, α is the damping parameter and $F = -\dfrac{\partial U}{\partial x}$ and is the force acting upon the particle.

By solving the equation and applying several different computational techniques one obtained the location of the final resting place of the particle. Using the potential $U(x) = (x^2 - 1)^2$ and differentiating it accordingly the force was obtained,

$$F_u = -4x(x^2 - 1)^2 \qquad\qquad (3.1.2.2)$$

Knowing that,

$$F = m\ddot{x} \qquad\qquad (3.1.2.3)$$

It was decided m = 1. So,

$$F = \ddot{x} \qquad\qquad (3.1.2.4)$$

A damping term was then introduced to equation (3.1.2.4),

$$F_u + F_{damping} = \ddot{x} \qquad\qquad (3.1.2.5)$$

Where $F_{damping} = -\alpha\dot{x}$, α is the damping parameter and $\dot{x}$ is the velocity of the particle. With this substitution we get,

$$\ddot{x} - F_u - F_{damping} = 0 \qquad\qquad (3.1.2.6)$$

Now substituting F_u and $F_{damping}$ the following equation was obtained,

$$\ddot{x} + 4x(x^2 - 1) + \alpha\dot{x} = 0 \qquad\qquad (3.1.2.7)$$

The damping parameter α was set to 0.1. This final equation was then used to construct a programme that enabled the particle to be represented mathematically.

With the parameters in place (the code in full can be seen in the appendix 6.1) and with the initial conditions, $x[0] = 0$ and $x'[0] = 0$ the code was initiated and a result was obtained. A graph was then produced to observe the oscillation of the particle. The positive y axis represented the right well and the negative represented the left well and the x axis represented time, t.

With this constructed correctly a loop was put into place to collate results over a range of initial conditions. The initial velocity of the particle ranged from -2.5 to 2.5, this was also the same for the initial position of the particle. Instead of looking at the oscillations of the particle a graph was plotted to show when the particle will overcome the barrier height in place at $x = 0$.

3.1.3   Results for the Single Particle in a Double Well Potential

The first set of results is from the single particle in a potential well. The code for these results can be found in the appendix. Figure (3.1.3.1) shows the results for the particle possessing an initial velocity of ($\dot{x}_0 = 0$) for the range of initial positions, ($-9 < x < 9$).
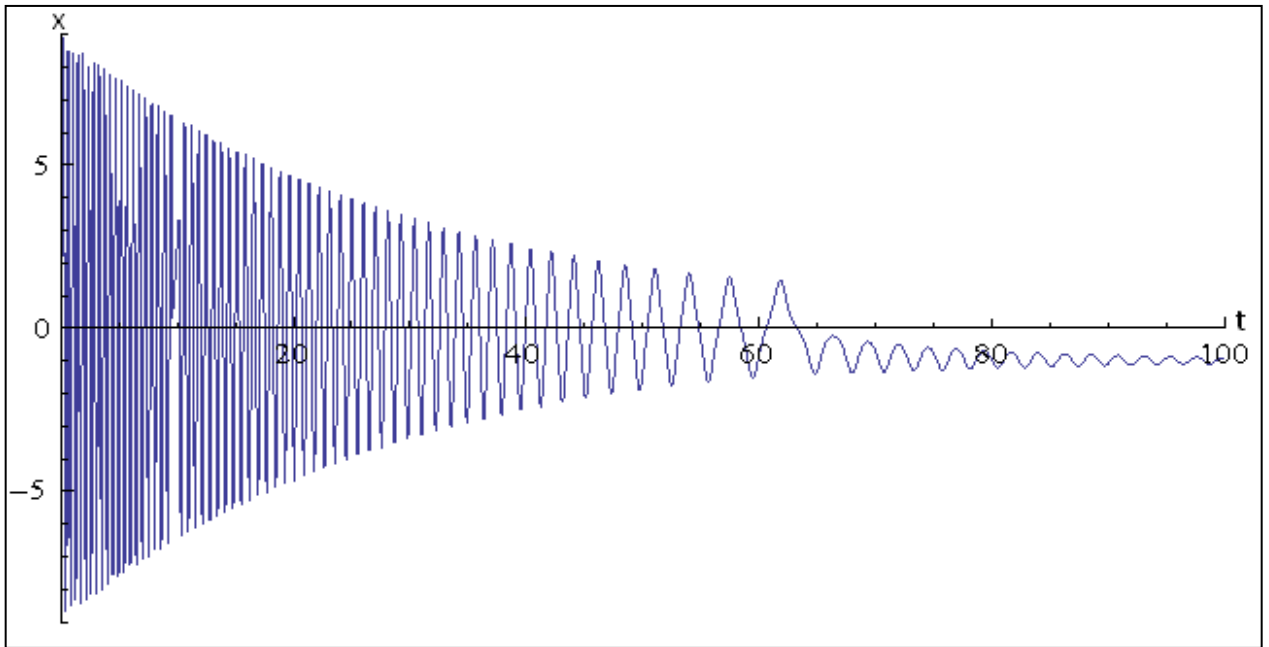
Figure (3.1.3.1) The result for the particle that has a initial position of -9, $((x_0 = -9)$ and initial velocity of 0, $(\dot{x}_0 = 0)$.
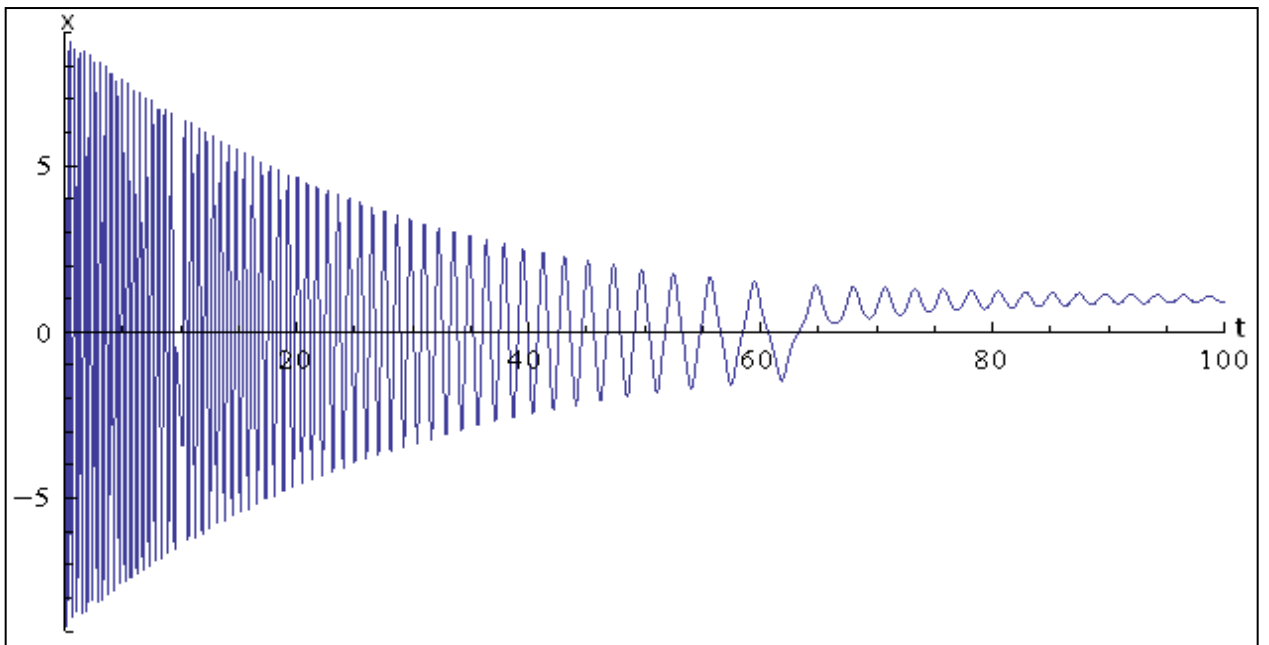
Figure (3.1.3.2) A graph to show the propagation of a single particle in the double well potential with x_0= 9 and $\dot{x}_0$= 0.

After taking these primary results down for various initial conditions a graph was designed to encompass the multiple results. A black dot represents the condition that gave the end result of the right well (particle resting in the positive x-axis) and a red dot for the left well (where the particle came to rest in the negative axis). For example, figure (3.1.3.1) would yield a red dot and figure (3.1.3.2) would yield a black dot. Figure (3.1.3.3) shows the results for the ranges, $(-10 < x_0 < 10)$ and $(0 < v_0 < 10)$.
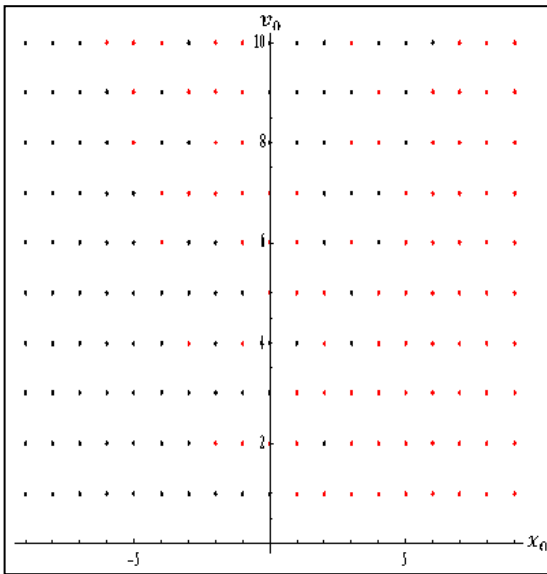
Figure (3.1.3.3) The graph for the particle scenario with the ranges, $(-10 < x_0 < 10)$ and $(0 < v_0 < 10)$.

As one can see there is a symmetry occurring in the corners of the graph but this is unsurprising due to the steepness of the double well potential at these ranges. The initial conditions therefore had to be filed down to observe whether a more distinct pattern/relationship would occur. The green dot represents a right well result and the black dot represents a left well result. Figure (3.1.3.4) shows the results for the conditions $(-2.5 < x_0 < 2.5)$ and $(-2.5 < v_0 < 2.5)$.

65
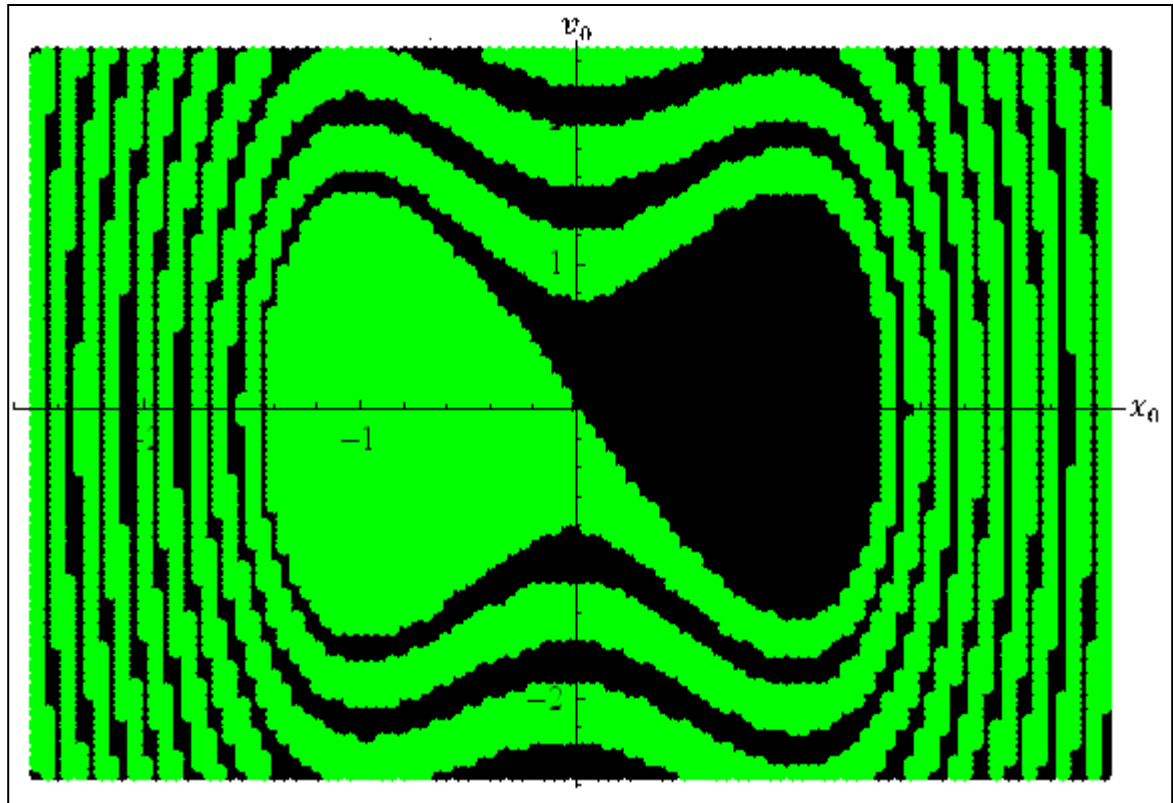
Figure (3.1.3.4) A graph to show the single particle in the double well potential for the ranges $(-2.5 < x_0 < 2.5)$ and $(-2.5 < v_0 < 2.5)$.

The results in (3.1.3.1) and (3.1.3.2) give us a clear indication of where in a double well potential a particle will come to rest. This is represented by the clear oscillation of the particle and whether it rests in the positive or negative x axis. From figure (3.1.1.4) it can be seen that the positive axis refers to the "right" well and the negative x axis refers to the "left" well. In the basic case of figure (3.1.3.1) the particle came to rest in the right well with the initial conditions, $x_0 = 9$ and $x_0' = 0$ and in figure (3.1.3.2) the particle came to rest in the left well with the initial conditions are $x_0 = -9$ and $x_0' = 0$.

The following part of the project was to write a program that would produce a whole set of results rather than a single one. By taking a range of the initial velocities from 0 to 10 and the initial positions from -10 to 10 we have produced figure (3.1.3.3). This graph produced in the results consisted of red and black dots. The red dot represented the particle resting in the "positive" right well and the black dot when the particles is resting in the "negative" left well. Figure (3.1.3.3) shows that there is no real distinction of a connection between the different initial velocities and positions. The reason this is so is due to the fact that the potential steepens dramatically at $(x > -2)$ and $(x > 2)$ respectively and so with the particle starting at an initial

position greater then these parameter proves to be of no use in finding an underlying relationship.

The parameters of the code were then changed accordingly and produced figure (3.1.3.4). This resulted in a prominent relationship being observed. The shape produced is a spiral, it is however not of perfect geometric form but still in essence behaves as any spiral would. One can trace around it from the centre with their finger and see that it does indeed spiral out.

In greater detail, at the smaller initial conditions the particle is not passing into the other well. That is why we can see a large proportion of dots at the centre to be green or black respectively. If we consider $(-1.4 < x_0 < 0)$ and $(v_0 = 0)$, one can see that ball does not have enough of an initial velocity to overcome the barrier height in the double well potential and rest in the positive well thus resulting in a green dot. As the velocity is increased however, we see that the particle does indeed start passing over the barrier height and resting in the other well. Taking this further, if we look towards $(x_0 < -1.5)$ we see that the particle has passed from the left well over to the right and then back into the left well again to rest. So as the colour shifts back and forth we can determine which initial conditions will give rise to a certain result. This analysis can be seen on the positive side of the graph due to the symmetry of the pattern.

3.1.4   Two Particles in a Double Well Potential

After constructing graphs of the results for the single particle case it was decided to move onto two particles in a double well potential, firstly a non-interaction and then an interaction between the particles. Instead of just the one equation describing the system, two were needed this time. As well as this, an interaction term was also introduced (for the non-interaction case it was set to zero).

The general equation now had the form,

$$\ddot{x} + 4x(x^2 - 1) + \alpha\dot{x} - F_{int} = 0 \qquad (3.1.4.1)$$

67

The interaction term proposed for this part of the experiment,

$$F_{int} = \frac{2\beta(x_1 - x_2)}{((x_1 - x_2)^2 + \varepsilon)^2} \qquad (3.1.4.2)$$

Where x_1 refers to particle 1 and x_2 is particle 2. β is the interaction strength parameter, and ε is the softening parameter. The choice of this particular interaction term comes from the analogy of Newtonian gravity in 3D. We have,

$$V = \frac{GM_1M_2}{(r_1 - r_2)} \qquad (3.1.4.3)$$

$$= \frac{-GM_1M_2}{((x_1 - x_2)^2 + (y_1 - y_2)^2 + (z_1 - z_2)^2)^{\frac{1}{2}}} \qquad (3.1.4.4)$$

Because $r_1 = (x_1y_1z_1)$ and $r_2 = (x_2y_2z_2)$ are vectors. The force, which is also a vector can be written as,

$$F = -\nabla V = -\frac{-GM_1M_2(r_1 - r_2)}{((x_1 - x_2)^2 + (y_1 - y_2)^2 + (z_1 - z_2)^2)^{\frac{3}{2}}} \qquad (3.1.4.5)$$

The potential V is a special case of a general formula,

$$V = \frac{\beta}{\left(((x_1 - x_2)^2 + (y_1 - y_2)^2 + (z_1 - z_2)^2)\right)^{\gamma}} \qquad (3.1.4.6)$$

In the 1D case this equation becomes,

$$V = \frac{\beta}{((x_1 - x_2)^2)^\gamma} \qquad (3.1.4.7)$$

Thus the force term F is,

$$F_1 = -\frac{\partial V}{\partial x_1} = \frac{2\beta(x_1 - x_2)}{((x_1 - x_2)^2)^{(\gamma+1)}} \qquad (3.1.4.8)$$

If we choose $\gamma = 1$, then we obtain

$$F_1 = \frac{2\beta(x_1 - x_2)}{((x_1 - x_2)^2)^2} \qquad (3.1.4.9)$$

To obtain the complete equation (3.1.4.2) we introduce the softening parameter ε (this does not have a physical meaning but is added in order to perform numerical integration as the computer programme cannot work with infinite numbers).

With this a coupling equation was constructed so that the particles will either be repulsive or attractive. A difference in sign is needed for the force term to make the system symmetric. This can be seen in the following equations.

$$\ddot{x} + 4x(x_1^2 - 1)^2 + \alpha\dot{x} - \frac{2\beta(x_1 - x_2)}{((x_1 - x_2)^2 + \varepsilon)^2} = 0 \qquad (3.1.4.10)$$

$$\ddot{x} + 4x\left(x_2^2 - 1\right)^2 + \alpha\dot{x} + \frac{2\beta(x_1 - x_2)}{\left((x_1 - x_2)^2 + \varepsilon\right)^2} = 0 \qquad \text{(3.1.4.11)}$$

In its place of only the single particle coming to rest in either the left or right well there were other combinations too because of the new particle introduced to the system. The particles would come to rest in either the same well (left or right) or would be separated between both of the wells. The particles were treated as indistinguishable therefore it did not affect which combination the particles came to rest in the separate wells as the result was allocated the same coloured plot. If the result was positive (both particles coming to rest in the same well) a black plot was allocated to those initial conditions and if a negative result was achieved (particles coming to rest in different wells) then a blue dot was assigned.

The initial velocity for each of the particles was set to zero, this allowed a graph to be produced of the initial position of particle two against that of particle one. Through the adjustment of the interval step between iterations one can control the resolution of the graph.

Once a result was obtained and examined it was decided that different values for the parameter β should be considered and how this effects the results obtained when there was no interaction between the particles.

3.1.5   Results for Two particles in a Double Well Potential

Next we looked at how two particles propagating in the same potential would react. Figure (3.1.5.1) shows the oscillation trails of two non-interacting particles. The blue oscillation corresponds to particle one and the mauve oscillation trail corresponding to particle two.
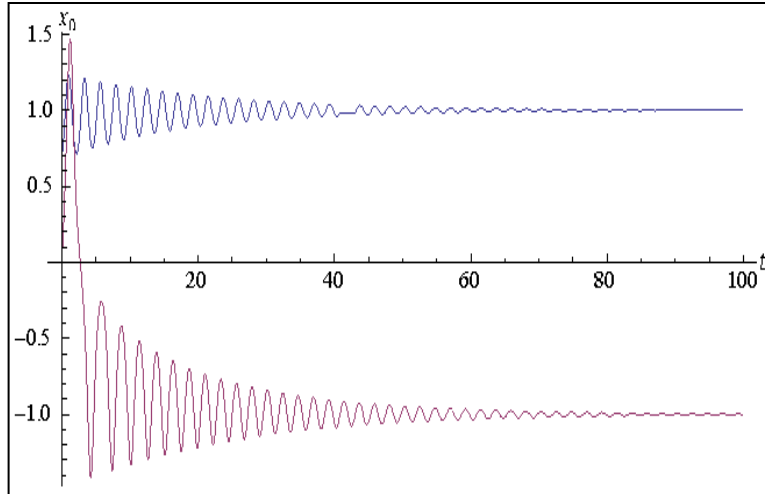
Figure (3.1.5.1) Two particles oscillating in the same double well potential.

After this stage the code was expanded to cover a particular range of initial positions for both particles. Figure (3.1.5.2) shows x_1 along the x axis and x_2 plotted on the y axis. Both of the particle's initial velocities were equalled to zero. The same dot allocation was used as in figure (3.1.3.4).
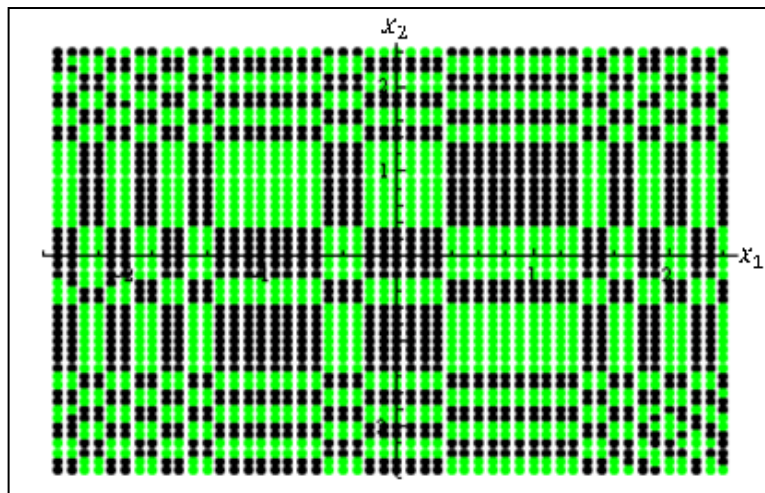
Figure (3.1.5.2) Two non-interacting particles with the following conditions, $\dot{x}_1 = \dot{x}_2 = 1$ and $(-2.5 < x_1 < 2.5)$ and $(-2.5 < x_2 < 2.5)$.

The following results are derived from the method (3.1.5) and show the two particles interacting.
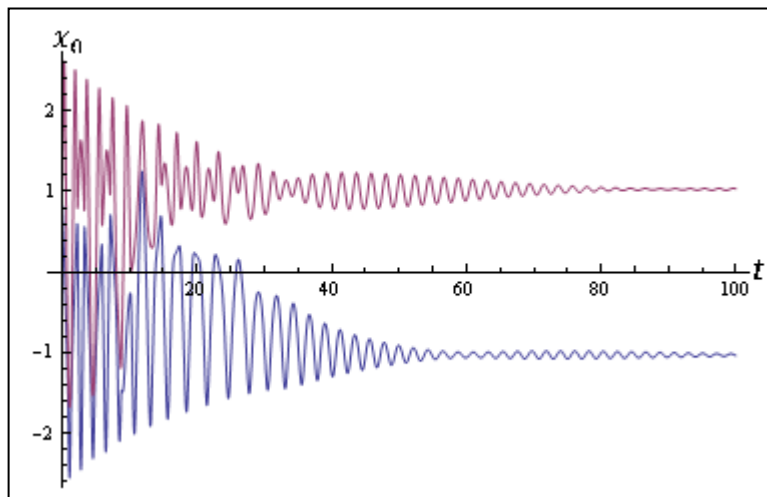
Figure (3.1.5.3) Two interacting particles with the initial conditions, $x_1 = 0.8, v_1 = 5.5, x_2 = 1$ and $v_2 = 0$.

The next set of results to follow show the impact of varying the parameter β. Each figure indicates the value of β used for that particular simulation.
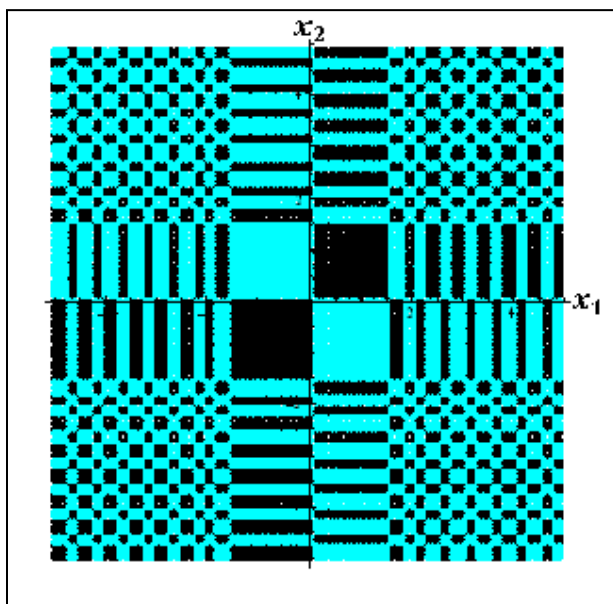
Figure (3.1.5.4) The graph above shows the result for β=0.0 with $(-5 < x_1 < 5)$ and $(-5 < x_2 < 5)$ respectively.
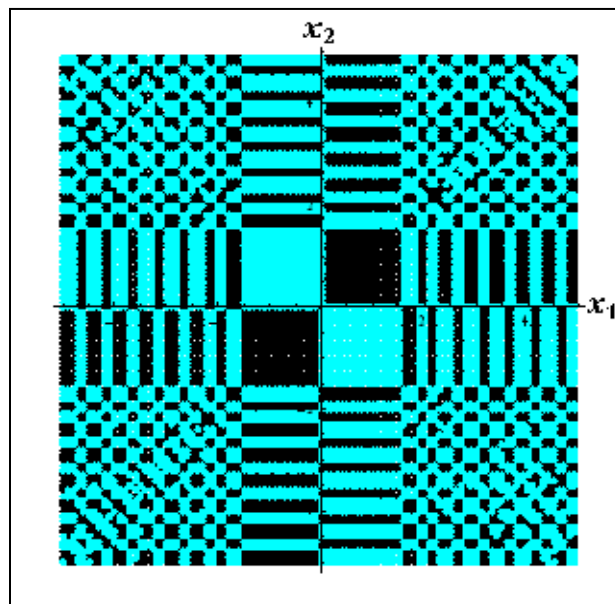
Figure (3.1.5.5) The graph above shows the result for β = 0.0001 with $(-5 < x_1 < 5)$ and $(-5 < x_2 < 5)$ respectively.
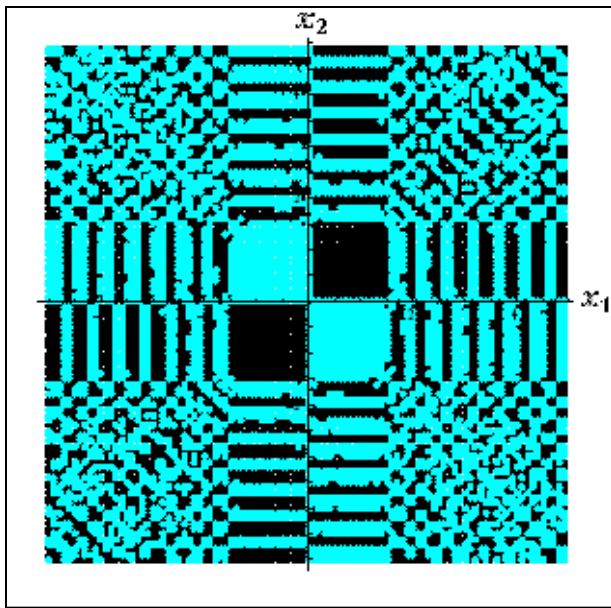
Figure (3.1.5.6) The graph above shows the result for β = 0.001 with (-5 < x_1 < 5) and (− 5 < x_2 < 5) respectively.
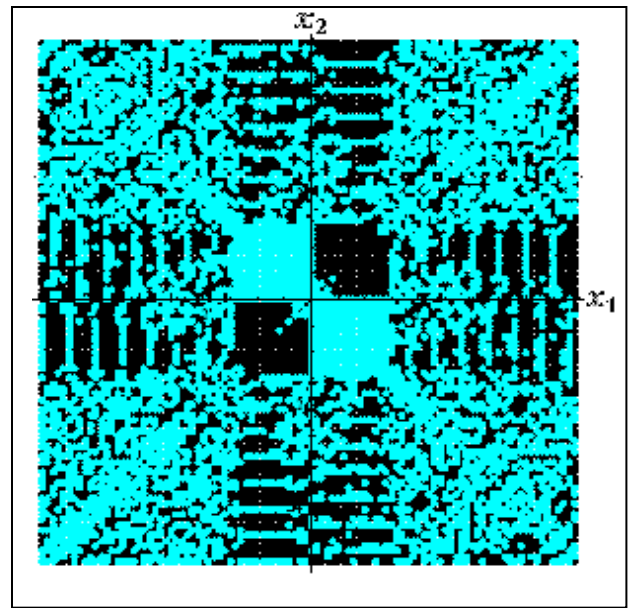
Figure (3.1.5.7) The graph above shows the result for β = 0.01 with (-5 < x_1 < 5) and (− 5 < x_2 < 5) respectively.

Figures (3.1.5.4) to (3.1.5.7) show the initial position of particle one represented on the x axis and the initial position of particle two is represented on the y axis. We took particular note of when β= 0.001 and zoomed into the area (2 < x_1 < 2.5) and (2 < x_2 < 2.5). This produced the result in figure (3.1.5.8).
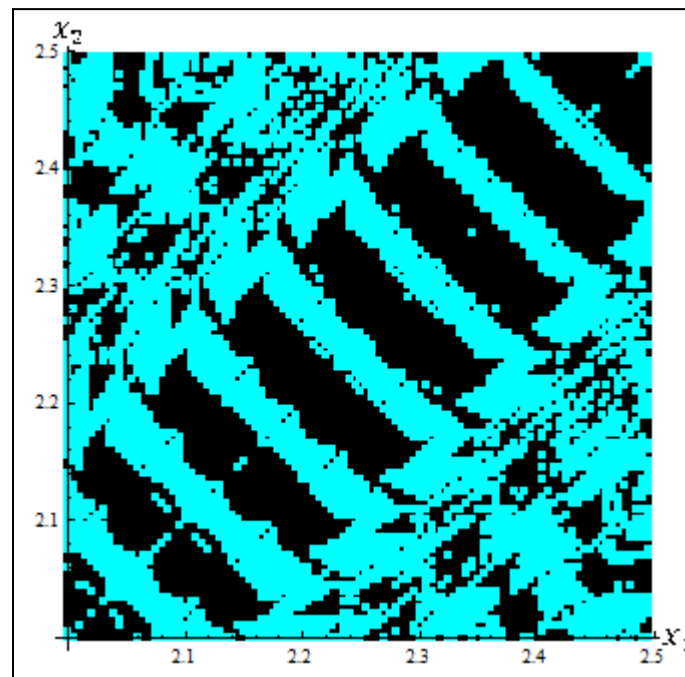
Figure (3.1.5.8) The close up of the region (2 < x_1 < 2.5) and (2 < x_2 < 2.5) where β=0.001.

73

We investigated the effect of two particles in the same double well potential. This was achieved with a code that incorporated two sets of equations instead of the single equation as before for the single particle problem. In figure (3.1.5.1) we looked at a non-interaction of two particles and after this was completed we moved onto a system that included an interaction. As the figure showed, we can see the two particles oscillating in the same potential and coming to rest in different wells. These particles do not interact, hence why they seemingly pass through one another. The blue line in the figure represents the oscillation of "particle 1" whereas the red line is "particle 2". The initial conditions were set at $x_1 = 0.7$ (initial position of particle one), $\dot{x}_1 = 0.3$ (initial velocity of particle one) and $x_2 = 0$ (initial position of particle two), $\dot{x}_2 = 1$ (initial velocity of particle two). These conditions were chosen to show how the particles oscillated rather than for a specific end condition.

As in the single particle case the range of initial positions were set to $(-2.5 < x_1 < 2.5)$ and $(-2.5 < x_2 < 2.5)$ but their initial velocities were set to, $\dot{x}_1 = \dot{x}_2 = 1$. The result of two particles in the same potential has achieved different results. Figure (3.1.5.2) shows the case where there is no interaction between the two particles. As the initial positions vary we see that we obtain a regular arrangement of rectangular blocks. This regular array of "blocks" corresponds to whether both particles rest in the same well or not. In our case the black dots represent the condition when both particles have come to rest in separate wells whereas the blue dots represent both particles resting in the same well whether it is in the left or right well.

For the interaction of two particles we introduced an interaction term denoted in equation (3.1.4.2). Once programmed into Mathematica as stated in method (3.1.4) we were able to produce a base graph of the oscillations of the two particles. This can be seen in figure (3.1.5.3) The initial conditions for the particles were $x_1 = 0.8$, $v_1 = 5.5$, $x_2 = 1$ and $v_2 = 0$ respectively. From this figure we see that the red and blue oscillation lines do in fact interact with one another and react with the knowledge that there is a particle in close proximity. This is a mathematical simulation however, we would like to focus on what would be physically happening if the case was a real experiment. As the figure portrays the particle interacting with one another until $t = 15s$ is reached in which case the particles end up in separate wells. This would yield a blue dot as the final positions of the particles once multiplied would give a negative result.

The interaction term has the parameter β which can be tuned to apply a greater or lesser interaction between the particles. Figures (3.1.5.4) to (3.1.5.7) show the progression of the value in β and how this affects the regular array that is present when $\beta = 0$. We have showcased the scenarios where β=0.0, 0.0001, 0.001, 0.01 and 0.1. It can be seen that as the interaction term is increased that the regularity of the rectangular array becomes decomposed in a sense causing a more chaotic result to appear. From this chaos we hoped to be able to find

natural fractal pattern. This is why we chose to zoom into the area suggested in figure (3.1.5.8) Through the use of different geometric parameters put in place we were able to obtain a set of diagonal "rectangles" that were uniform in size and distance to one another. We hoped that with the aid of other geometric changes that a fractal pattern would occur as one zoned in on this but unfortunately this was not found at that time. We have denoted our best effort for the reader to perhaps using this as a base line to then springboard off into another line of research.

3.1.6   A Single Soliton

After considering particles in a double well potential, solitons were next to be investigated. Modifications had to be made to the code that was constructed for the previous case as new parameters were introduced to the problem. Firstly, was the new potential that would be used which would have to take into account the external magnetic field which is applied to the system that causes the soliton attempting to align itself with it.

The potential for a soliton in an AJJ,[42]

$$u(x) \approx \mu(sech^2 x + \bar{h}x^2) - 2\pi\gamma x \qquad (3.1.6.1)$$

Where γ is the bias current, μ is a parameter that corresponds to the microshort's strength, x is the position of the soliton measured along the junction and,

$$\bar{h} \equiv \frac{h\pi sech(\pi/2r)}{\mu r^2} \qquad (3.1.6.2)$$

Where $\bar{h}$ represents the magnetic field in the system. The bias current $\gamma = 0$. A double well is once again produced and is shown in figure (3.1.6.1)

---

[42] Ibid. A.N. Price, A. Kemp, D.R. Gulevich, F.V. Kusmartsev and A.V. Ustinov. "Vortex Qubit Based on an Annular
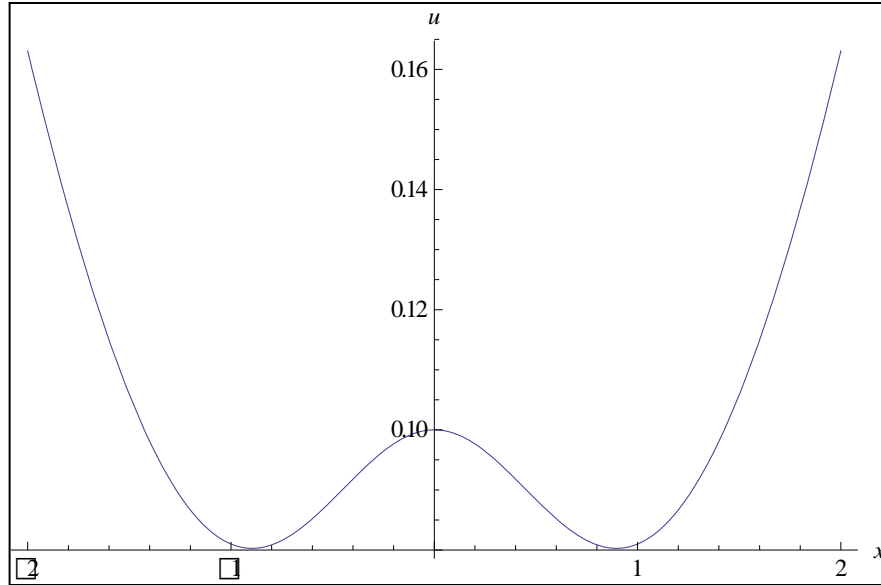
Figure (3.1.6.1) Double well potential with the fluxon parameters.

The equation of motion was used as a basis once again and the terms were differentiated and substituted appropriately,

$$\ddot{x} + 2\mu\bar{h}x - 2\mu sech^2(x)\tanh(x) + \alpha\dot{x} = 0 \qquad (3.1.6.3)$$

The damping parameter α = 0.1, $\bar{h} = 0.3$ and μ = 0.1. This yielded the following equation,

$$\ddot{x} + 0.06x - 0.2sech^2(x)\tanh(x) + 0.1\dot{x} = 0 \qquad (3.1.6.4)$$

The initial velocity and initial position ranged from $(-10 < x < 10\,)$ and the time parameter was set to t = 100s. This gave the fluxon enough time to come to rest in one of the wells. The same procedure was applied for obtaining a result in that when the fluxon came to rest in the left well it was assigned a black dot for the initial conditions that yielded the result and a green

dot for the right well. Then by producing a graph of the initial velocity and initial position it was seen whether a relationship occurred due to the initial conditions applied to the problem.

3.1.7   Result for the Single Fluxon

We then looked at how the new potential (3.1.4.4) affected a fluxon in the one particle system. Figure (3.1.7.1) shows a typical oscillation of the fluxon in the double well potential. The conditions applied were, $(v_0 = 0, x_0 = 2, t = 100)$.
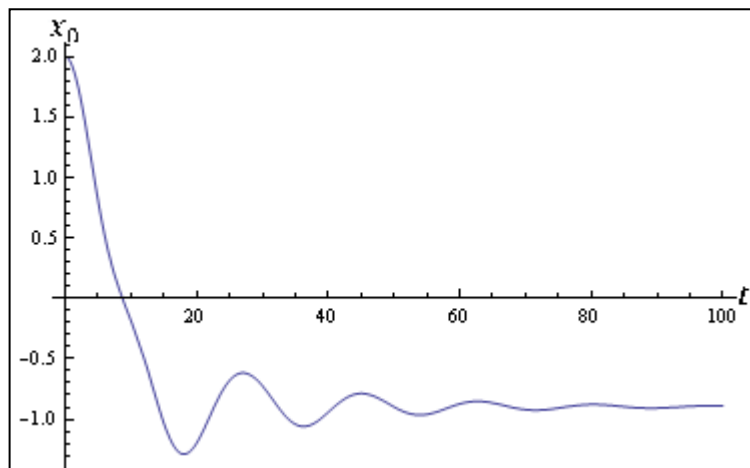
Figure (3.1.7.1) The oscillation of the single soliton in a double well potential ending with a negative result.

By using this equation a graph was once again obtained with the initial velocities and positions of the fluxon with the range $(-10 < x_0 < 10)$ and $(-10 < v_0 < 10)$. As with the single particle system, a black dot represents a soliton resting in the right well and a green dot represents the fluxon resting in the left well. The result can be seen in figure (4.3.1).

77
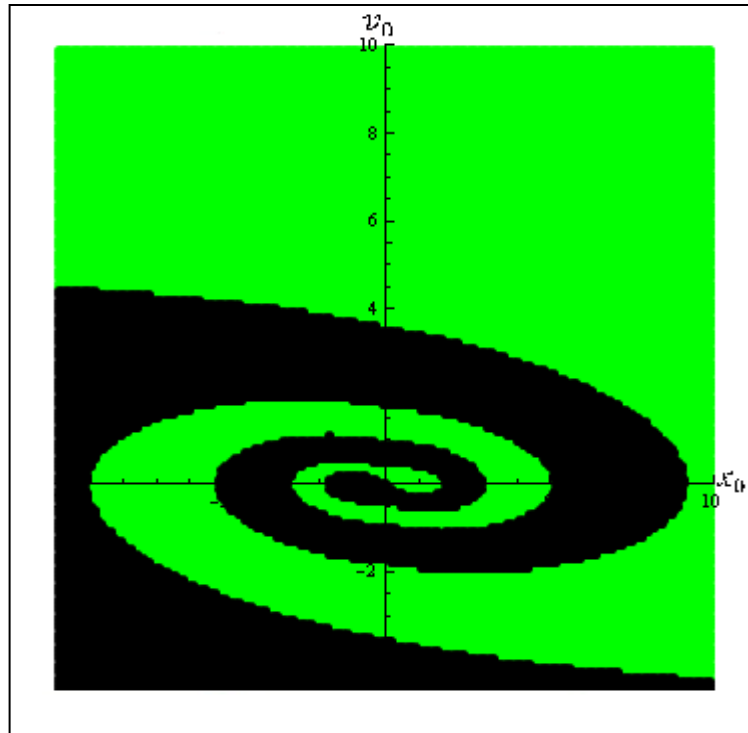
Figure (3.1.7.2) A graph to show the result of a fluxon propagating in a double well potential.

After this examination of single and double particles the research moved onto how a fluxon would behave in these conditions. The process of this stage of the research was similar to the previous example but changed the particle for a fluxon. The code was amended to accommodate these changes and a result for the singular fluxon was obtained and shown in figure (3.1.7.1). This figure showed the fluxon oscillating gently (there was not as many erratic peaks as in the particle systems) and coming to rest in the negative x axis and therefore the left well. With this is mind we went onto examining (as in the particle system) numerous initial conditions for the velocity and position. What we obtained from that is seen in figure (3.1.7.2). This time around the result is distinctly uniform in shape and is most definitely a spiral.

3.1.8 Two Interacting Fluxons

The next case concerned itself with two fluxons. These fluxons have the added notion that they will not only contend with the microshort but with one another. The same form of equation was used as for the single fluxon case which has now resulted in coupled equations due to the two

fluxons. As well as this an interaction term had to be introduced. This would have a different form than the two particle system and was as follows,

$$u = e^{-\beta(x_1 - x_2)^2} \tag{3.1.8.1}$$

Where x_1 and x_2 correspond to the positions of the fluxons. With this new interaction potential term, the force term can be derived through the following processes,

$$F_{int} = -\frac{\partial u}{\partial x_1} = -\frac{\partial}{\partial x_1} e^{-\beta(x_1 - x_2)^2} \tag{3.1.8.2}$$

$$= -e^{-\beta(x_1 - x_2)^2} \frac{\partial}{\partial x_1} [-\beta(x_1 - x_2)^2] \tag{3.1.8.3}$$

$$= -e^{-\beta(x_1 - x_2)^2} [-2\beta(x_1 - x_2) \cdot \frac{\partial}{\partial x_1}(x_1 - x_2)] \tag{3.1.8.4}$$

$$-\frac{\partial}{\partial x_1}[x_1 - x_2] = \frac{\partial}{\partial x_1} x_1 - \frac{\partial}{\partial x_1} x_2 = 1 - 0 = 1 \tag{3.1.8.5}$$

So finally,

$$F_{int} = -e^{-\beta(x_1 - x_2)^2} [-2\beta(x_1 - x_2) \times 1] \tag{3.1.8.6}$$

$$= 2\beta(x_1 - x_2)e^{-\beta(x_1 - x_2)^2} \tag{3.1.8.7}$$

So following the same steps for the interaction term with respect to x_2 one obtained,

$$= -2\beta(x_1 - x_2)e^{-\beta(x_1-x_2)^2} \qquad (3.1.8.8)$$

And this is of the opposite sign because,

$$\frac{\partial}{\partial x_2}[x_1 - x_2] = \frac{\partial}{\partial x_2}x_1 - \frac{\partial}{\partial x_2}x_2 = 0 - 1 = -1 \qquad (3.1.8.9)$$

The general force term was,

$$F_{int} = \pm 2\beta(x_1 - x_2)e^{-\beta(x_1-x_2)^2} \qquad (3.1.8.10)$$

Where x_1 and x_2 denote each of the fluxons and β is a parameter that dictates the strength of the interaction. The equations in full with respect to both fluxons were,

$$\begin{cases} \ddot{x}_1 + 2\mu\bar{h}x_1 - 2\mu sech^2(x_1)\tanh(x_1) + \alpha\dot{x}_1 + 2\beta(x_1 - x_2)e^{-\beta(x_1-x_2)^2} = 0 & (3.1.8.11) \\ \ddot{x}_2 + 2\mu\bar{h}x_2 - 2\mu sech^2(x_2)\tanh(x_2) + \alpha\dot{x}_2 - 2\beta(x_1 - x_2)e^{-\beta(x_1-x_2)^2} = 0 \end{cases}$$

As with the two particle system, focus was on the parameter β and how the interaction strength would affect the system. The values of β investigated were 0.0001, 0.001, 0.01 and 0.1 respectively. By comparing these results to the instance where β = 0.0 it was seen how the strength of interaction changed the final positions of the fluxons.

3.1.9 Results for Two Fluxons

The two fluxons resting in the same well result was indicated by a blue dot, and two fluxons resting in different wells was indicated by a white dot. The figures below show the evolution of the scenario with an increase in the interaction term through the parameter β.
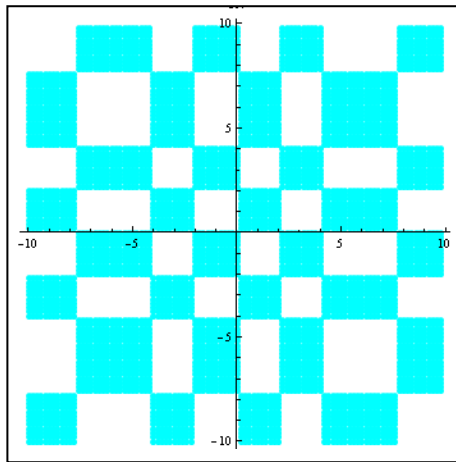
Figure (3.1.9.1) Beta = 0.000
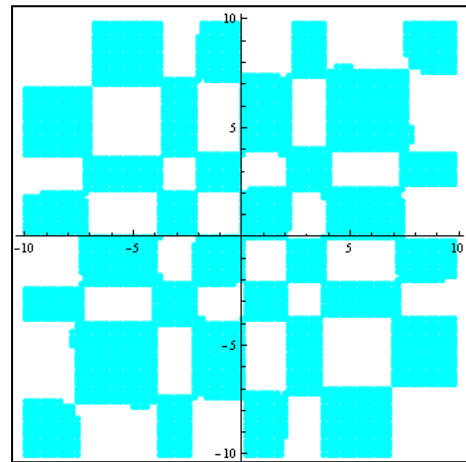
Figure (3.1.9.2) Beta = 0.001
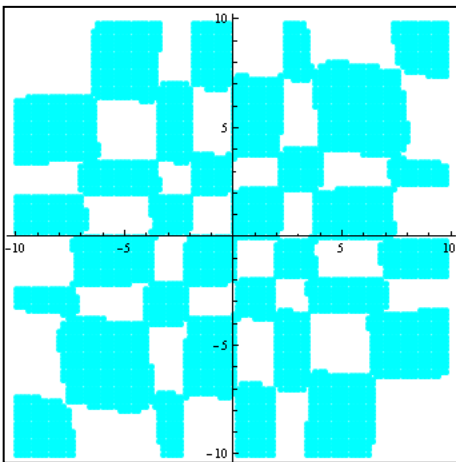
Figure (3.1.9.3) Beta = 0.002
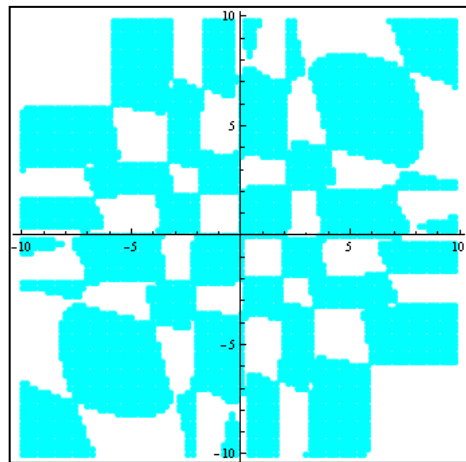
Figure (3.1.9.3) Beta = 0.003
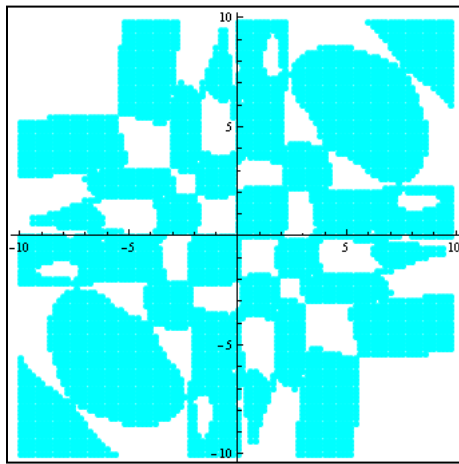
Figure (3.1.9.5) Beta = 0.004
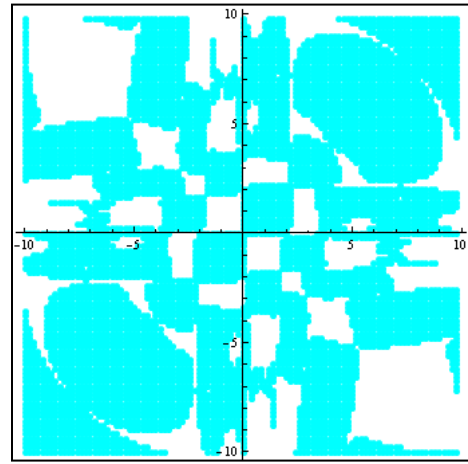
Figure (3.1.9.6) Beta = 0.005
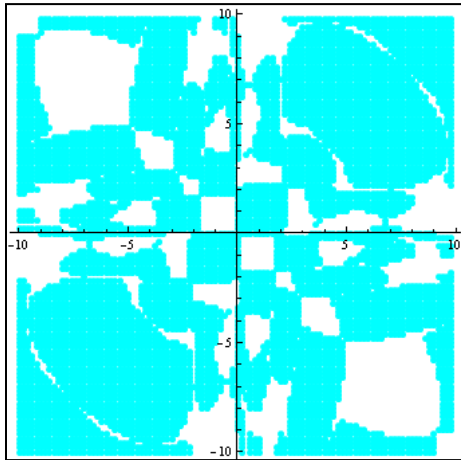
Figure (3.1.9.7) Beta = 0.006
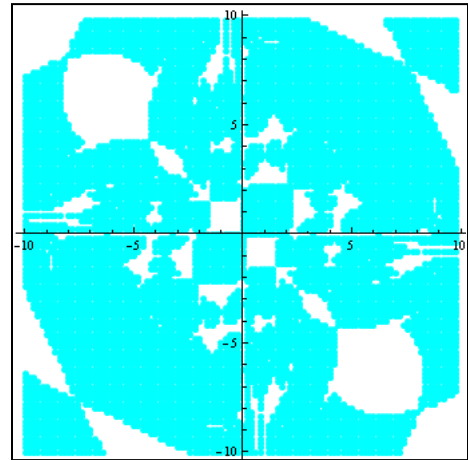
Figure (3.1.9.8) Beta = 0.007
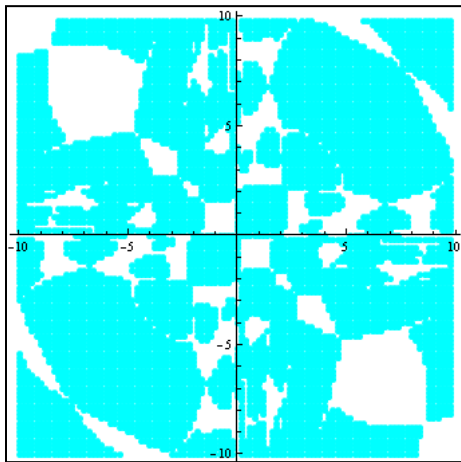
Figure (3.1.9.9) Beta = 0.008
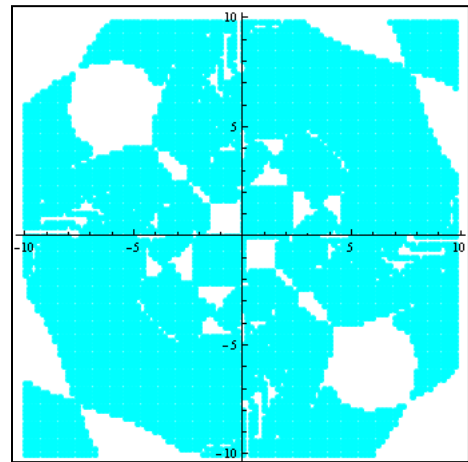
Figure (3.1.9.10) Beta = 0.009

82
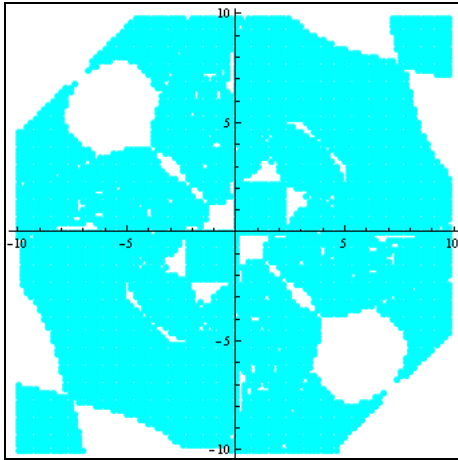
Figure (3.9.1.11). Beta = 0.01

We introduced another fluxon into the double well potential and applied virtually the same method as in the particle process. Again, the parameter β was varied to indicate whether a fractal pattern or different array of regular geometries was observed. As can be seen in figures (3.1.9.1) to (3.1.9.11) we obtained a slowly decomposing set of regular arrangements of geometries. The decomposition is symmetrical in the opposing diagonal axis but does not show any sort of regular pattern formation that we hoped to achieve at this point. As β is increased the resulting dots that made up the latter edges of each axis became more distorted. However the core area made up of four predominant squares do in fact overall keep their shape with the increments up until $\beta = 0.01$ with the positive right hand quadrant and negative left quadrant keeping their form most of all. This demonstrates that even with an increase in such a parameter that the result for localised initial conditions will tend to remain the same.

3.1.10 Interaction Radius of Solitons in Microshort Potential.

We have used Mathematica to look into various properties that a fluxon may have in the double well potential. In the following results we paid close attention to the relationship between the radius of interaction and the values of L and β, where L is the distance between the wells of the potential and β is the interaction term. Using the equation (3.1.10.1) we were able to calculate interaction radius. This can be seen below,

$$R_{int} = \frac{1}{\sqrt{\beta}}$$

(3.1.10.1)

The following three cases show the constraints, $L \ll R_{int}$, $L = R_{int}$ and $L \gg R_{int}$.

3.1.11 $L \ll R$

Here the results show what happens between the two fluxons when the distance between the wells L is small compared to the interaction radius, R_{int}. The fluxons are set at initial positions of -2 and 2. Then one fluxon's initial position is varied so that it ends up closer towards the other fluxon. The value of β = 0.01. With $L = 2.8$ the value of $R_{int} = 10$.
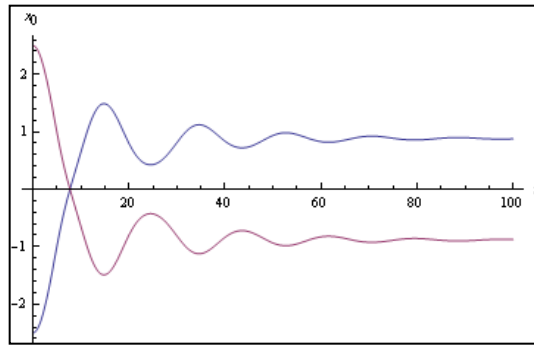
Figure (3.1.11.1) Fluxon 1 with an initial position $x_0 = -2.5$.
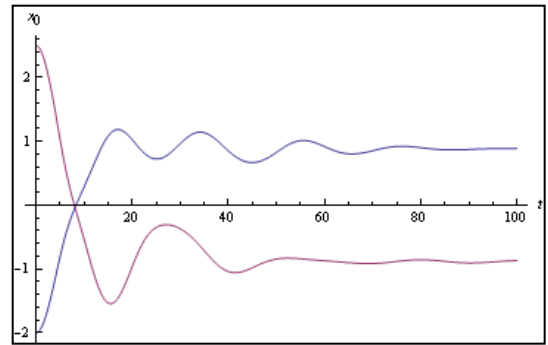
Figure (3.1.11.2) Fluxon 1 with an initial position $x_0 = -2.0$.
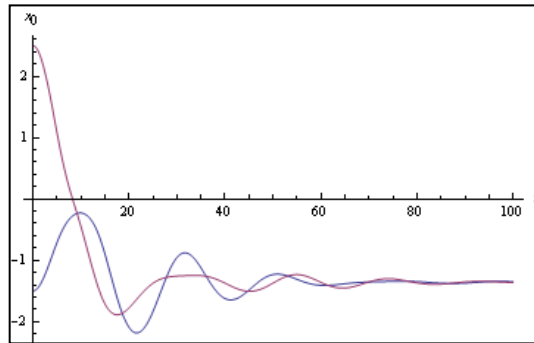
Figure (3.1.11.3) Fluxon 1 with an initial position $x_0 = -1.5$.
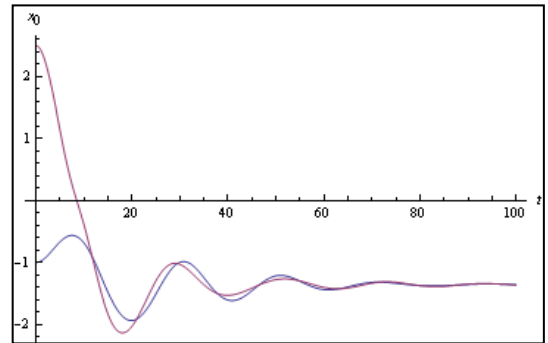
Figure (3.1.11.4) Fluxon 1 with an initial position $x_0 = -1.0$.
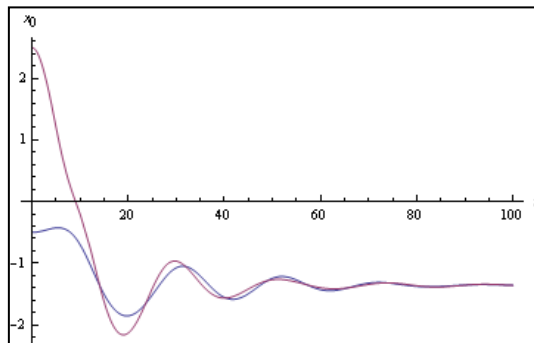
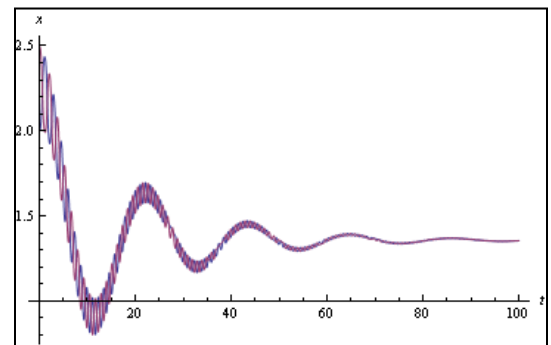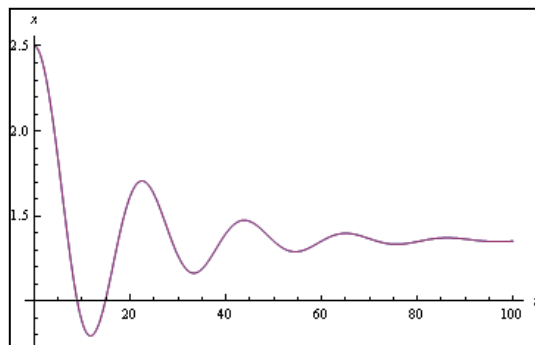**Figure (3.1.11.5) Fluxon 1 with an initial position $x_0 = -0.5$.**
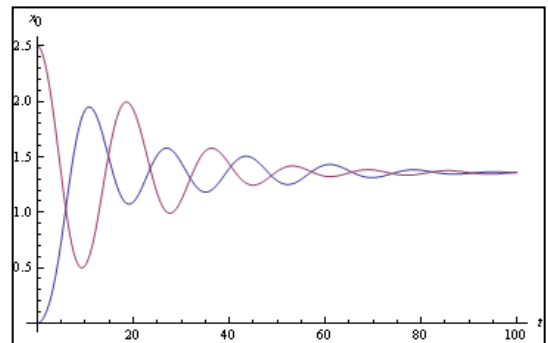
Figure (3.1.11.6) Fluxon 1 with an initial position $x_0 = 0.0$.

84
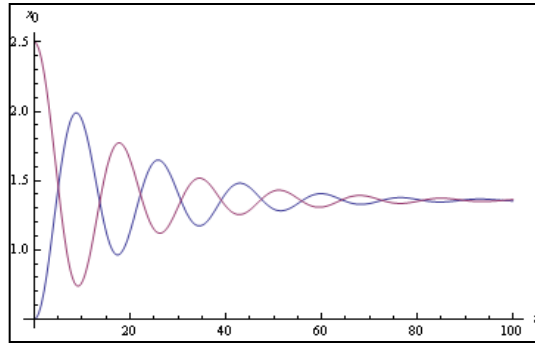
Figure (3.1.11.7) Fluxon 1 with an initial position
$x_0 = 0.5.$
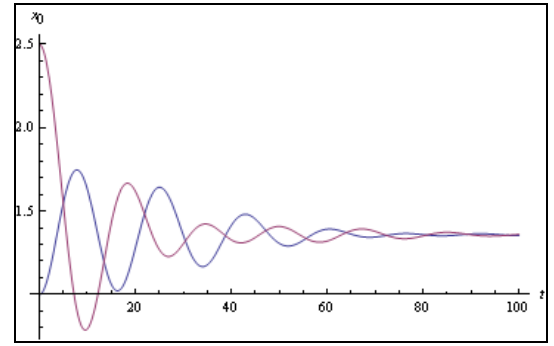
-**Figure (3.1.11.8) Fluxon 1 with an initial position**
$x_0 = 1.0.$
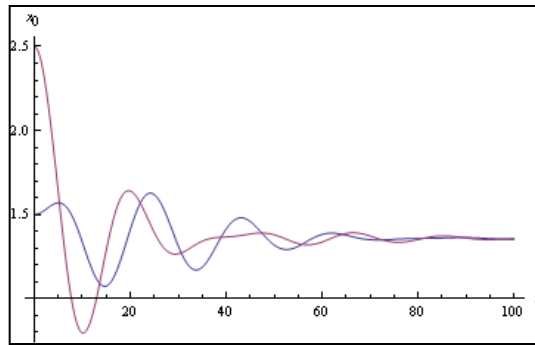
Figure (3.1.11.9) Fluxon 1 with an initial position
$x_0 = 1.5.$
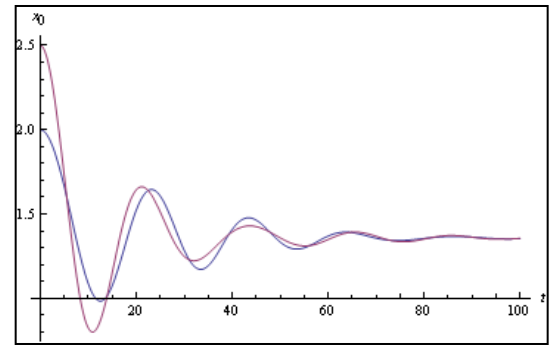
Figure (3.1.11.10) Fluxon 1 with an initial position
$x_0 = 2.0.$
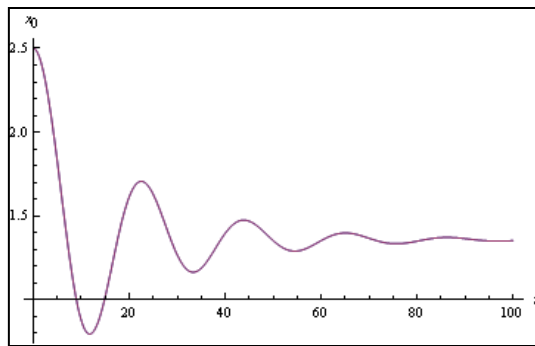
Figure (3.1.11.11) Fluxon 1 with an initial position
$x_0 = 2.5.$

3.1.12 $L = R$

This set of results are similar to the previous set in which one fluxon is "moved" towards the other. The value of β was set to 0.13. This resulted from the parameters, $L = R_{int} = 2.8$.
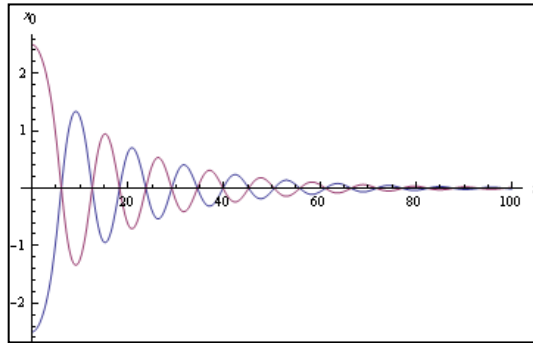
Figure (3.1.12.1) Fluxon 1 with the initial position, x_0 = -2.5.
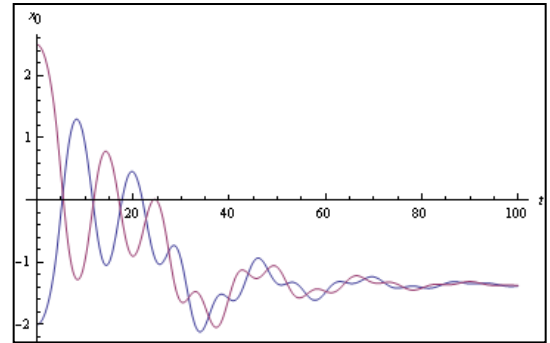
Figure (3.1.12.2) Fluxon 1 with the initial position of $x_0 = -2.0$.
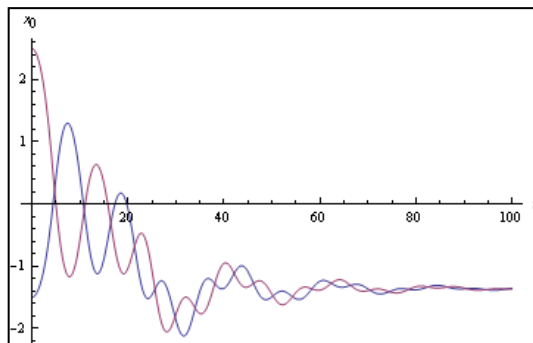
Figure (3.1.12.3) Fluxon 1 with the initial position $x_0 = -1.5$.
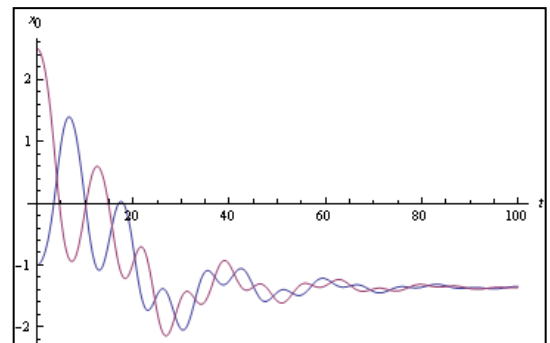
Figure (3.1.12.4) Fluxon 1 with the initial position $x_0 = -1.0$.
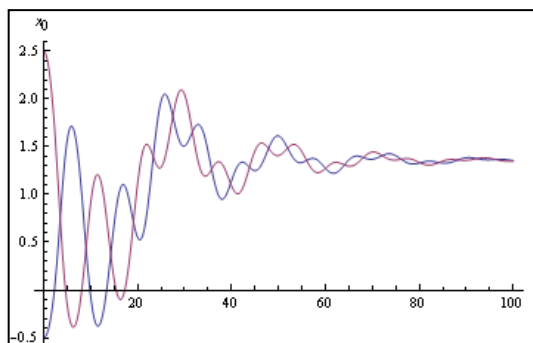
Figure (3.1.12.5) Fluxon 1 with the initial position $x_0 = -0.5$.
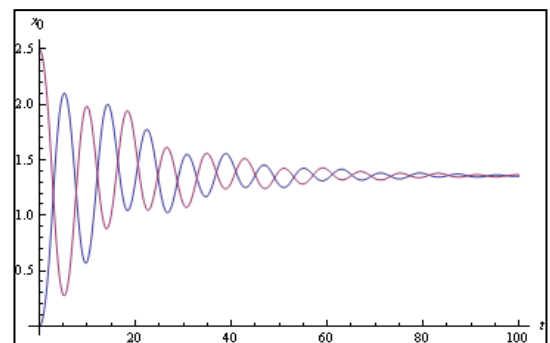
Figure (3.1.12.6) Fluxon 1 with the initial position $x_0 = 0.0$.
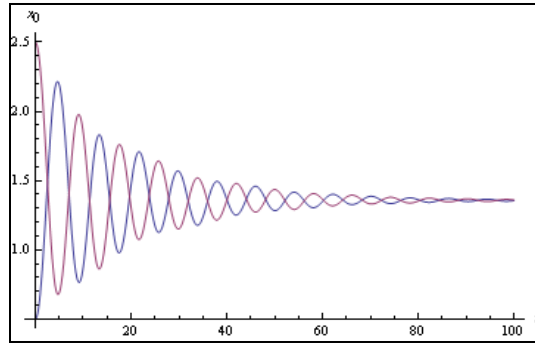
Figure (3.1.12.7) Fluxon 1 with the initial position $x_0 = 0.5.$
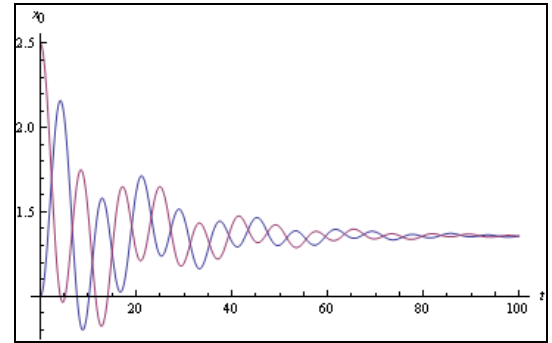
Figure (3.1.12.8) Fluxon 1 with the initial position $x_0 = 1.0.$
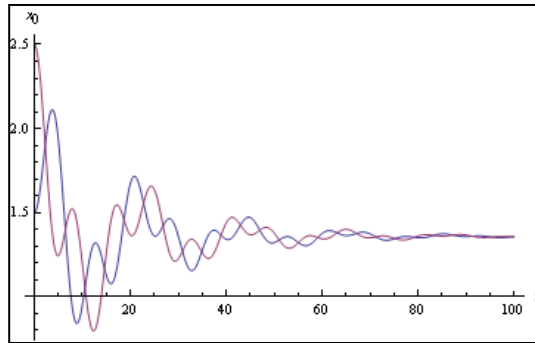
Figure (3.1.12.9) Fluxon 1 with the initial position $x_0 = 1.5.$
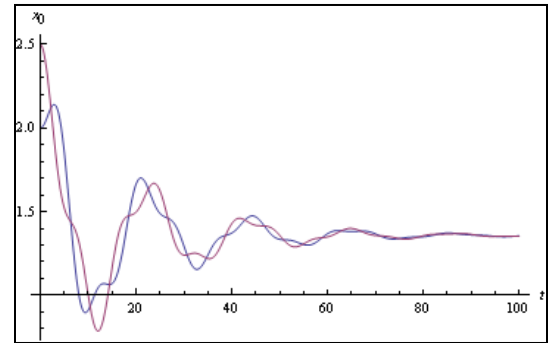
Figure (3.1.12.10) Fluxon 1 with the initial position $x_0 = 2.0.$
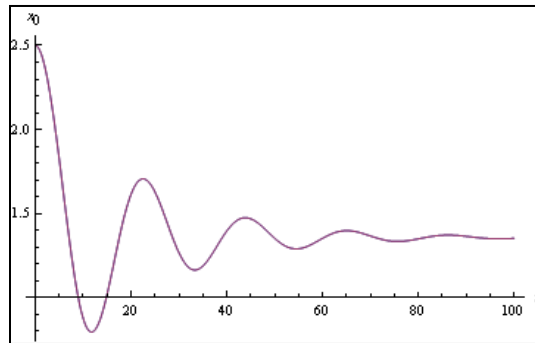
Figure (3.1.12.11) Fluxon 1 with the initial position $x_0 = 2.5.$

87

3.1.13 $L \gg R$

The same method was adopted for this third and final scenario with $\beta = 10$. Thus resulting in $R_{int} = 0.032$.
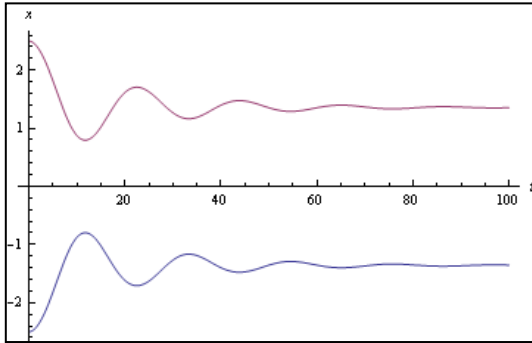
Figure (3.1.13.1) Fluxon 1 with the initial position, x₀ = -2.5
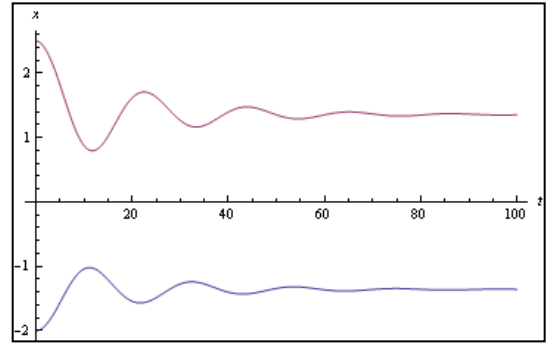
Figure(3.1.13.2) Fluxon 1 with the initial position, x₀ = -2.0
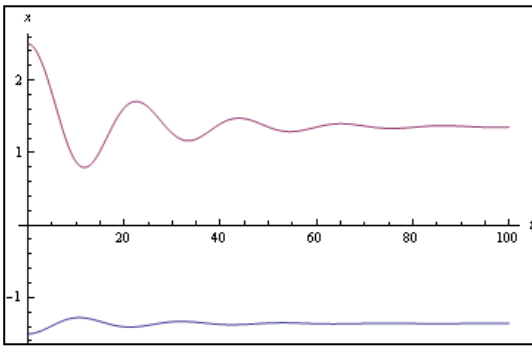
Figure (3.1.13.3) Fluxon 1 with the initial position x₀ = -1.5
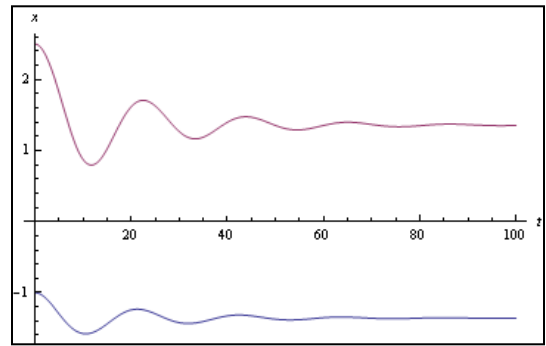
Figure (3.1.13.4) Fluxon 1 with the initial position x₀ = -1.0
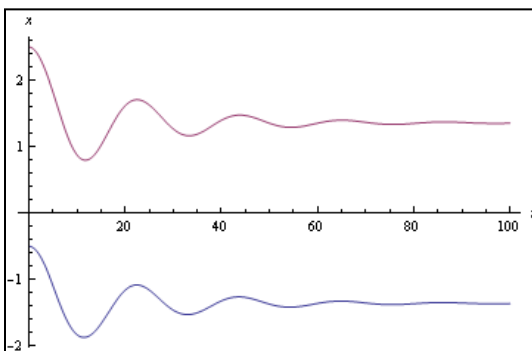
Figure(3.1.13.5Fluxon 1 with the initial position x₀ = -0.5
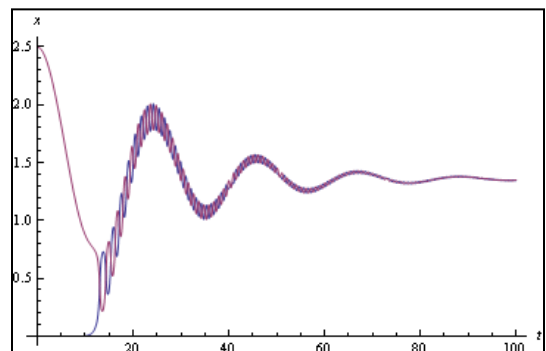
Figure (3.1.13.6) Fluxon 1 with the initial position x₀ = 0.0
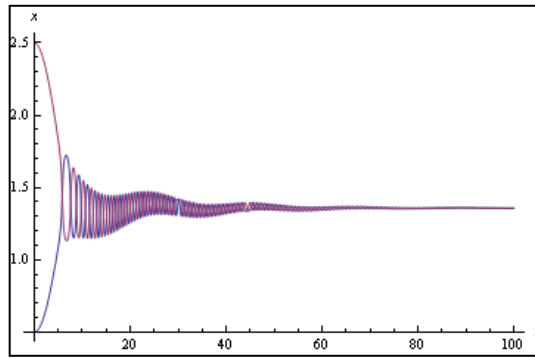
Figure (3.1.13.7) Fluxon 1 with the initial position $x_0 = 0.5$
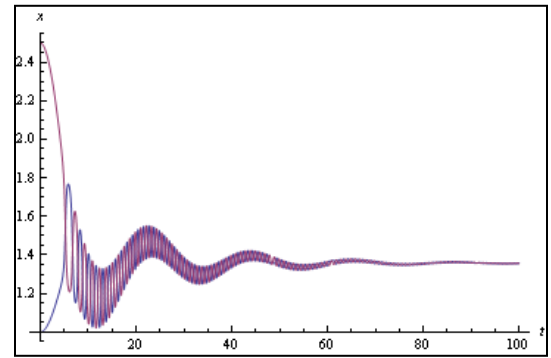
Figure (3.1.13.8) Fluxon 1 with the initial position $x_0 = 1.0$
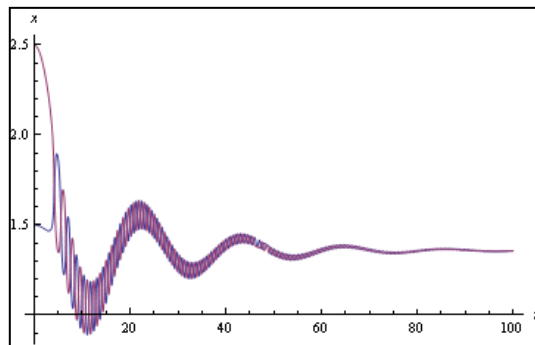
Figure (3.1.13.9) Fluxon 1 with the initial position $x_0 = 1.5$

Figure (3.1.13.10) Fluxon 1 with the initial position $x_0 = 2.0$

Figure (3.1.13.11) Fluxon 1 with the initial position $x_0 = 2.5$

The next stage of research concerned itself with examining the effects of L and R_{int} and with the relationship proposed in equation (3.1.10.1). The first case where $L \ll R_{int}$, the fluxons crossed paths and seemingly passed through one another initially and then as the time t progressed they repelled from one another. The figures (3.1.11.3) to (3.1.11.5) show that these

two fluxons attracted to one another and finally come to rest in negative axis. The figures after this show a positive result and that the two are attracted to one another but do only oscillate quite gently as compared to later results.

With the $L = R$ scenario, we start off with a symmetrical oscillation graph with an interaction with both of the fluxons. This does not occur at these initial starting points in the other cases. There is also a variety of negative and positive axes results. The figures (3.1.12.1), (3.1.12.6) and (3.1.12.7) show the fluxons oscillating in the same localised state whereas the other figures show movement over the potential barrier and also movement in the wells.

If we consider the case where $L \gg R_{int}$, we see that the fluxons commence with not interacting at all and actually deflecting away from each other. This can be seen by the symmetry of the two oscillations. As the fluxon approached the other fluxon we see that this is the case until the first fluxon is located on the potential barrier. At this point the fluxons then intertwine with there oscillations and end up "bound" together in the positive axis. As the fluxon is placed in the same well as the second fluxon we see that with these parameters set the fluxons are attracted to one another and located in the same oscillation path.

3.2   COMSOL Multiphysics

3.2.1   Propagating Fluxon in an AJJ

COMSOL Multiphysics allows us to design programmes that model fluxons in an AJJ with a microshort and is used in the following three different geometric cases. Again the simplest case was designed first and then the complexity was raised to the system to achieve a full realistic working model. Firstly an AJJ was drawn and can be seen in figure (3.2.1.1)
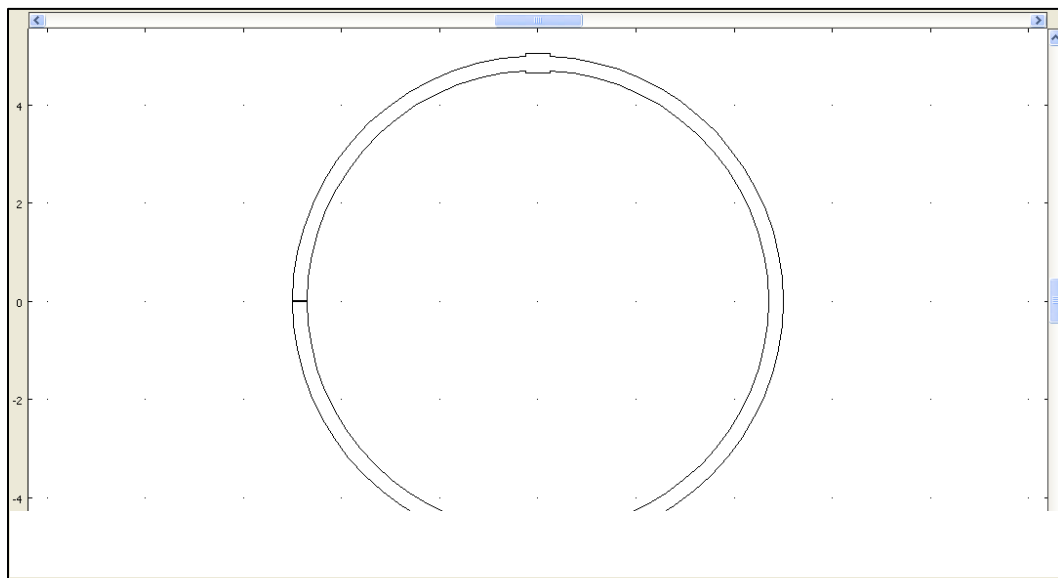
Where R = 5, $(R - \Delta R) = 4.7$, $\Delta R = 0.3$ and corresponds to the thickness of the junction. The microshort width was set to 0.4 in total. A break in the geometry was allocated at the co-ordinates (0, -5). This was done to allow the fluxon to become stable and provide a starting point for the simulation. The subdomain settings were then applied. This was through the use of the basic sine-Gordon (2.4.4) soliton solution and with the application of some extra parameters to accommodate the shape of the junction. The equation used to model the fluxon in the AJJ in Comsol had the following final form,

$$u(t_0) = \left(\left(4 \tanh^{-1} \left(e^{\left(\frac{x - x_0}{\sqrt{(1 - v^2)}} \right)} \right) \times (y < 0) \right) + 2\pi(y \geq 0) \right) \tag{3.2.1.1}$$

With,

$$ut(t_0) = \frac{4}{\left(1 + e^{(a(x - x_0))^2}\right) \times \left(-(av)e^{(a(x - x_0))}\right)} \times (y < 0) \tag{3.2.1.2}$$

Equation (3.2.1.1)'s extra parameters allowed the fluxon to propagate around the junction rather than negating the circular aspect to the junction by travelling in a horizontal fashion.

Boundary conditions were then applied to the system, and this is explained in detail in figure (3.2.1.1). These conditions were constructed using,[43]

$$K\left(n_x H_y - n_y H_x\right) = n \cdot \nabla \varphi \qquad (3.2.1.3)$$

Where $K = \dfrac{1}{\lambda_J \, j_c}$, $\lambda_J = \sqrt{\dfrac{\Phi_0}{2\pi\mu_0 d j_c}}$. H_x and H_y is the external magnetic filed in the x and y directions. The normal to the AJJ boundaries are n_x and n_y respectively. These conditions were applied in Neumann boundary condition form menu.
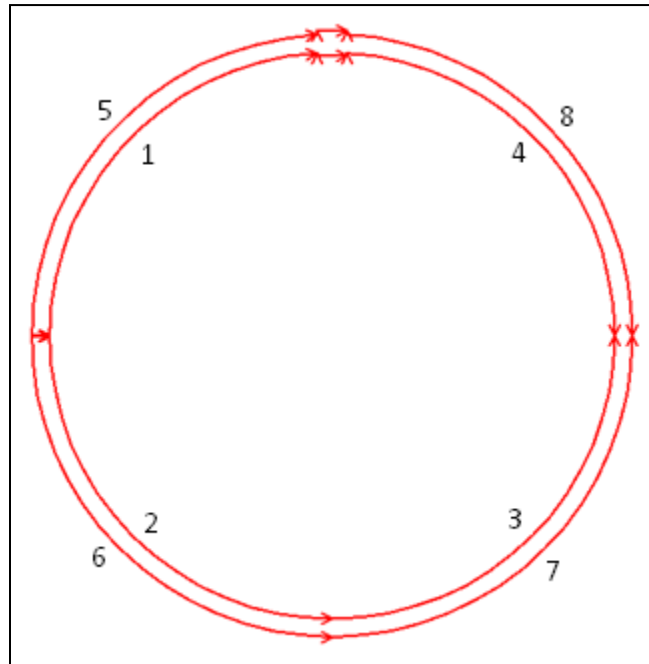
Figure (3.2.1.1) A schematic showing which boundary conditions are applied.

Figure (3.2.1.1) of the AJJ is a boundary condition plot and shows the "arcs" where each corresponding condition is applied. Figure (3.2.1.2) and figure (3.2.1.3) show close ups of the microshort and the break in the junction with corresponding boundary conditions applied.

---

[43] D.R. Gulevich and F.V. Kusmartsev. "Field Theory of Two Dimensional Josephson Junctions". (Unpublished).
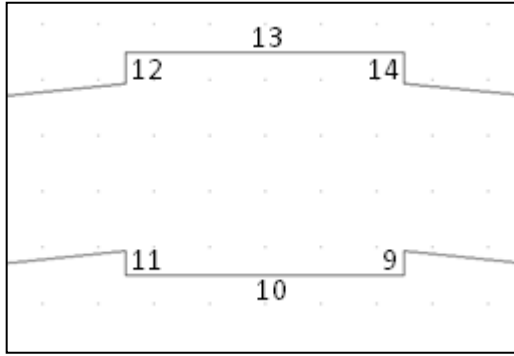
Figure (3.2.1.2) Close up of the microshort schematic.
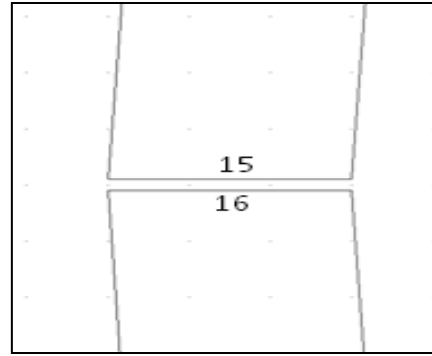
Figure (3.2.1.3) Close up of the "break" in the AJJ.

From using equation (3.2.1.3) the boundary conditions were calculated as follows,

1: $G = -(K * H * x)/(R - dR)$ 9: $G = -(K * H * x)$

2: $G = -(K * H * x)/(R - dR)$ 10: $G = 0$

3: $G = (K * H * x)/(R - dR)$ 11: $G = (K * H * x)$

4: $G = (K * H * x)/(R - dR)$ 12: $G = (K * H * x)$

5: $G = (K * H * x)/R$ 13: $G = 0$

6: $G = (K * H * x)/R$ 14: $G = -(K * H * x)$

7: $G = -(K * H * x)/R$ 15: $G = 0$

8: $G = -(K * H * x)/R$ 16: $G = 0$

With $H = 0.08$, $R = 5$, $dR = 0.3$ and $K = 6.9 \times 10^{-8}$. Mesh parameters were then added to the system. Due to the microshort and AJJ's shape a general mesh already installed in the software was unsuitable and a custom mesh had to be designed. This was done by accessing the free parameter mesh menu and changing the following parameters and so the maximum element size = 0.4, maximum element scaling size = 1, element growth rate = 1, mesh curvature factor = 1, the mesh curvature cutoff = 0.6 and resolution of narrow regions = 0.01 , thus creating a well grafted and balanced mesh. The mesh was altered over the microshort via the "increase mesh" tab to enable a more concentrated calculation to be obtained at this point. The

timer settings were changed to give a time step of 0.1s for the interval of 0 to 45s. The relative

tolerance = 0.001 and the absolute tolerance = 0.00001.

3.2.2   Results for Annular Josephson Junction.

The following are snapshots from the annular junction devised in COMSOL with the parameters
from chapter (3.2.1).
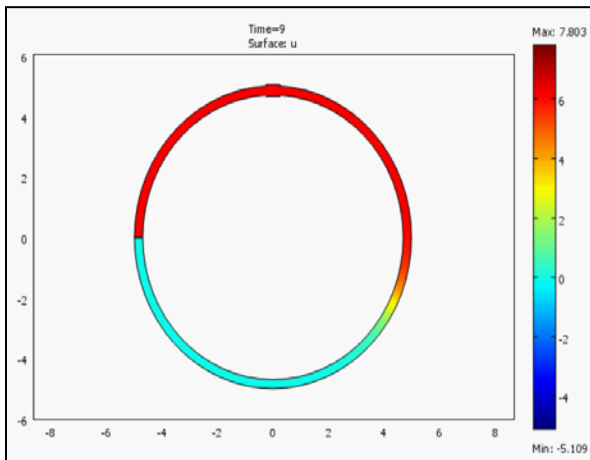

Figure (3.2.2.1) t=9s.
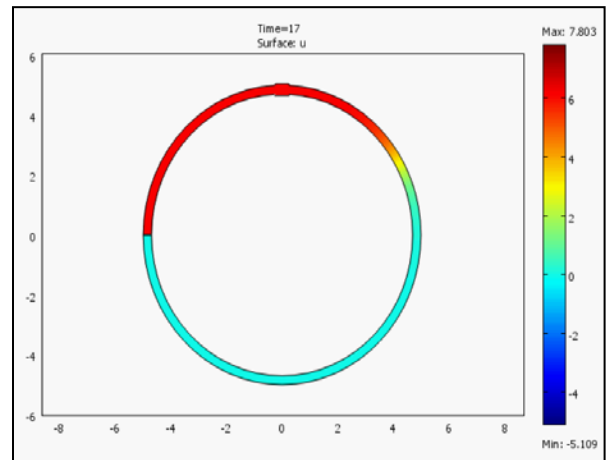
Figure (3.2.2.2) t=17s.
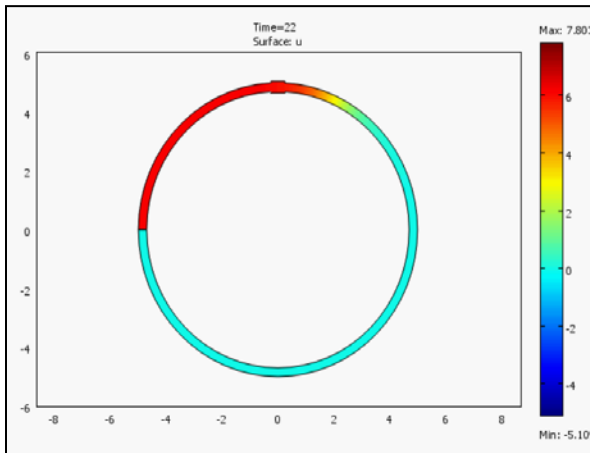
Figure(3.2.2.3) t=22s.
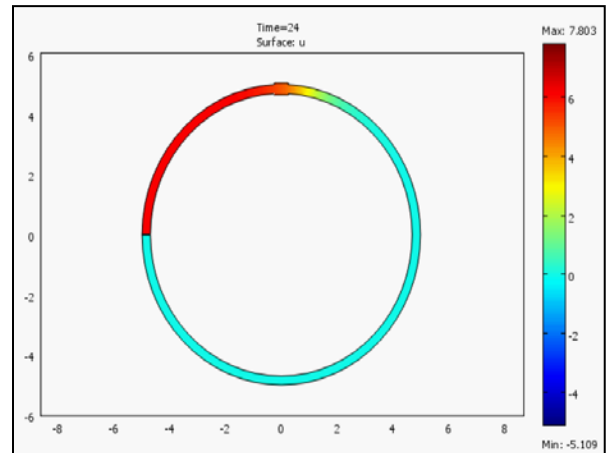
Figure(3.2.2.4) t=24s.
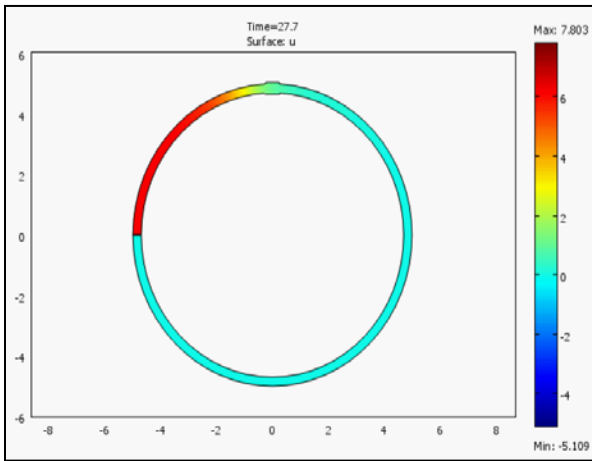
Figure(3.2.2.4) t=27.7s.
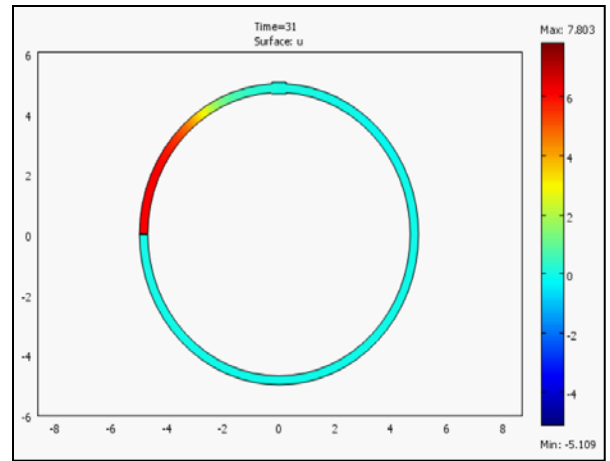
Figure(3.2.2.4) t=31s.
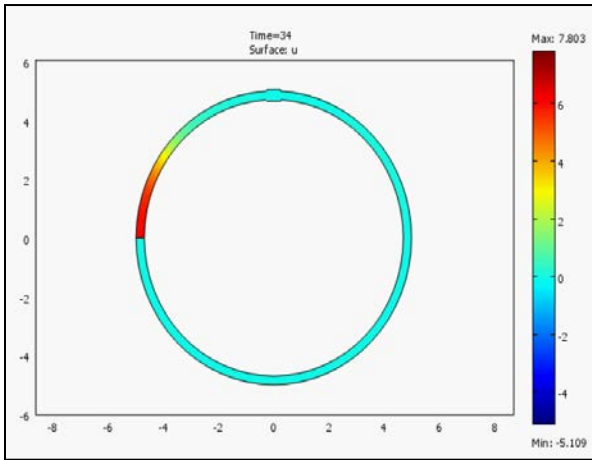
Figure (3.2.2.7) t=34s.
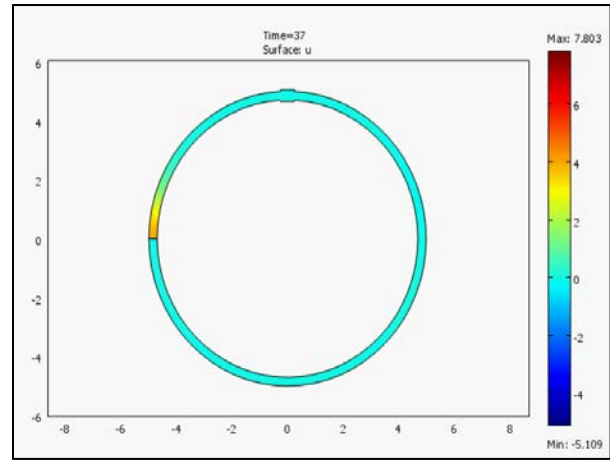
Figure (3.2.2.8) t=37s.
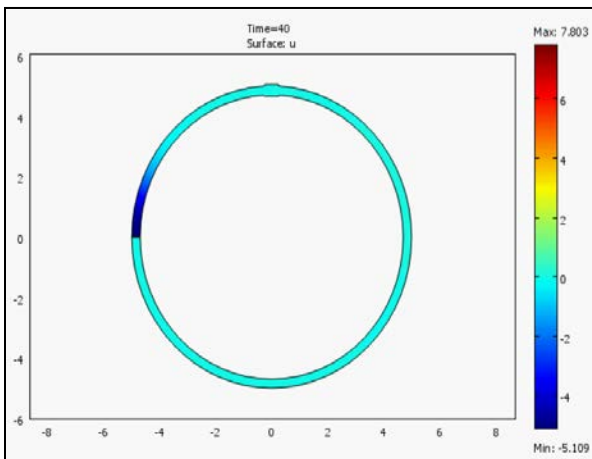
Figure (3.2.2.9) t=40s.

3.2.3   Square Junction

To try and find different properties that a fluxon may exhibit another geometry considered along with the AJJ was the square Josephson junction. As there had been discoveries made with a "linear" junction it made sense to try out this scenario. In this case the microshort was positioned at the top of the junction with a break once again placed in the junction to provide a starting boundary point for the fluxon. A drawing of this set up is seen in figure (3.2.3.1)
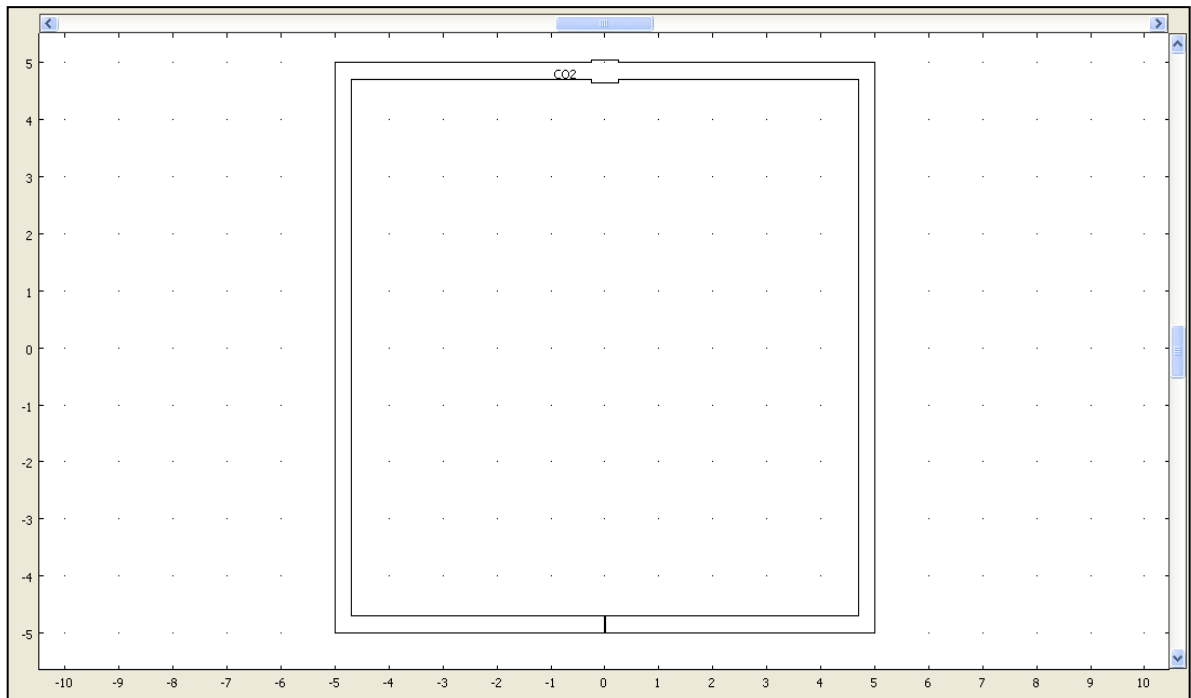
Figure (3.2.3.1) A schematic of the square Josephson junction.

The square geometry has lengths d = 10 and a junction width Δd = 0.3 which is also the same as the previous case.

The subdomain settings were the same as the AJJ's, including the form for the fluxon. The boundary conditions however were differed and so by using equation (3.2.1.3) the altered boundary conditions were applied. The figures, (3.2.3.2) to (3.2.3.4) show which condition is applied to each boundary.
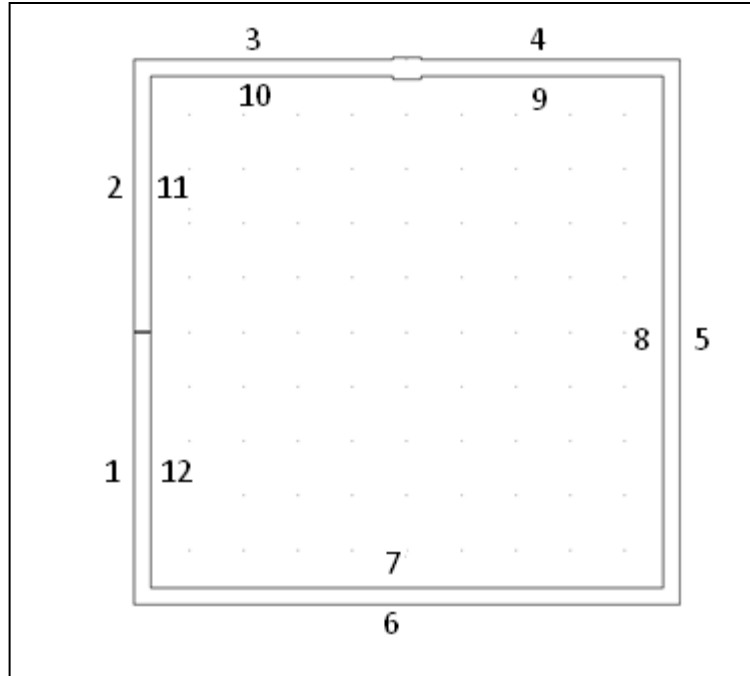
Figure (3.2.3.2) A schematic of the square junction with numbered sides allocated to a certain boundary condition.
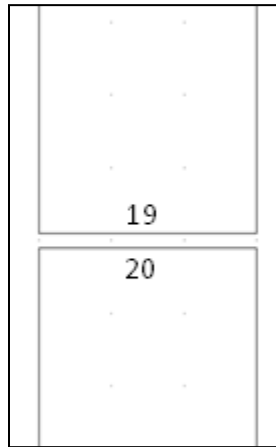
Figure (3.2.3.3) A close up of the "break" in the geometry.
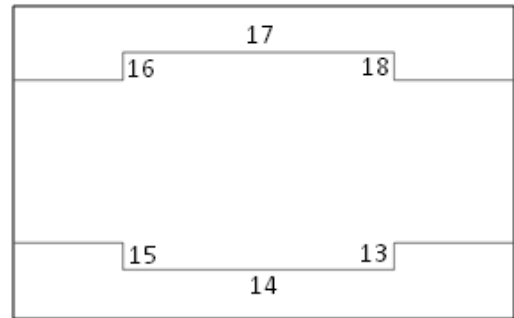
Figure (3.2.3.4) A close up of the microshort.

The following conditions apply to the corresponding numbered side. Boundaries 19 and 20 have been set to zero as a way of giving the fluxon a stable initial starting point.

$1: G = (K * H * x)$ $11: G = -(K * H * x)$

$2: G = (K * H * x)$ $12: G = -(K * H * x)$

$3: G = 0$ $13: G = -(K * H * x)$

$4: G = 0$ $14: G = 0$

$5: -(K * H * x)$ $15: G = (K * H * x)$

$6: G = 0$ $16: G = (K * H * x)$

$7: G = 0$ $17: G = 0$

$8: G = (K * H * x)$ $18: G = -(K * H * x)$

$9: G = 0$ $19: G = 0$

$10: G = 0$ $20: G = 0$

3.2.4   Results for Square Junction

The following are snapshots from the annular junction devised in COMSOL with the parameters from chapter (3.2.3).
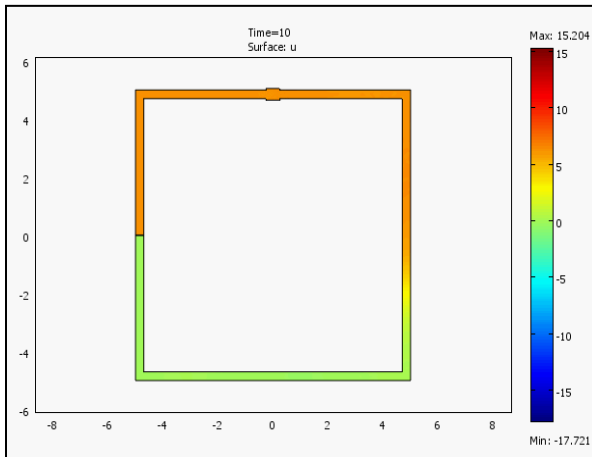
Figure (3.2.4.1) t = 10s.
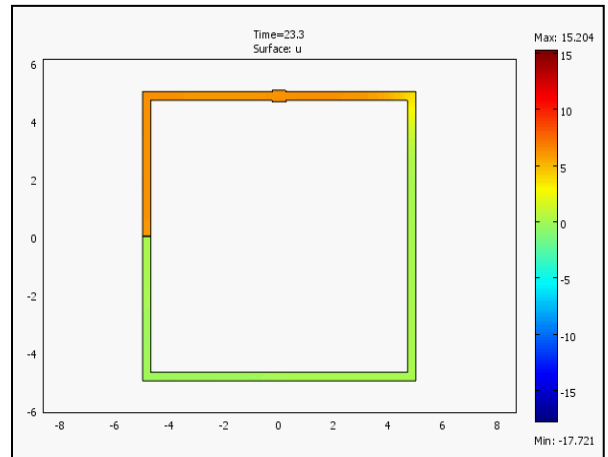
Figure (3.2.4.2) t=23.3s.
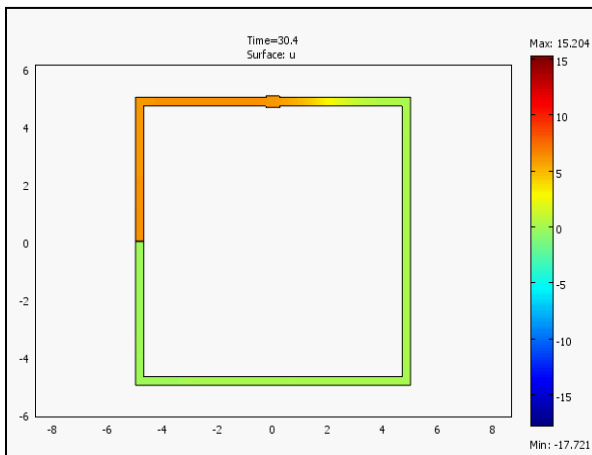
Figure (3.2.4.3) t=30.4s.
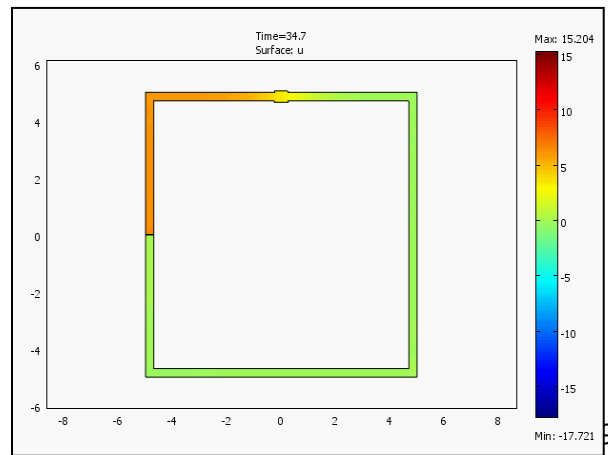
Figure (3.2.4.) t=34.7s.
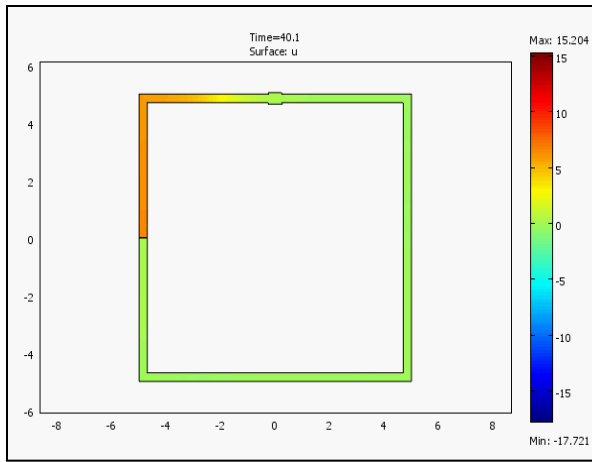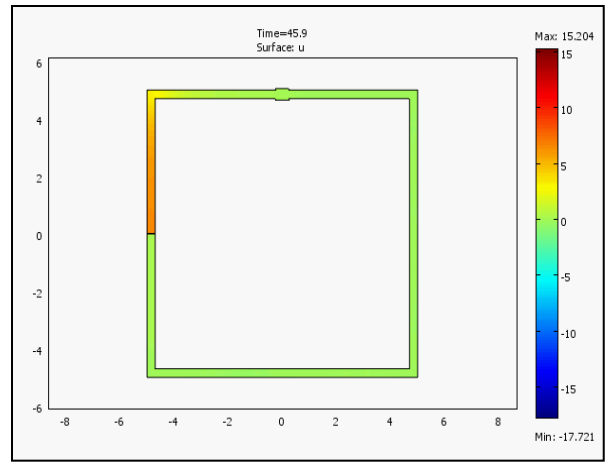
Figure (3.2.4.5) t=40.1s.   Figure (3.2.4.6) t=45.9s.

3.2.5 Heart Junction

The heart junction was proposed in "Fluxon States in Heart-Shaped Josephson Junctions" by Alexander Kemp.[44] From this research it was decided to investigate this different Josephson junction geometry with regards to fluxon propagation in a microshort. Figure (3.2.5.1) shows the junction design with the microshort in place.
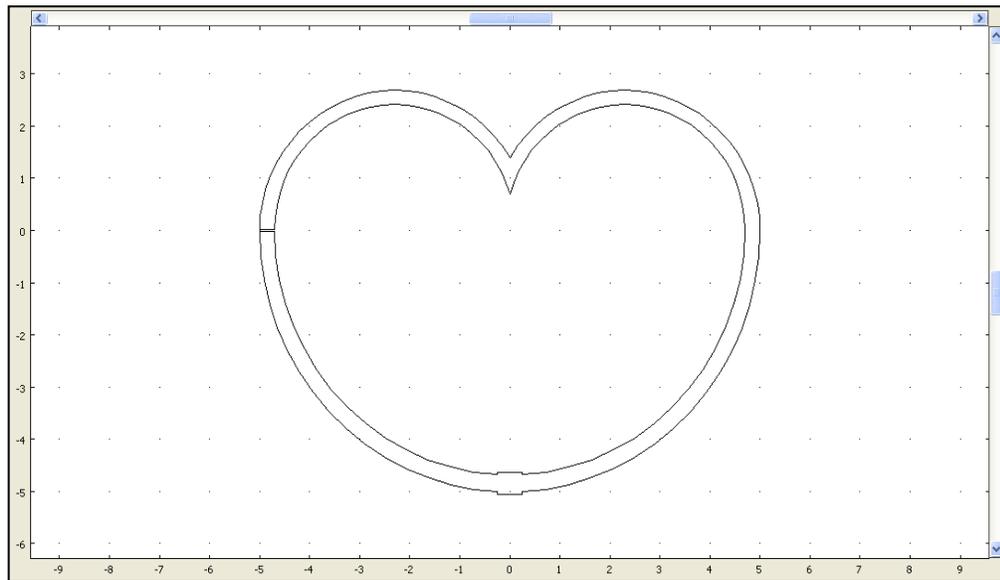
Figure(3.2.5.1) The heart geometry constructed in Comsol.

The geometry was constructed using the same radial distances as for the AJJ case. However the "top" part of the heart was calculated using the following relationship,

---

[44] A. Kemp. "Fluxon States in Heart-Shaped Josephson Junctions". (01/03/01).

$$r = \frac{R}{\sin(\beta) + 1} \tag{3.2.5.1}$$

Where r is the internal radius of the "upper arc", R is the radius of the junction, and β is the angle made from the midpoint of the upper arc to the deflection at the top of the junction. We used the following values to obtain the above heart shape, $R = 50 \times 10^{-6}m$ and $\beta = 60^{\circ}$. Through the calculation of r we were able to obtain figure (3.2.5.1). The microshort was allocated at the bottom of the junction.

As with the previous cases the width of the junction and the microshort were set at the same value. The heart junction then had its plot parameters, mesh, and subdomain settings equalled to the AJJ case seeing as they are similar in shape and the circular nature in propagation the fluxon undertakes. The boundary conditions were constructed using equation (3.2.1.3) and are labelled to the corresponding boundary.
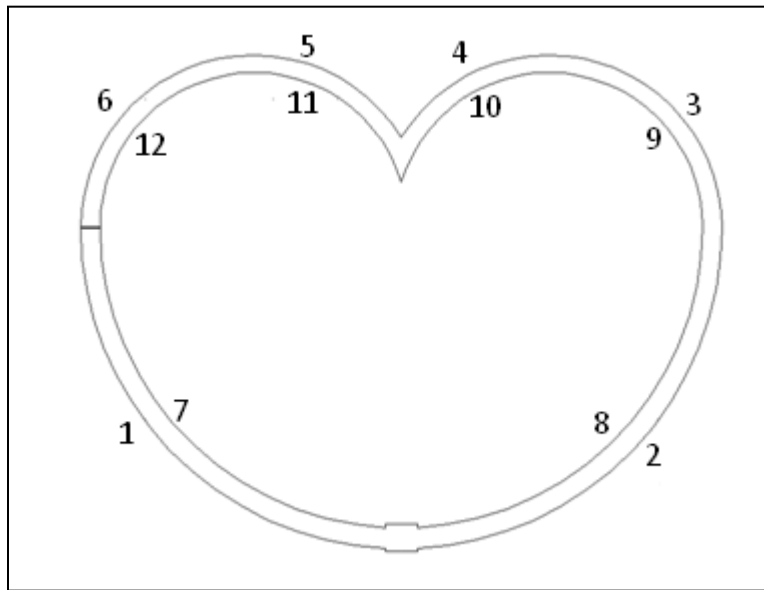
Figure (3.2.5.2) Labelled boundaries for the heart junction.
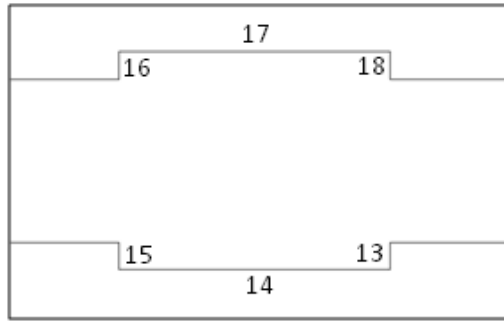
Figure (3.2.5.3) A close up of the microshort.
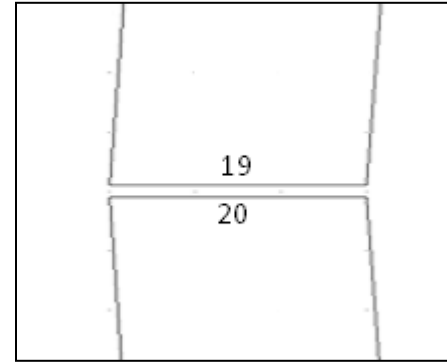

Figure (3.2.5.4) A close up of the "break" in the junction.

The boundary conditions were as follows,

$1: G = -(K * H * x)/R$

$2: G = (K * H * x)/R$

$3: G = -(K * H * x)/r$

$4: G = (K * H * x)/r$

$5: G = -(K * H * x)/r$

$6: G = (K * H * x)/r$

$7: G = -(K * H * x)/(r - dr)$

$8: G = -(K * H * x)/(r - dr)$

$9: G = (K * H * x)/(r - dr)$

$10: G = -(K * H * x)/(r - dr)$

$11: G = (K * H * x)/(r - dr)$

$12: G = -(K * H * x)/(r - dr)$

$13: G = -(K * H * x)$

$14: G = 0$

$15: G = (K * H * x)$

$16: G = (K * H * x)$

$17: G = 0$

$18: G - (K * H * x)$

$19: G = 0$

$20: G = 0$

3.2.6   Results for Heart Junction

The following are snapshots from the heart junction devised in COMSOL with the parameters from chapter (3.2.5).
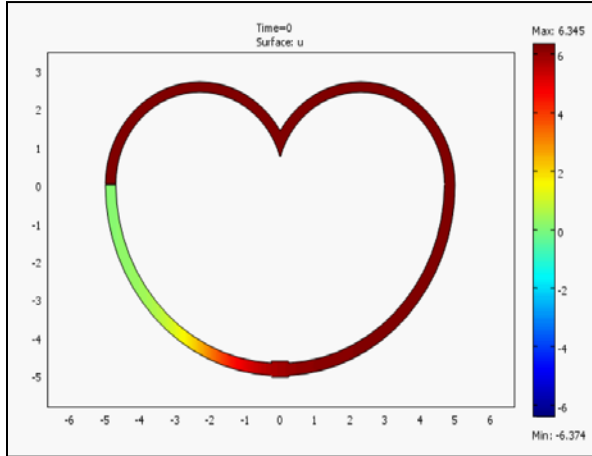
Figure (3.2.5.1) t=0s.

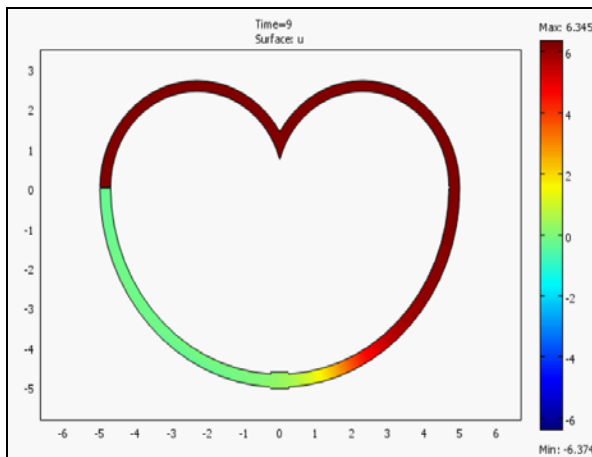**Figure (3.2.5.2) t=3s.**

Figure(3.2.5.3) t=5s.

Figure (3.2.5.4) t=7s.

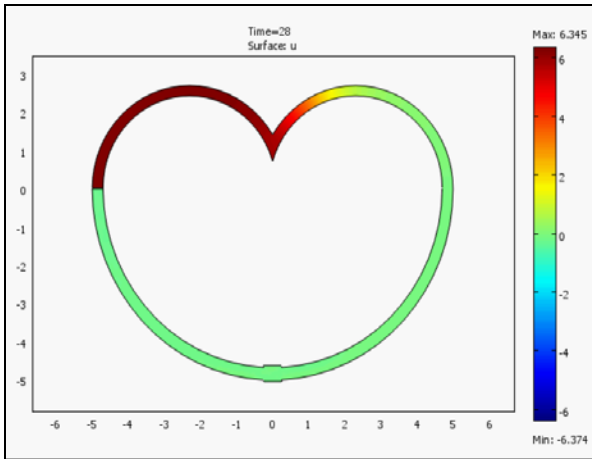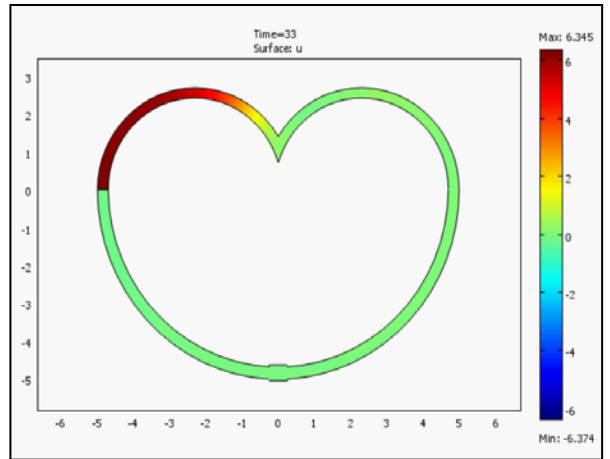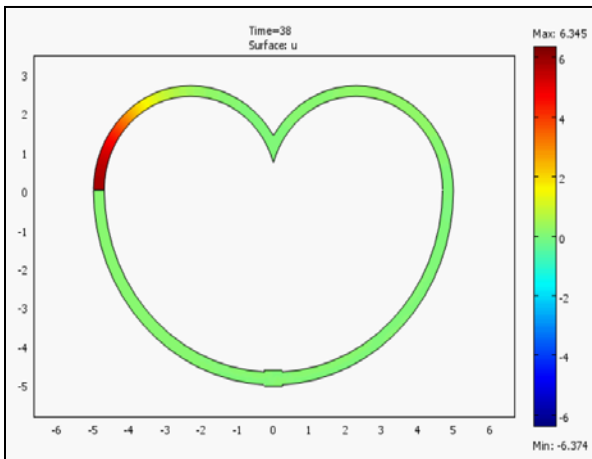**Figure (3.2.5.5) t=9s.**
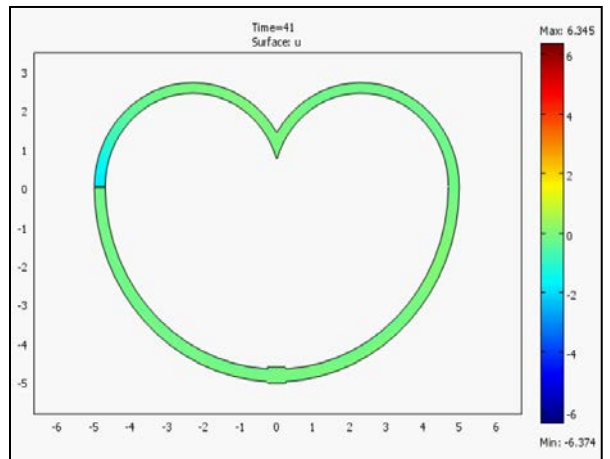

Figure (3.2.5.6) t=11s.

102

Figure (3.2.5.7) t=28s.

Figure(3.2.5.8) t = 33s.

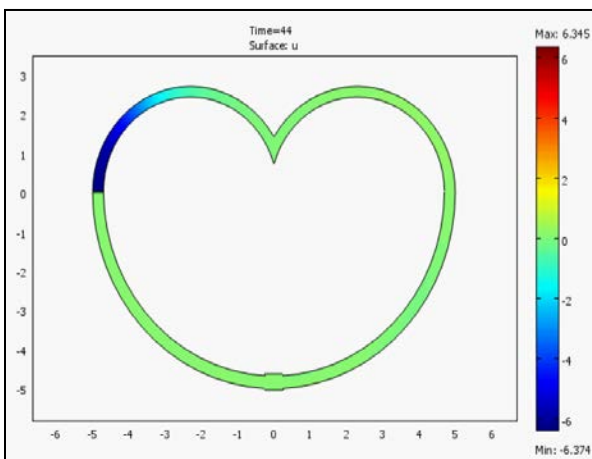**Figure(3.2.5.9) t=38s.**

Figure(3.2.5.10) t=41s.

Figure (3.2.5.11) t=44s.

Next we pursued the fluxon propagating in a Josephson junction via Comsol. We started with the annular case as described in the method (3.2.1). From the result figures (3.2.2.1) to (3.2.2.9) it can be seen that there is a propagating fluxon in the junction. As it approached the microshort we hoped that the fluxon would undergo a transformation in the sense of either creating a new fluxon (akin to previous studies indicated in the literature review) or experience some form of difficulty passing through this addition to the junction. However, we did not yield any of these results and the fluxon passed through the microshort as if it was not present. Even when the fluxon approached the break in the junction it underwent an expected phase change.

The square geometry also left us disappointed. The set of figures in results (3.2.3.4) show that it had taken longer for the propagating fluxon to approach the microshort. As in the annular case the microshort did not affect the fluxon in any way. The same result was found in the heart junction however the fluxon propagated like the fluxon in the AJJ and was faster than the square junction. This showed that further research was needed to obtain a result where the microshort would provide the fluxons to possess new properties that are currently not known.

4 **Conclusion**

The research has compiled a variety of results in examining double well potentials with propagating particles/solitons and fluxons in them. The Mathematica part of the research showed a relationship between initial position and velocity of the particle which resulted in distorted spiral being formed. If we look at the fluxon case where a new potential was applied we also see a spiral which is more regular in shape than the particle result however is still a spiral. We were unable to find an underlying fractal pattern in the interaction of particles section. We did find a regular set of shapes in result (3.1.5.8) which was the best result we obtained in this instance.

The interaction between solitons in the double well potential showed a decomposing set of graphs in form and yielded no fractal patterns. However it did show that at smaller ranges the fluxons will still obtain the same result even as the interaction parameter β was increased.

The Comsol results did prove to be quite disappointing. Having not yielded the expected results one must look at possible ways to improve the simulations so that they may indeed result in a more intriguing manner. The parameters applied to the Comsol simulations are first to be improved. With different values that can be classed as theoretically plausible we could have achieved a satisfying result. As well as this the microshort is made to be of a plausible size in relation to the junction but this can also be examined and improved which could also contribute to a better result being obtained.

As for the process of the research we could have managed the time spent on the Mathematica more efficiently. Due to being unfamiliar with the programme at the start of the study a lot of time was allocated to learning the basics and building the complexity to the standard of our codes presented in this thesis. This is a minor cause of time delay but it is felt that the Mathematica overtook the study for a large portion of the research and so when work came to be done in Comsol not as much time could be devoted to it. This makes us contemplate whether more viable results for the Comsol section could be obtained.

Despite these minor factors into why the results wanted were not obtained it is all a very good starting point for someone else to build upon to gain a new understanding of fluxon propagation in Josephson junctions. Many devices have relied upon the Josephson junctions and will continue to do so. These are highlighted in the literature review accordingly. This research hopes to provide the needed tools for further research to be able to contribute to these new devices and applications in condensed matter physics.

5 <u>Appendix</u>

5.1   Codes for Point Particle

5.1.1   Varying the Initial Velocity.

The first set of codes established the oscillation of a point particle. These oscillations were used to give an initial starting point on the larger project goal. The code below is one example of this initial point. With the aid of a looping function one was allowed to obtain many graphical results to show what happened at various initial conditions. In this case the velocity was the variable. The initial velocity (v_0) of the point particle was set at 1 with the final condition being $v_0 = 10$.

```
v0=1;
Do[Print[v0];
 sol=NDSolve[{x''[t] +4*x[t]*(x[t]^2-1)+ 0.1*x'[t] ☐ 0, x[0] ☐ 4,
x'[0] ☐  v0}, x, {t, 0, 100}, MaxSteps → 10000];
 v0=v0+1;
 Print[Plot[Evaluate[{x[t]}/.sol], {t, 0, 100}, PlotRange→{{0,
100}, {-10, 10}}]], {i, 10}]
```

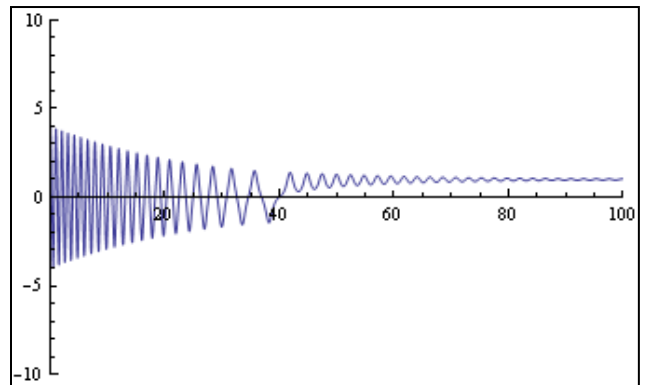The following graphs were yielded,
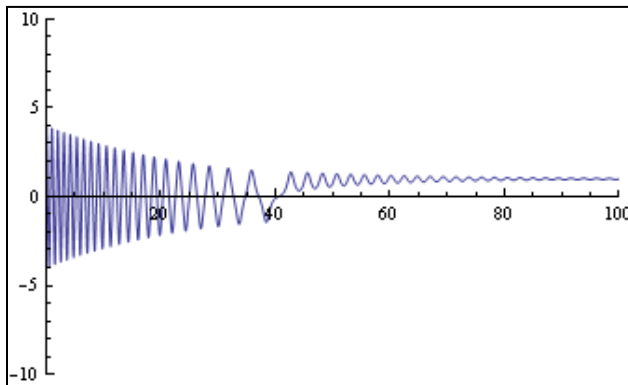
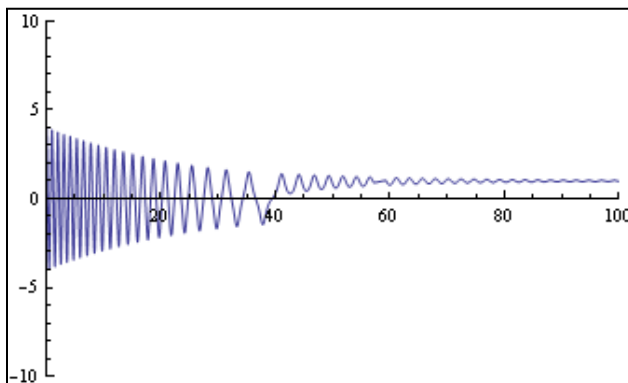**Figure (5.1.1.1) v_0 = 9**

Figure (5.1.1.2)v_0 = 8
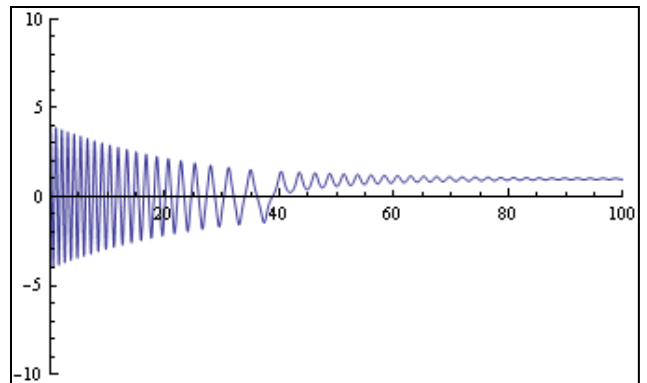

Figure (5.1.1.3) v_0 = 7
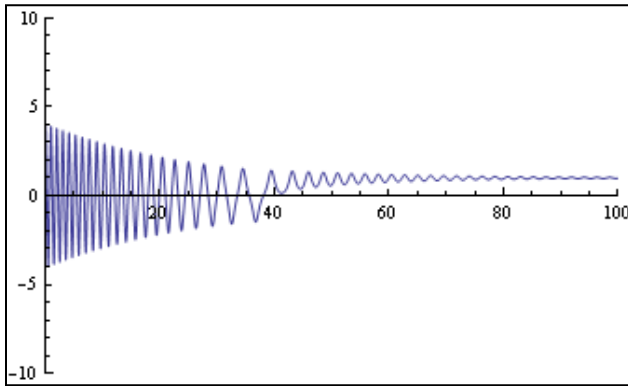

Figure (5.1.1.4) v_0 = 6
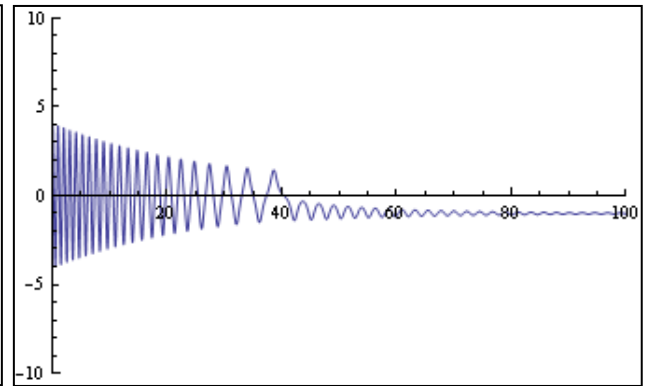
Figure (5.1.1.5) $v_0 = 5$
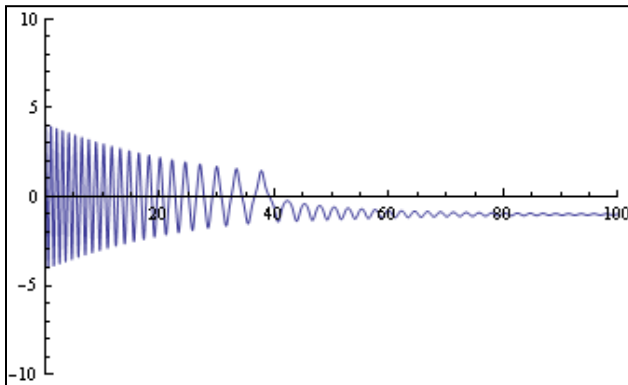

Figure (5.1.1.6) $v_0 = 4$

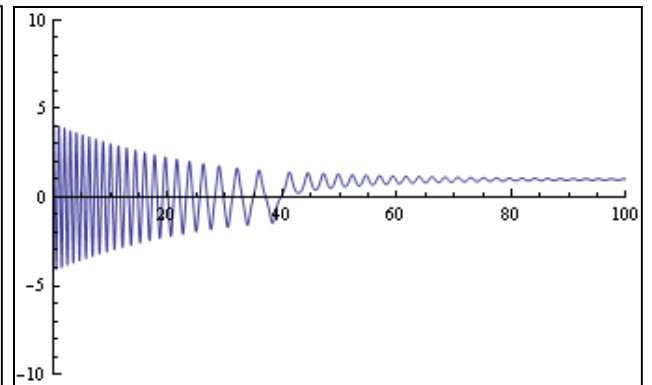**Figure (5.1.1.7)** $v_0 = 3$

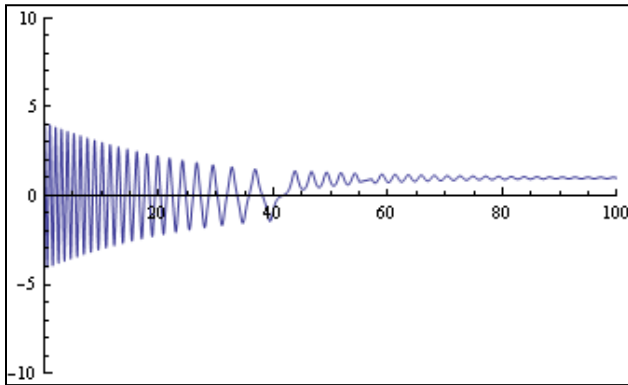**Figure (5.1.1.8)** $v_0 = 2$
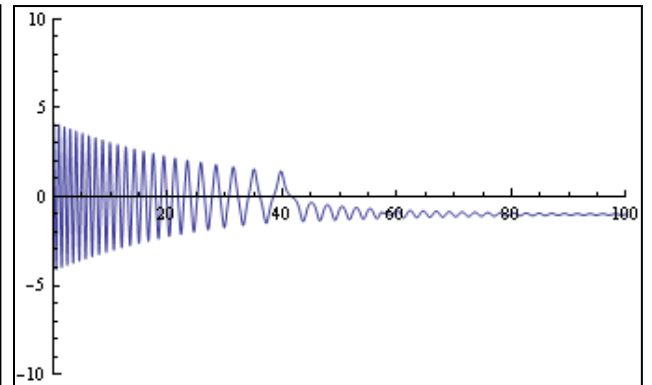

`Figure  (5.1.1.9)` $v_0 = 1$

Figure (5.1.1.10) $v_0 = 0$

5.1.2 Varying the Initial Position.

This code is similar in structure to the previous but with the initial position of the point particle being the variable quantity rather than the velocity.

```
x0=-5;
Do[Print[x0];
 sol=NDSolve[{x''[t] +4*x[t]*(x[t]^2-1)+ 0.1*x'[t] □ 0, x[0] □
x0, x'[0] □  2}, x, {t, 0, 100}, MaxSteps → 10000]; x0=x0+1;
 Print[Plot[Evaluate[{x[t]}/.sol], {t, 0, 100}, PlotRange→{{ 0,
100}, {-5, 5}}]], {i, 11}]
```

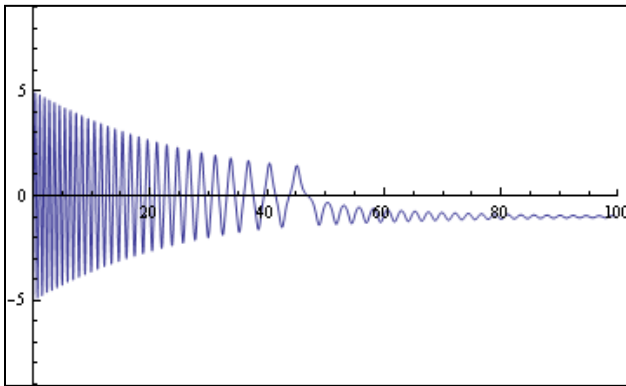

Figure (5.1.2.1) x_0 = -5

Figure (5.1.2.2) (b) x_0 = -4

Figure (5.1.2.3) x_0 = -3

Figure (5.1.2.4) x_0 = -2

Figure (5.1.2.5) (d) x_0 = -1

Figure (5.1.2.6) x_0 = 0

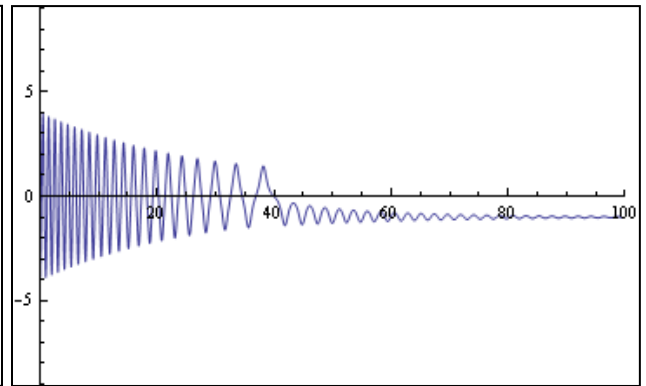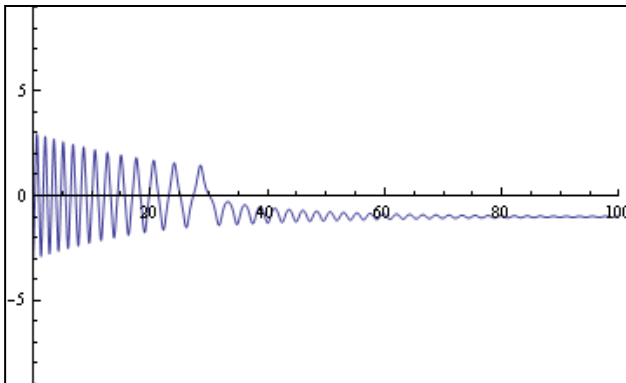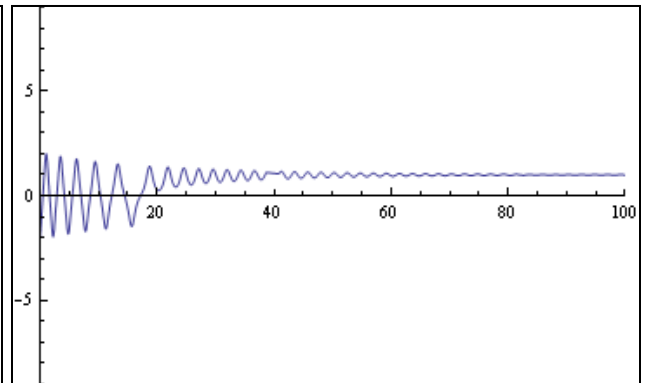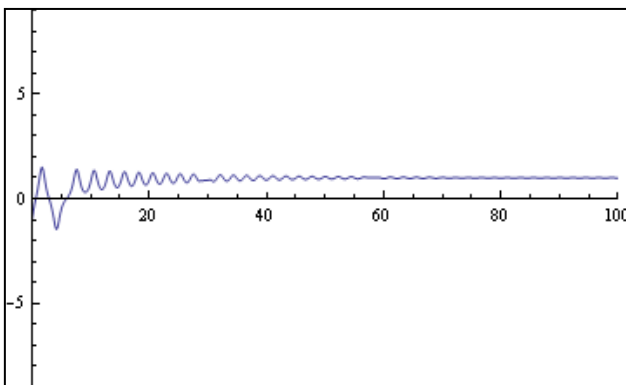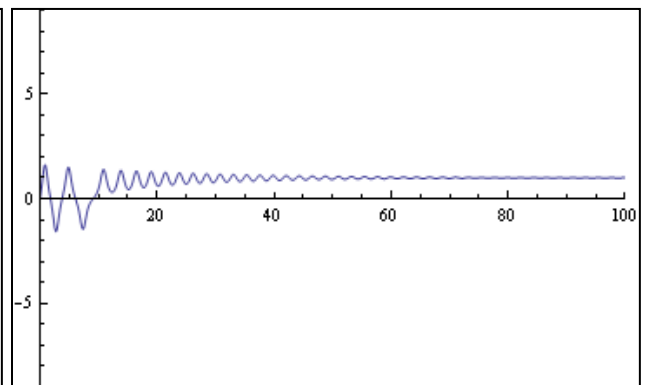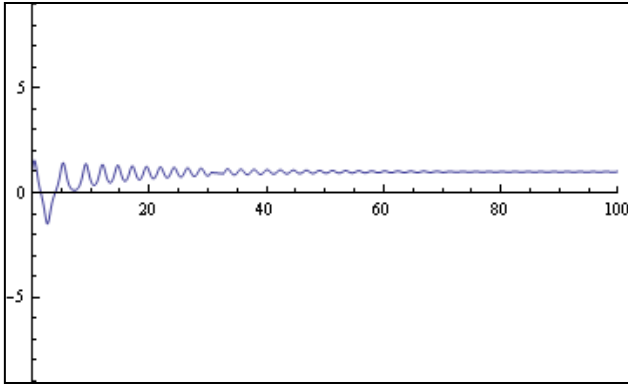**Figure (5.1.2.7) $x_0 = 1$**
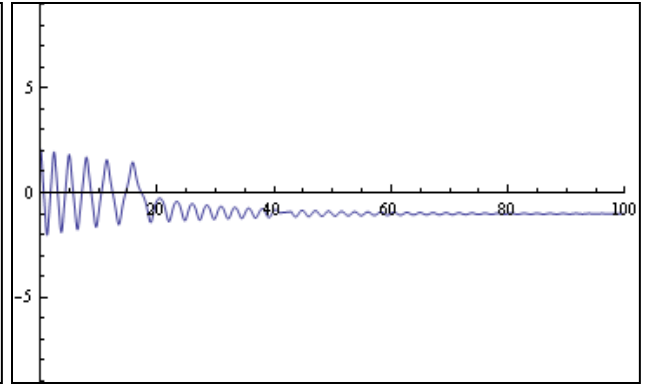
Figure (5.1.2.8) $x_0 = 2$
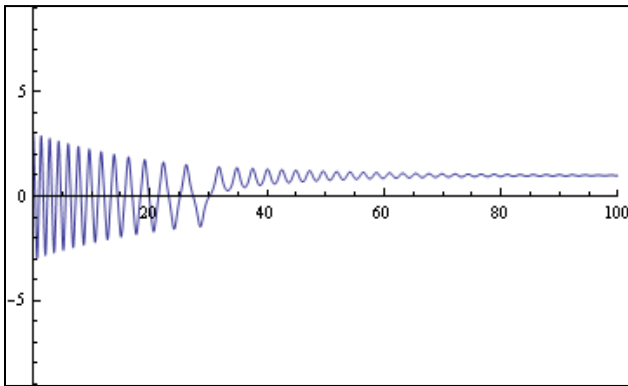
Figure (5.1.2.9) $x_0 = 3$
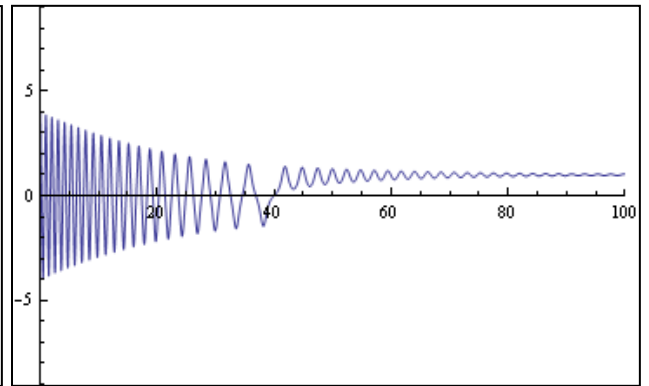
Figure (5.1.2.10) $x_0 = 4$
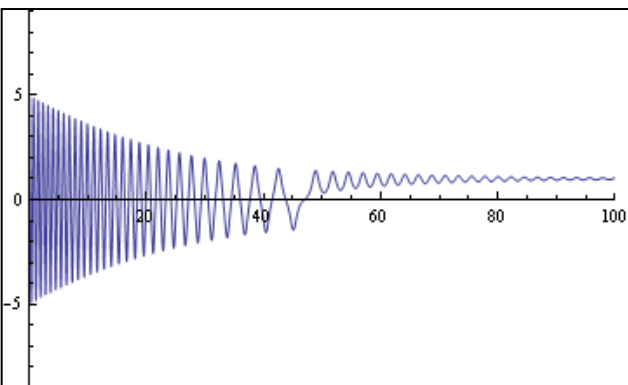
Figure (5.1.2.11) $x_0 = 5$

5.1.3 Single Particle Final Code

The code then evolved so that we could encompass two variables rather than just the solitary one. Here we have a single particle and it's velocity (v) and position (x) are the variables. With aid of an append term, one can sort out the results which yield a "left" or "right" state result. Then the code finished up by plotting these results in a graph.

```
v0=1;
list1={};
list2={};
Do[x0=-9;
  Do[
    sol=NDSolve[{x''[t] +4*x[t]*(x[t]^2-1)+ 0.1*x'[t] □ 0, x[0]
□ x0, x'[0] □  v0},x, {t, 0, 100}, MaxSteps → 50000][[1]];
    If[(x[70]/.sol)>0,
    list1= Append[list1, {x0,v0}],
    list2= Append[list2, {x0,v0}]];

  x0=x0+1;
  , {i, 19}];

  v0=v0+1;
  , {j, 10}];
list1 {};
list2;

ListPlot[{list2, list1}, PlotStyle→{Black,Red}, AxesLabel→{x, v}
]
```

From these graphs and codes we were able to zoom into the positions and velocities that would suit the problem and give us a working solution. The quantities are stated in the method part of the research.

5.2   Code for Interacting particles

The following code shows how we constructed the two particles to behave in the same system.

```
sol=NDSolve[{x₁''[t]+4 x₁[t] (x₁[t]^2-1)+0.1 x₁'[t]==0,
    x₂''[t]+4 x₂[t] (x₂[t]^2-1)+0.1 x₂'[t]==0,x₁[0]==0.5,  x₂[0]==0,
x₁'[0]==0.9, x₂'[0]==1}, {x₁,x₂}, {t, 0, 100}]

Plot[Evaluate[{x₁[t], x₂[t]}/.sol], {t, 0, 100}]
```

The code in full that yielded the results obtained is as follows,

```
list1={};
list2={};

v1=0;
v2=0;

(* x1 being the original position of particle 1, x2 being the
original position of particle 2, v1 is the original velocity of
particle 1 and v2 is the original velocity of particle 2 *)

alpha=0.001;
x2=2; dx=0.01;
While[x2<2.5,
  x1=2; While[x1<2.5,sol=NDSolve[{x₁''[t]+4 x₁[t] (x₁[t]^2-1)+0.1
x₁'[t]-(alpha*2)*(x₁[t]-x₂[t])/((x₁[t]-x₂[t])^2+0.01)^2==0,
      x₂''[t]+4 x₂[t] (x₂[t]^2-1)+0.1 x₂'[t]+(alpha*2)*(x₁[t]-
x₂[t])/((x₁[t]-x₂[t])^2+0.01)^2==0,x₁[0]==x1,  x₂[0]==x2, x₁'[0]==v1,
x₂'[0]==v2}, {x₁,x₂}, {t, 0, 50}, MaxSteps→16000][[1]];
   If[(x₁[50]/.sol)* (x₂[50]/.sol)>0,  list1=Append[list1, {x1,
x2}], list2=Append[list2, {x1, x2}]];
    x1=x1+dx];
     x2=x2+dx];

graph1=ListPlot[list1, PlotStyle→{Black, PointSize[0.015]},
AxesLabel→{x1, x2}];

graph2=ListPlot[list2, PlotStyle→{Cyan, PointSize[0.015]},
AxesLabel→{x1,x2}];
```

5.3   Code for a Single Soliton

Now through the use of a new double well potential and transferring from a point particle to a fluxon. The changes can be seen in the following code in the form of the equation which now encompasses the correct parameters for the new scenario.

```
v0=-10;
list1={};
list2={};
While[v0<10,
  x0=-10;
  While[x0<10,
     sol=NDSolve[{x''[t]+(0.078 x[t])-0.2
Sech[x[t]]^2*Tanh[x[t]]+ 0.1*x'[t] □ 0, x[0] □ x0, x'[0] □
v0},x, {t, 0, 100}, MaxSteps → 15000][[1]];
     If[(x[50]/.sol)>0,
     list1= Append[list1, {x0,v0}],
     list2= Append[list2, {x0,v0}]];
   x0=x0+0.1;
    ];

  v0=v0+0.1;
  ];

graph1=ListPlot[list1, PlotStyle→{Black, PointSize[0.015]},
AxesLabel→{x1, x2}, AspectRatio→1];
graph2=ListPlot[list2, PlotStyle→{Green, PointSize[0.015]},
AxesLabel→{x1,x2}, AspectRatio→1];

Show[graph1, graph2]
```

5.4   Code for Interacting Solitons

For the interaction as stated in the appropriate sections of this thesis we see the addition of the second fluxon. With the animate function applied to the end of the code we were able to see how the results progressed as beta increased.

```
beta=0.0; betamax=0.01; betastep=0.001;
listall1={};
listall2={};

While[beta≤betamax,
 list1={};
 list2={};
 v1=0;
 v2=0;

 x2=-10; dx=0.2;
 While[x2<10,
  x1=-10;
  While[x1<10,
   sol=NDSolve[{x₁''[t]+(0.06*x₁[t])-
0.2*Tanh[x₁[t]]*Sech[x₁[t]]^2+(0.1*x₁'[t])+2*beta (x₁[t]-
x₂[t])*Exp[-beta (x₁[t]-x₂[t])^2]▢0,
       x₂''[t]+(0.06*x₂[t])-
0.2*Tanh[x₂[t]]*Sech[x₂[t]]^2+(0.1*x₂'[t])-2*beta (x₁[t]-
x₂[t])*Exp[-beta (x₁[t]-x₂[t])^2]▢0,
       x₁[0]▢x1,x₂[0]▢x2,  x₁'[0]▢v1, x₂'[0]▢v2}, {x₁,x₂}, {t, 0,
100},MaxSteps→16000][[1]];

   If[(x₁[50]/.sol)* (x₂[50]/.sol)>0,  list1=Append[list1, {x1,
x2}], list2=Append[list2, {x1, x2}]];
    x1=x1+dx];
     x2=x2+dx];
 Print[beta];
 listall1=Append[listall1, list1]; listall2=Append[listall2,
list2];
 beta=beta+betastep;]

Nsteps=1+(betamax/betastep)
```

```
ListAnimate[Table[ListPlot[listall1[[n]], PlotStyle→{Black,
PointSize[0.015]}, AxesLabel→{x1, x2}, AspectRatio→1], {n, 1,
Nsteps}]]
```

6 <u>Bibliography</u>

<u>Books</u>

Barone A, Paterno G. Physics and Applications of the Josephson Effect. (New York: John Wiley & Sons, 1982)

Dodd R.K. Solitons and Nonlinear Wave Equations (London: Academic Press, 1982)

Drazin P.G, Johnson R.S, Solitons: An Introduction (Cambridge University Press, 1989)

Filippov A.T. The Versatile Soliton (Springer Distributor, 2010)

Fordy A.P. Soliton Theory: a survey of results. (Manchester University Press, 1990)

Infeld E, Eowlands G. Nonlinear Waves, Solitons and Chaos (Cambridge University Press, 1990)

McMahon D. Quantum Computing Explained (John Wiley and Sons Inc, 2008)

Rajaraman R. Solitons and Instantons (North-Holland Physics Publishing, 1987)

<u>Papers</u>

Price A.N, Kemp A, Gulevich D.R, Kusmartsev F.V and Ustinov A.V. "Vortex Qubit Based on an Annular Josephson JunctionContaining a Microshort" (03/07/08)

Clark J. "SQUIDs" (Scientific American 271, #2, August 1994, p 46)

Gulevich D.R, Kusmartsev F.V, Savel'ev S, Yampol'skii V.A and Nori F. "Shape and Wobbling Wave Excitations in 2D Josephson Junctions: exact solutions of 2+1 sine-Gordon model" (Loughborough University, RIKEN, Ukranian Academy of Science and University of Michigan, 15/8/08)

Gulevich D.R, Kusmartsev F.V, Savel'ev S, Yampol'skii V.A. and Nori, F. "Shape Waves in 2D Josephson Junctions: Exact Solutions and Time Dilation", (Loughborough University, RIKEN, Ukranian Academy of Science and University of Michigan, 18/9/08)

Ustinov, A.V, "Solitons in Josephson Junctions – Basic model and fluxon properties", (University Erlangen-Nürnberg, 1998)

Lomdahl P.S, Soerensen O.H and Christiansen P.L "Soliton Dynamics and Zero Field Steps in Josephson Tunnel Junctions." (26/10/81).

Vernik I.V, Lazarides N, Sorensen M.P, Ustinov A.V, Pederson N.F and Oboznov V.A, "Experiments with Solitons in Annular Josephson junctions" (Russian Academy of Science, University of Tübinger, University of Denmark, 5/2/1996).

Gulevich D.R, Kusmartsev F.V. "Flux Cloning in Josephson Transmission Lines" (Loughborough University, 07/07/06)

Gulevich D.R, Kusmartsev F.V. "Field Theory of Two-Dimensional Josephson Junctions" (Loughborough University, unpublished)

Gulevich D.R, Gaifullin M, Kusmartseva O.E, Kusmartsev F.V and Hirata K. "Josephson Fluxon Pump:Theoretical aspects and Experimental Implementation of Elementary Flux Quanta Generator with BSCCO" (Loughborough University, National Institute for Materials Science, 13/06/08).

Konwent H. Machnikowski P and Radoszt A. "A certain Double Well Potential Related to SU(2) Symmetry" (1995)

Brauman J.I, "Some Historical Background on the Double Well Potential Model" (1995).

Shaju P.D, Kuriakose V.C. "Double Well Potential in Annular Josephson Junction" (Christ College, Cochin University of Science and Technology, 27/09/04)

McLaughlin D.W, Scott A.C. "Perturbation Analysis of Fluxon Dynamics" (01/10/78)

Lisitskii M.P, Ammendola G, Balashov D.V, Barone A, Cristiano R, Esposito E, Frunzio L, Gubankov V.G, Nappi C, Pagano S, Parlato L, Peluso G, Pepe G. "Annular Josephson Junctions for Radiation Detectiton: Fabrication and Investigation of the Magnetic Behaviour" (C.N.R, Universita Federico, Russian Academy of Sciences and Osservatorio Astronomico di Capodimonte, 2000)

Websites

"Carrier Wave", [Online] Farlex, Available from:
http://www.thefreedictionary.com/carrier+wave [Accessed on 28/12/08]

"Freak Waves Spotted From Space", [Online] MarineTalk2, Available from:
http://www.marinetalk.com/articles-marine-companies/art/Freak-Waves-Spotted-from-Space-xxx000120257IN.html [Accessed on 12/11/08]

"Freak Waves, Rogue Waves, Extreme Waves and Ocean Wave Climate", [Online] University of Bergen, Available from: http://www.math.uio.no/~karstent/waves/index_en.html [Accessed on 12/11/08]

"Sine-Gordon Equation". Wolfram Mathworld [Online] Available from: http://mathworld.wolfram.com/Sine-GordonEquation.html [Accessed on 08/12/08]

"Benoit Mandlebrot" [Online] NNDB, Available from: http://www.nndb.com/people/752/000022686/ [Accessed on 10/08/12]

R. Müller, "The Magnetic Pendulum" Avalable from:

"What are Josephson Junctions? How Do They Work?" [Online] Scientific American, Available from: http://www.scientificamerican.com/article.cfm?id=what-are-josephson-juncti [Accessed on 26/ 8/ 09]

"Josephson Junctions" [Online] UCL, Available from: http://www.ee.ucl.ac.uk/~pwarburt/jj.htm [Accessed on 5/4/09]

The Free Dictionary, "Cooper Pairs", [Online] Farlex, Available from: http://www.thefreedictionary.com/Cooper+pair [Accessed on 5/4/09]

"Josephson Devices", [Online] HyperPhysics, Available from: http://hyperphysics.phy-astr.gsu.edu/Hbase/solids/squid.html#c3 [Accessed on 10/5/09]

"SQUID Magnetometer", [Online] HyperPhysics, Available from: http://hyperphysics.phy-astr.gsu.edu/Hbase/solids/squid.html [Accessed on 15/5/09]

Quantum Solitons, [Online] Available from: http://physicsworld.com/cws/article/print/1285 [Accessed on 11/1108]

"Quantum Chip Sends Information by Bus" [Online] Scientific American, Available from http://www.scientificamerican.com/article.cfm?id=quantum-chip-bus-information [Acessed on 15/5/10]

Images

The image of the carrier wave:

http://www.mathpages.com/home/kmath210/Image3229.gif

The images of the Nordic coastline, The new year wave, The wave train experiment and The breather wave:
http://www.math.uio.no/~karstent/waves/index_en.html

The image of the SQUID:

http://hyperphysics.phy-astr.gsu.edu/Hbase/solids/squid.html

The image of the interacting amplitude solitary shape waves:
http://dml.riken.jp/pub/nori/pdf/PRL_101_127002.pdf

The image of soliton waves and noise:
http://physicsworld.com/cws/article/print/1285/1/world-12-2-8-1

The image of the tuneable potential

http://arxiv.org/pdf/0807.0488v2.pdf

The image of the tilted potential:

http://www.sciencedirect.com/science/article/pii/S0375960104013556